Aus der

Lehrstuhl für Virologie, Max-von-Pettenkofer-Institut

Institut der Ludwig-Maximilians-Universität München

Leitung: Prof. Dr. Oliver Keppler

SARS-CoV-2 Nsp3 and Nsp13 utilize host E3 ubiquitin ligase RCHY1 to suppress host antiviral responses and facilitate virus replication

Dissertation

zum Erwerb des Doktorgrades der Naturwissenschaften

an der Medizinischen Fakultät der

Ludwig-Maximilians-Universität München

vorgelegt von

Yi Ru

aus

Henan, China

Jahr

2025

Mit Genehmigung der Medizinischen Fakultät
der Ludwig-Maximilians-Universität München

Betreuer:	PD Dr. Dr. Albrecht von Brunn
Zweitgutachter:	Prof. Dr. Christian Ries
Dekan:	Prof. Dr. med. Thomas Gudermann
Tag der mündlichen Prüfung:	18.12.2025

SARS-CoV-2 Nsp3 and Nsp13 utilize host E3 ubiquitin ligase RCHY1 to suppress host antiviral responses and facilitate virus replication

Table of content

Zusammenfassung (Deutsch):

Das Coronavirus 2 des Schweren Akuten Respiratorischen Syndroms (SARS-CoV-2) hat eine globale Gesundheitskrise ausgelöst, die weltweit über 7 Millionen Todesopfer gefordert hat. Seine rasche Entwicklung und Anpassung stellen nach wie vor eine große Bedrohung für die menschliche Gesundheit dar. Daher ist es dringend erforderlich, die molekularen Mechanismen zu verstehen, die die Wechselwirkungen zwischen SARS-CoV-2-Proteinen und zellulären Wirtsfaktoren steuern, um wirksame therapeutische Strategien zu entwickeln.

RING finger and CHY zinc finger domain-containing protein 1 (RCHY1) ist eine E3-Ubiquitin-Ligase, die ihre Substrate wie p53 und p63 durch Ubiquitinreste modifiziert, was zu deren Abbau in Proteasomen führt. Frühere Studien der Arbeitsgruppe zeigten, dass die virale SARS-Unique-Domäne (SUD) und die Papain-ähnliche Protease-Domäne (PLpro) des Nicht-Strukturproteins Nsp3 von SARS-CoV mit RCHY1 interagieren und es stabilisieren, wodurch der Abbau des antiviralen Proteins p53 erleichtert wird. Diese Interaktion könnte eine Strategie des Coronavirus darstellen, um der antiviralen Abwehr des Wirts entgegenzuwirken. Wie SARS-CoV-2-Proteine RCHY1 und seine Substrate regulieren, ist jedoch noch weitgehend unbekannt.

In dieser Studie wurde die Interaktion von SARS-CoV-2 Nsp3 mit RCHY1 über seine SUD- und PLpro-Domänen identifiziert. Es wurde festgestellt, dass Nsp3 die Proteinexpressionsmenge von RCHY1 erhöht. Darüber hinaus zeigten *in vivo* Ribopuromycylierungs- und Ubiquitinierungstests, dass die Stimulation von RCHY1 durch Nsp3 sowohl aus einer erhöhten RCHY1-Protein-Translation als auch aus einem verringerten RCHY1-Abbau resultiert. RCHY1 ist ein direktes Ziel der PLpro-Domäne von Nsp3, da PLpro RCHY1 in einer von der katalytischen Aktivität von PLpro abhängigen Weise deubiquitinieren und deISGylieren kann. Darüber hinaus reduzierte Nsp3 RCHY1-Substrate wie p53 und p63, indem es die RCHY1-Expression hochregulierte. Eine Überexpression von p53 und p63 hemmt nachweislich die Replikation des humanen Coronavirus. Desweiteren senkt Nsp3 den ISGylierungsgrad von p53 und p63 drastisch. Wir vermuten, dass die Nsp3-induzierte Verringerung und De-ISGylierung von p53 und p63 die Replikation von Coronaviren erleichtern könnte. Darüber hinaus interagiert RCHY1 mit einem hochkonservierten Nicht-Strukturprotein von SARS-CoV-2, Nsp13, und modifiziert es posttranslational. In Gegenwart von RCHY1 unterdrückte Nsp13 die NF-κB-Signalaktivität.

Zusammengenommen deuten unsere Ergebnisse darauf hin, dass SARS-CoV-2 Nsp3 den Abbau der antiviralen Faktoren p53 und p63 durch Stabilisierung von RCHY1 fördert, während Nsp13 RCHY1 zur Hemmung des NF-κB-Signalwegs nutzt. Dies könntenStrategien von SARS-CoV-2 zur Schwächung des Wirtsimmunsystems darstellen.

Abstract (English):

Severe Acute Respiratory Syndrome Coronavirus 2 (SARS-CoV-2) has triggered a global health crisis, resulting in over 7 million deaths worldwide. Its rapid evolution and adaptation persist as a major threat to human health. Consequently, there is an urgent need to understand the molecular mechanisms governing the interactions between SARS-CoV-2 proteins and host cellular factors to develop effective therapeutic strategies.

RING finger and CHY zinc finger domain-containing protein 1 (RCHY1) is an E3 ubiquitin ligase that modifies its substrates such as p53, p63 by ubiquitin residues, leading to their degradation in proteasomes. Our previous study revealed that the viral SARS-unique domain (SUD) and papain-like protease (PLpro) domain of non-structural protein Nsp3 from SARS-CoV interact with and stabilize RCHY1, facilitating the degradation of the antiviral protein p53. This interaction may offer a strategy for the coronavirus to counteract the host's antiviral defenses. However, how SARS-CoV-2 proteins regulate RCHY1 and its substrates remains largely unknown.

In this study, the interaction of SARS-CoV-2 Nsp3 with RCHY1 through its SUD and PLpro domains was identified. Nsp3 was found to increase the protein expression level of RCHY1. In addition, *in vivo* ribopuromycylation and ubiquitination assays demonstrated that the stimulation of RCHY1 by Nsp3 results from both increased RCHY1 protein translation and decreased RCHY1 degradation. RCHY1 is a direct target of the Nsp3 PLpro domain, as PLpro can deubiquitinate and deISGylate RCHY1 in a manner dependent on the catalytic activity of PLpro. In addition, Nsp3 reduced RCHY1 substrates such as p53 and p63 by upregulating RCHY1 expression. Overexpression of p53 and p63 has been shown to inhibit human coronavirus replication. Additionally, Nsp3 dramatically downregulates the ISGylation level of p53 and p63. We speculate that Nsp3-induced reduction and deISGylation of p53 and p63 may facilitate coronavirus replication. Moreover, RCHY1 interacts with and post-translationally modifies a highly conserved non-structural protein of SARS-CoV-2, Nsp13. In the presence of RCHY1, Nsp13 suppressed NF-κB signaling activity.

Taken together, our results indicate that SARS-CoV-2 Nsp3 promotes the degradation of antiviral factors p53 and p63 by stabilizing RCHY1, while Nsp13 uses RCHY1 to inhibit the NF-κB signaling pathway, which may be strategies of SARS-CoV-2 to weaken the host immune system.

List of figures

List of tables

List of abbreviations

abbreviation	full name
a.a.	amino acid
ACE2	angiotensin-converting enzyme 2
ANOVA	Analysis of variance
ASFV	African swine fever virus
BSA	Bovine serum albumin
ca	catalytic mutant
cDNA	Complementary DNA
CHX	Cycloheximide
CMV	Cytomegalovirus
co-IP	co-immunoprecipitation
CoVs	Coronaviruses
DAPI	4',6-diamidino-2-phenylindole
ddH_2O	Doubly distilled water
DMEM	Dulbecco's modified Eagle's medium
DMSO	Dimethyl sulfoxide
DMV	double-membrane vesicle
DPBS	Dulbecco's Phosphate Buffered Saline
DTT	Dithiothreitol
E	envelope
ELISA	enzyme-linked immunosorbent assay
FBS	fetal bovine serum
HCoV	human coronavirus
HEPES	N-2-Hydroxyethylpiperazine-N-2-Ethane Sulfonic Acid
HIV-1	Human Immunodeficiency Virus type 1
h.p.i.	hours post-infection
HPV	Human Papillomavirus
IAV	influenza A virus
IFN	Interferon
IP	immunoprecipitation
IRF3	Interferon regulatory factor 3
IRF7	Interferon regulatory factor 7
ISG	Interferon-stimulated gene
KDa	kilodalton
LB	lysogeny broth

M	membrane
MDM2	murine double minute 2
MEM	Minimal Essential Medium
MERS	Middle East Respiratory Syndrome
MOI	multiplicity of infection
mRNA	Messenger RNA
N	nucleocapsid
NF-kB	Nuclear factor-κB
NP-40	Nonidet™ P40
Nsp	nonstructural protein
N2H	NanoLuc two-hybrid
ORFs	open reading frames
PAGE	polyacrylamide
PBS	Phosphate-buffered saline
PCR	Polymerase chain reaction
PEDV	Porcine Epidemic Diarrhea Virus
PEG	polyethylene glycol
PEI	polyethylenimine
PFA	Paraformaldehyde
PLpro	papain-like protease
PTMs	Post-translational modifications
P/S	penicillin/streptomycin
qPCR	quantitative PCR
RCHY1	RING finger and CHY zinc finger domain-containing protein 1
RING	Really Interesting New Gene
RT	Room temperature
S	spike
SARS-CoV	Severe acute respiratory syndrome coronavirus
SARS-CoV-2	Severe acute respiratory syndrome coronavirus 2
SDS	sodium dodecyl sulfate
SEV	Sendai virus
SUD	SARS Unique Domain
TBS	Tris-buffered saline
TBST	Tris-buffered saline with Tween® 20 detergent
TNFα	Tumor necrosis factor α

ubi	ubiquitin
VSV	Vesicular stomatitis virus
VSV-G	VSV glycoprotein G
WB	Western blot
wt	Wild type
YPD	yeast extract peptone dextrose
Y2H	yeast-two-hybrid
ZIKV	Zika virus

1. Introduction

1.1 The pandemic of COVID-19

Since the initial identification of coronavirus disease 2019 (COVID-19), the global incidence of the disease has been reported to be over 700 million cases, with a mortality rate of over 7 million cases worldwide by April 2025 [1]. Unvaccinated or partially vaccinated older individuals with underlying health conditions are particularly susceptible to severe disease outcomes [2]. In patients with non-fatal diseases, long COVID can persist for months and impact multiple organ systems [3]. In contrast to the geographically restricted impact of severe acute respiratory syndrome coronavirus (SARS-CoV) and Middle East respiratory syndrome coronavirus (MERS-CoV), the global distribution of severe acute respiratory syndrome coronavirus 2 (SARS-CoV-2) and the potential for the emergence of new variants that may compromise the efficacy of vaccines, underscores the urgent need for safe, effective and readily available therapeutics for the treatment of patients infected with SARS-CoV-2 [4].

Therefore, it is essential to deepen our understanding of the molecular mechanisms underlying the interactions between SARS-CoV-2 proteins and host proteins. This profound knowledge is indispensable for the advancement of therapeutic interventions against coronaviruses.

1.2 SARS-CoV-2 genome and proteins

Coronaviruses (CoVs) are a group of viruses that are responsible for causing respiratory tract diseases in humans. There are seven distinct members of the CoV family, with HCoV-229E, -NL63, -OC43 and HKU-1 being mildly pathogenic and responsible for the symptoms of the common cold. In contrast, MERS-CoV, SARS-CoV and the newly emerged SARS-CoV-2 are classified as severe respiratory tract infections, with the potential to cause lung failure and death [5].

SARS-CoV-2 has been classified as an enveloped beta-coronavirus, which is a genus within the family *Coronaviridae*. The genome of SARS-CoV-2 consists of a single-stranded positive-sense RNA molecule of 29,903 nucleotides[6]. The first two-thirds of the SARS-CoV-2 genome encodes two large polyproteins, pp1a and pp1ab, which can be cleaved into sixteen non-structural proteins [7, 8](Nsp1-16) (Figure 1). The last one-third of SARS-CoV-2 genome encodes several accessory proteins: orf3, orf6, orf7a, orf7b, orf8, orf9b, orf10, and four structural proteins: spike (S), membrane (M), nucleocapsid (N), envelope (E), which play crucial roles in the entry of viruses into host cells, their packaging, assembly, and release of virus particles [9-12].

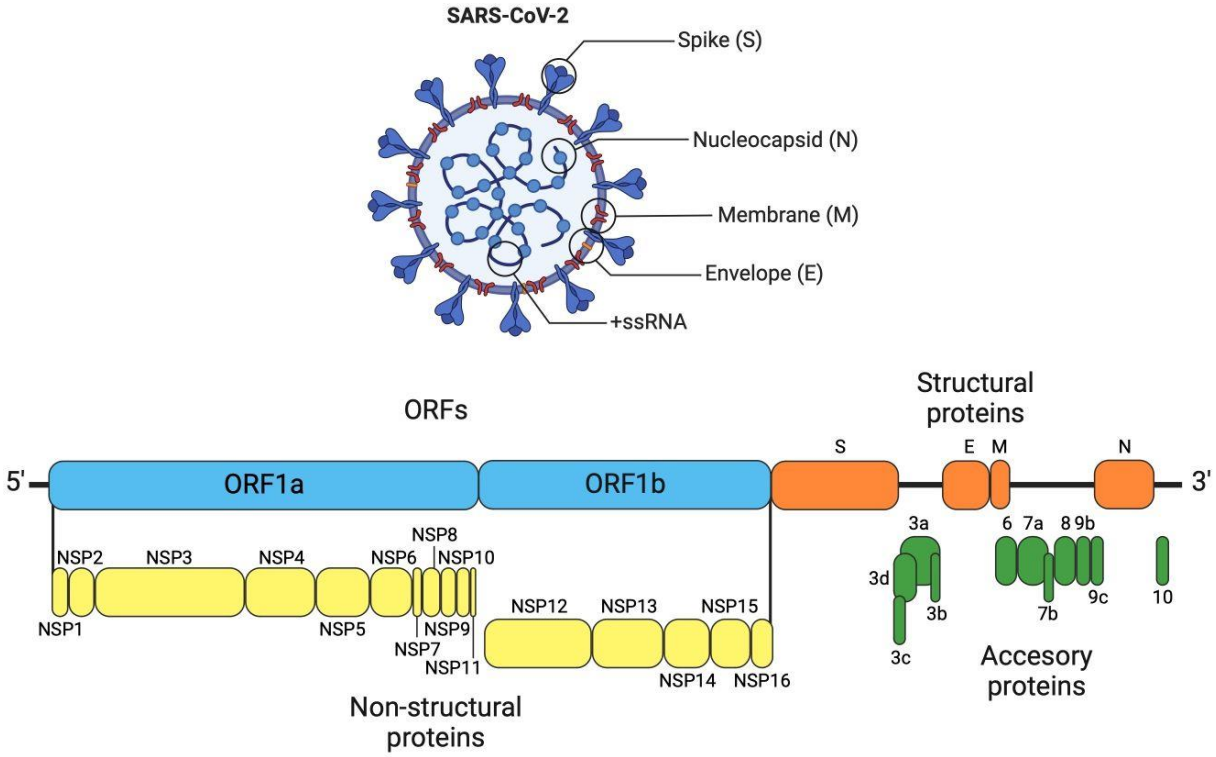

Figure 1. Genome and structure of SARS-CoV-2. Figure from [13].

1.2.1 SARS-CoV-2 non-structural protein Nsp3

Nsp3 is the largest non-structural protein of SARS-CoV-2, which is more than 200 kDa of the molecular mass. It plays a crucial role in several essential steps of the coronavirus life cycle, including the formation of replication/transcription complex and the process of polyprotein [14, 15]. Furthermore, Nsp3 has been demonstrated to play a pivotal role in the process of ER-associated double-membrane vesicle (DMVs) formation [16-18]. These vesicles serve to separate viral replication away from cellular sensors and do not induce early interferon expression by double-stranded RNA [19, 20] and have been observed to impede the host's capacity to recognize viral infection [21].

Nsp3 can be divided into 14 to 16 subdomains (Figure 2). SARS unique domain (SUD) of Nsp3 was first identified in SARS-CoV [22] and absent in coronaviruses which cause only mild symptoms in human hosts. Therefore, it has been hypothesized that SUD may be implicated in the extreme pathogenicity of SARS-CoV. It has been demonstrated that two subdomains of SUD, SUD-N and SUD-M can bind to G-quadruplexes, which are four strands of nucleic acid configurations rich in guanine. The binding capability of SUD potentially has a role in counteracting the immune response of the infected host cell, thereby facilitating viral replication [23]. SUD can also induce the degradation of NF-κB modulator NEMO. Such a process modulates the host's inflammatory responses and aids in its evasion of the immune system [24].

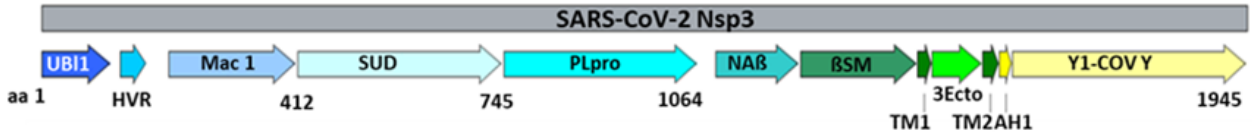

Figure 2. Schematic diagram of SARS-CoV-2 Nsp3 subdomains. UBl1: ubiquitin-like domains. HVR: hypervariable region. SUD: SARS unique domain. PLpro: Papain-like protease domain. NAB: nucleic-acid binding domain, βSM: beta-coronavirus-specific marker. TMs: transmembrane regions.

PLpro is another domain of Nsp3 with multiple functions. It is responsible for the cleavage of Nsp1, Nsp2, and Nsp3, releasing them from polyproteins. Furthermore, PLpro has been demonstrated to possess deubiquitinating and deISGylating activities (Figure 3), which remove the ubiquitin or IFN-stimulated gene 15 (ISG15) molecules from the host protein, thereby interfering with host immune responses [25, 26].

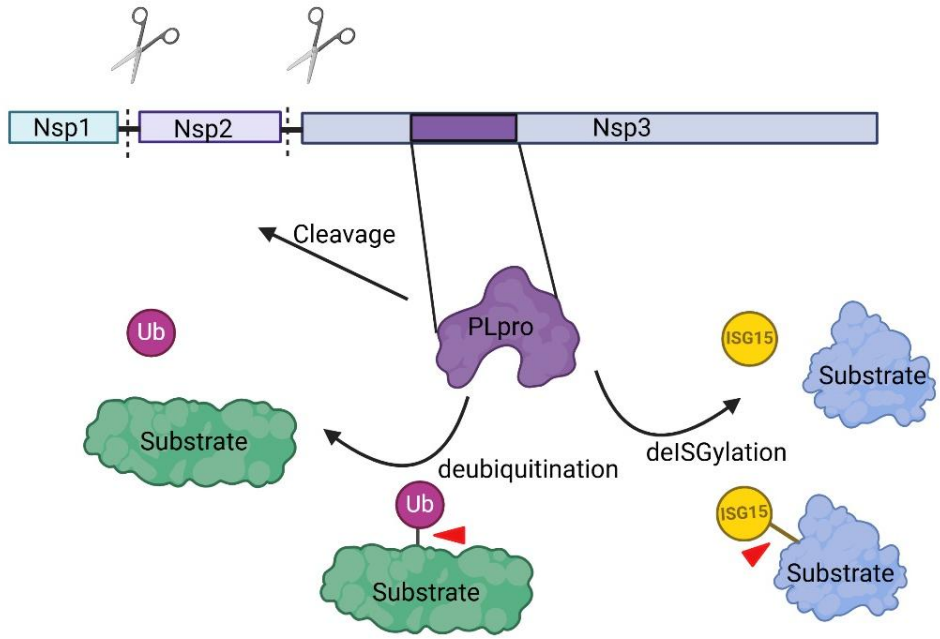

Figure 3. PLpro functions. (Created by BioRender).

For instance, SARS-CoV-2 PLpro has been demonstrated to remove ISG15 from Interferon regulatory factor 3 (IRF3) and to inhibit type I interferon responses. Remarkably, the SCoV-PLpro inhibitor GRL-0617 has been shown to maintain the antiviral interferon pathway, and to reduce viral replication in infected cells [25]. Moreover, PLpro has been observed to interact with the host cytoplasmic viral nucleic acid sensor MDA5, thereby inducing a counteraction of ISG15-mediated activation of MDA5 through the process of active deISGylation. This provides a strategy by which SARS-CoV-2 is able to evade MDA5-mediated immune surveillance [27].

1.2.2 SARS-CoV-2 non-structural protein Nsp13

Nsp13, another SARS-CoV-2 non-structural protein focused on in this study, belongs to the helicase superfamily 1B, which has the ability to catalyze the unwinding of double-strand DNA or RNA in a 5′ to 3′ direction by using the energy of nucleotide triphosphate hydrolysis [28]. In addition to its helicase activity, Nsp13 can function as an RNA 5′ triphosphatase and participate in the viral capping process together with Nsp10, Nsp12, Nsp14, Nsp16 to mimic host mRNA to avoid host detection [28].

Nsp13 also plays a role in the disruption of host's immune response such as the IFN signaling. In a study by Xia et. al, it was found that Nsp13 can suppress IFN-I signaling by binding to TBK1 and blocking its phosphorylation [29]. Besides, Nsp13 has been shown to inhibit IFN signaling through its ability to target JAK1-mediated phosphorylation of STAT1, which is dependent on Nsp13 helicase activity [30].

Given the evidence of the important functions of SARS-CoV-2 proteins in virus replication and counteracting host immune responses, it is essential to deepen our understanding of the molecular mechanisms underlying the interactions between SARS-CoV-2 proteins and host proteins to develop more effective therapies against coronaviruses.

1.3 Post-translational regulation in host defense against virus infection

Post-translational modifications (PTMs) are defined as covalent modifications of proteins following ribosomal translation. Coronavirus proteins have been found to be subject to a variety of PTMs that are catalyzed by host enzymes. These PTMs such as ubiquitination, ISGylation, and phosphorylation have been shown to have a significant impact on the viral pathogenesis process [31].

1.3.1 Ubiquitination

Ubiquitination is a post-translational modification process in which the ubiquitin molecule is covalently attached to a target protein in the cell for various purposes including protein degradation and immune signaling. This process is typically catalyzed by three distinct types of enzymes: ubiquitin-activating enzymes (E1), ubiquitin-conjugating enzymes (E2), and ubiquitin ligases (E3). These enzymes function in a sequential manner, characterized by a series of regulatory steps, which ensure the precise control of the ubiquitination process. During this procedure, E1 catalyzes the ATP-dependent activation of ubiquitin and transfers it to E2. This is followed by the E3 ligase, which functions as the scaffold to facilitate the ubiquitin transfer from E2 to substrate. This

reaction is repeated, resulting in additional ubiquitin molecules being sequentially attached to one another, thereby generating a polyubiquitin chain. Subsequently, the substrates linked with Lys-48 based ubiquitin chains are identified and degraded into short peptides by proteasomes with the release of free ubiquitin (Figure 4) [32, 33].

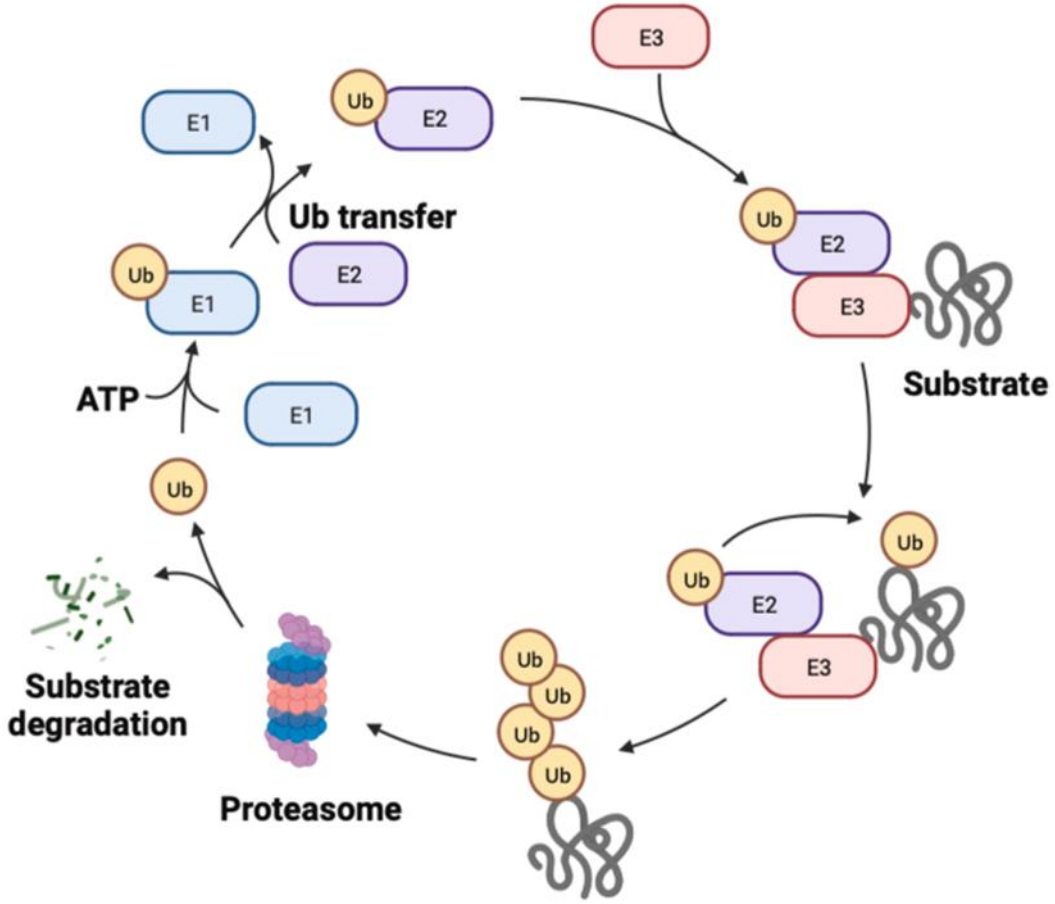

Figure 4. The ubiquitin-proteasome system. Figure modified from [33].

Coronaviruses have been observed to exploit the host linear ubiquitin chain assembly complex (LUBAC) to facilitate the attachment of linear polyubiquitin chains to the SARS-CoV-2 Nsp14. This linear ubiquitinated Nsp14 has been shown to recruit and activate the IKK complex, thereby initiating NF-κB activation and subsequent expression of proinflammatory factors [34]. In certain instances, some E3 ligases have been observed to exert antiviral properties against SARS-CoV-2. Yu et. al found that multiple E3 ligases, including HECT, UBA, ubiquitin protein ligase E3 component n-recognin 4 (UBR4), and UBR5, could ubiquitinate and induce the degradation SARS-CoV-2 ORF9b, a protein that functions as an interferon (IFN) antagonist. This process has been demonstrated to enhance IFN production and diminish SARS-CoV-2 replication [35].

1.3.2 Human E3 ligase RCHY1

The E3 ligases of the ubiquitination process can be divided into three families: the RING (really interesting new gene) domain family, homologous to E6-associated protein at the carboxy-terminus (HECT) domain family, and U-box family. The RING domain was initially hypothesized to function in DNA binding and recognition [36]. Bailly et al. demonstrated that the yeast DNA-damage repair protein Rad18 mediates histone ubiquitination via its RING domain [37]. Since then, many studies have extensively investigated the link between the RING domain and ubiquitination modification.

RCHY1 is a type of E3 ligase that modifies its substrates, including p53 [38], p63 [39] and HDAC1[40], through the addition of ubiquitin residues, thereby inducing their degradation within proteasomes. It has been reported that some viruses can utilize RCHY1 to counteract host defense, which is beneficial for virus replication. Mukerjee et al. demonstrated that p53 prevented the phosphorylation of RNA polymerase II, leading to the inhibition of viral transcriptional elongation in HIV-infected cells. The hypothesis of RCHY1 involvement in p53 downregulation during HIV-1 infection, was later confirmed by increased RCHY1 levels in HIV-1 infected human monocyte cell line U-937 [41]. For SARS-CoV, our research group was the first to identify an interaction between RCHY1 and SUD, PLpro of Nsp3, leading to an increase in RCHY1 protein levels. This, consequently, results in the degradation of the RCHY substrate antiviral protein p53. This interaction may represent a strategy employed by the coronavirus to evade the host's antiviral defenses [42].

1.3.3 ISGylation

ISGylation plays a key role in the innate immune response especially during viral infections. It is a process in which ubiquitin-like interferon-stimulated gene 15 protein (ISG15) is covalently conjugated to lysine residues of target proteins [43]. Similar to ubiquitination, ISG15 is covalently conjugated to target proteins through a sequential enzymatic cascade involving three key enzymes: ubiquitin-activating enzyme E1 (UBE1L), ubiquitin-binding enzyme E2 (UBCH8), and ubiquitin ligase E3 (HERC5/TRIM25/ARIH1) [44]. The removal of ISG15 from the substrate is catalyzed by the ubiquitin-specific peptidase 18 (USP18) [45, 46] (Figure 5).

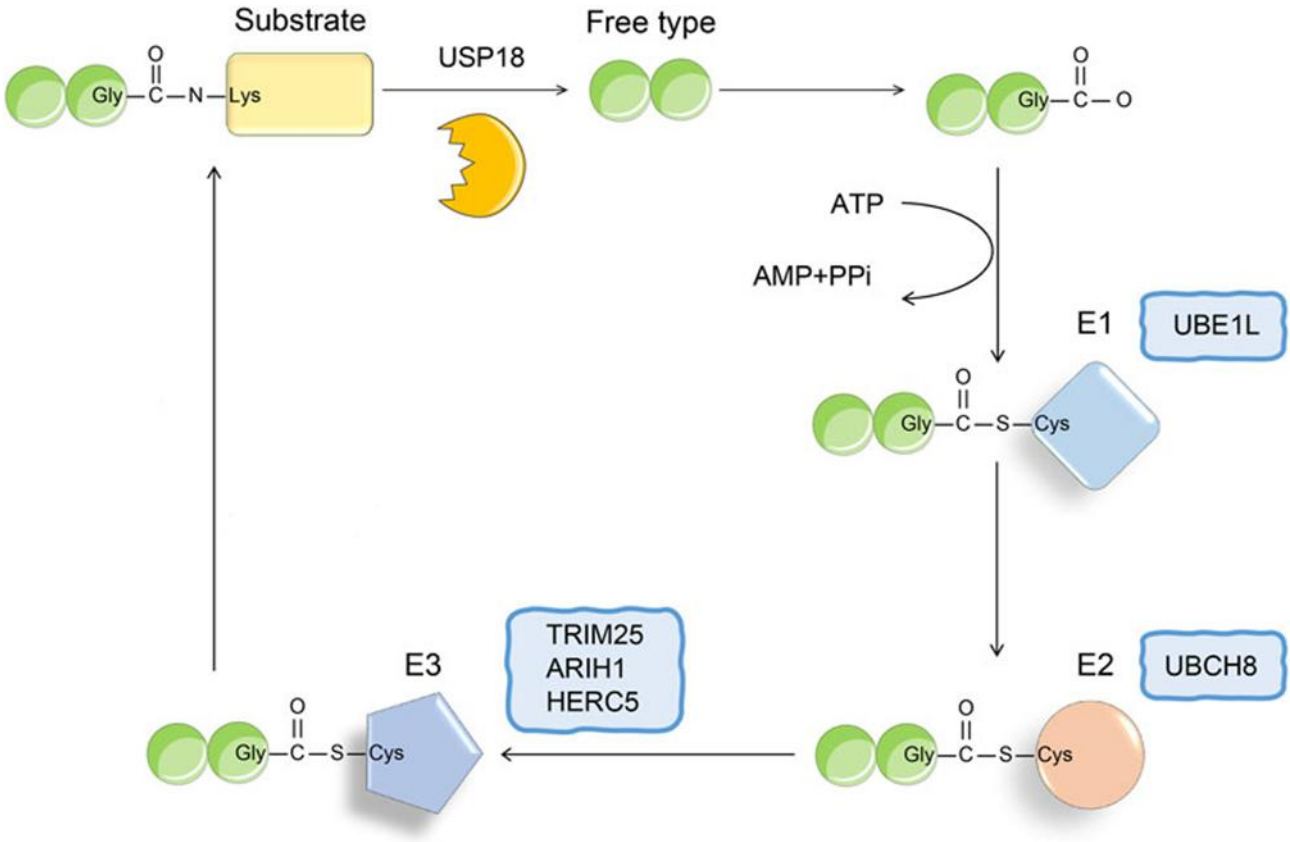

Figure 5. The conjugation of ISG15. Figure modified from [47].

It has been demonstrated that this modification is associated with a number of antiviral effects, including the inhibition of the entry, replication or release of a variety of intracellular pathogens [48]. The knockout of ISG15 gene in mice has been demonstrated to lead to an increased susceptibility to various pathogens such as norovirus [49] and Chikunguya virus [50]. It is notable that only a limited number of cellular enzymes have the capacity to remove ISG15, thereby enabling this modification to function as a virus-induced danger signal. Some viruses have evolved mechanisms to counteract ISG15 activity. For instance, the protein IE1 of human cytomegalovirus (HCMV) has been shown to interfere with ISG15 expression through a STAT1-dependent mechanism. In addition, its viral protein UL26 has been observed to impede ISG15 conjugation [51].

In the context of SARS-CoV-2, the PLpro domain of Nsp3 has been shown to decrease IFN-β and NF-kB-p65 to attenuate host antiviral immunity [25]. ISGylation of the N protein by the host HERC5 ISGylation machinery can disrupt N oligomerization and inhibit viral RNA synthesis. This antiviral restriction mechanism is hindered by the PLpro deISGylation activity of SARS-CoV-2 Nsp3 [52].

1.4 P53 and p53 family proteins

p53, a well-characterized RCHY1 substrate, functions as a transcription factor regulating cell cycle arrest, DNA repair, apoptosis, and autophagy. This makes it a critical tumor suppressor [53]. The regulation of p53 protein levels is a complex process that involves several E3 ubiquitin protein ligases, including RCHY1 [38] and MDM2[54]. These ligases facilitate the proteasomal degradation of p53, a process that is crucial for maintaining cellular homeostasis. RCHY1 contributes to the downregulation of p53 activity through direct physical interaction and ubiquitin-dependent degradation [38]. This process is independent of MDM2 and plays a pivotal role in regulating p53 activity.

In addition to its role as a tumor suppressor, p53 serves as a central antiviral factor in host cells. For instance, it has been observed that p53 increased the clearance of influenza A virus (IAV) and alleviated IAV-induced disease in mice. The absence of p53 was found to induce a delayed response in the expression of cytokines and antiviral genes in both the lung and the bone marrow in mouse models [55]. Ma-Lauer and her colleagues observed that Nsp3 SUD and PLpro domain of SARS-CoV interacted with and stabilized RCHY1, thereby promoting the degradation of the antiviral protein p53. This interaction may represent a strategy employed by the coronavirus to evade the host's antiviral defenses [42].

The p53 family of transcription factors consists of three proteins: p53, p63, and p73. They have similar structures in transactivation domain (TA), DNA binding domain (DBD), and oligomerization domain (OD) [56]. As illustrated in Figure 6, two additional alternative domains are present at the C-terminus of p63 and p73. The first of these is the sterile alpha motif (SAM), which is involved in protein-protein interaction, and the second is the transcription inhibition domain (TID) [57]. TAp63α or TAp73α are also known as full-length p63 or p73. The process of alternative splicing of C-terminal exons results in the p63 and p73 γ variants. The generation of the ΔNp63 isoforms is initiated by an alternative promoter located within intron three [58]. A comparable isoform, termed ΔNp73, has been observed in p73 [59].

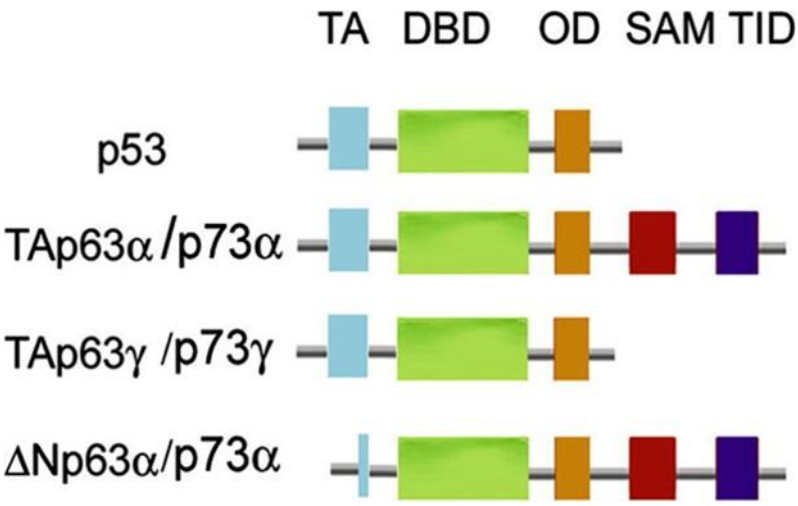

Figure 6. Structural organization of p53 family proteins and their isoforms. transactivation domain (TA), DNA binding domain (DBD), oligomerization domain (OD). Sterile alpha motif (SAM) is involved in protein-protein interaction. Transcription inhibition domain (TID). Figure modified from [57].

In a manner similar to that of p53, p63 can be polyubiquitinated by RCHY1 and subsequently degraded by the proteasome [39]. P63 is a pivotal factor in the developmental process of the epidermis during the embryonic stage. It plays a crucial role in the process of epidermal keratinocyte morphogenesis, proliferation and differentiation. In this process, p63 directly activates a variety of target genes, which are involved in various processes including cellular proliferation, differentiation and adhesion [60]. Furthermore, p63 is widely recognized for its role in carcinogenesis. For instance, a higher percentage of squamous cell carcinomas was observed in $p63^{+/-}$ mice compared with wild-type mice. This finding suggests the tumour-suppressing role of p63 [61]. Guo et al found that TAp63 isoforms functioned as tumour suppressors by regulating senescence via p53-independent pathways [62]. Another isoform of p63, ΔNp63α mainly plays an oncogenic role in cancer such as skin cutaneous melanoma [63] and breast cancer [64].

In DNA viruses such as Herpes simplex virus 1 (HSV-1), the infection was observed to disturb the balance between pro-survival ΔNp63α and the pro-apoptotic TAp63γ. This disturbance could potentially be a consequence of the activation of the DNA damage response, which is triggered as a consequence of viral replication [65]. In another DNA virus human papillomavirus (HPV), the viral protein E6/E7 expression can regulate ΔNp63α transcriptionally, increasing both its mRNA and protein levels. Additionally, ΔNp63α mRNA level was higher in HPV-positive Head and Neck Cancer cell lines [66]. However, the role of p63 in RNA virus replication such as coronavirus remains elusive.

1.5 Potential therapeutic targets for coronavirus

The current strategies for treating the infection caused by coronavirus can be categorized as follows: the identification of potential therapeutic targets that are virus-based or host-based [67].

Researchers have identified some potential therapeutic agents that target the viral proteins. For example, the inhibitors of SARS-CoV-2 protease Mpro, Lycorine HCl and MG-101, and inhibitors of PLpro, Sitagliptin and Daclatasvir HCl, reduced viral titers and exhibited low cytotoxicity in Huh7.5 cells [68]. Nsp13 of SARS-CoV-2 displays a high degree of conservation relative to that of SARS-CoV, exhibiting 99.8% protein sequence identity [69]. Therefore, Nsp13 is an ideal target for developing broad-spectrum antiviral therapeutics, with potential efficacy against SARS-CoV and future emerging coronaviruses [28]. Nsp13 inhibitors which target the helicase active center show effective suppression on human coronavirus 229E and SARS-CoV-2 [70].

A further strategy for treating a coronavirus infection involves the targeting of host proteins to increase the expression of certain antiviral proteins or interfere with the process of virus replication. For example, the ubiquitin-proteasome system plays a pivotal role in the infection cycles of some viruses such as mouse hepatitis virus. As revealed by Raaben et al, proteasome inhibitors MG132, epoxomicin and Velcade (Bortezomib) have demonstrated clear coronaviral inhibition activity in cell culture, mainly by affecting the early steps of coronaviral infection, such as virus entry and RNA synthesis [71]. It has been observed that two known MDM2 inhibitors, Nutlin-3 or RG-7112, activate the p53 pathway and decrease the release of SARS-CoV-2, thereby down-regulating the pro-inflammatory status induced by viral infection in A549-hACE2 cells [72].

1.6 Aims of this study

The outbreak of COVID-19 continues to pose a significant threat to global public health. Potential approaches or therapies against COVID-19 are still under consideration. It is therefore imperative to gain insights into the host interaction partners of the SARS-CoV-2 virus proteins, and their influence on virus effective replication. In a previous study, our laboratory has found that SARS-CoV SUD and PLpro interact with and stabilize RCHY1. The RCHY1-dependent mechanism by which SARS-CoV neutralizes the antiviral activity of p53 was identified [42]. However, how SARS-CoV-2 proteins regulate RCHY1 and its substrates remains unknown.

Both SUD and PLpro domains of Nsp3 share high amino acid sequence identity in SARS-CoV and SARS-CoV-2 [25, 73], therefore, it has been hypothesized that SARS-CoV-2 SUD and PLpro interact with and stimulate RCHY1 expression to reduce endogenous p53 via RCHY1. To test this hypothesis, the interaction between RCHY1

and SARS-CoV-2 SUD and PLpro was investigated by co-immunoprecipitation (co-IP). The expression level of RCHY1 and endogenous levels were evaluated in the presence or absence of Nsp3 by Western blot. Furthermore, the investigation of additional RCHY1 substrates affected by SARS-CoV-2 protein was also one of the aims of this study. Therefore, the RCHY1 substrates were selected from a human cDNA library [74] and cloned into pDEST vectors fused to GFP or HA tags by gateway cloning. The influence of Nsp3 on RCHY1 and RCHY1's substrates has been determined by Western blot.

How SARS-CoV-2 benefits from the reduction of RCHY1 substrates induced by Nsp3 was investigated subsequently. Human coronaviruses infection assays were performed in cells overexpressing these RCHY1 substrates. Virus replications was assessed by Western blot (nucleocapsid protein expression) and quantitative real-time polymerase chain reaction (qPCR) using virus-specific probes.

In addition to SARS-CoV-2 Nsp3, other SARS-CoV-2 proteins that interact with RCHY1 are of great interest. To identify such interactions yeast two-hybrid screening was performed and the results were confirmed by co-IP. Finally, the influence of this SARS-CoV-2 protein on host antiviral responses or related signaling pathways was studied in the presence or absence of RCHY1.

2. Material and Methods

2.1 Material

2.1.1 Chemicals

25 KD polyethylenimine (PEI) (Polysciences)

Lipofectamine 3000 (Thermo Fisher Scientific)

MG132 (Sigma Aldrich)

Puromycin (Gibco, Thermo Fisher Scientific)

Paraformaldehyde (PFA) (Carl Roth GmbH)

4′,6-diamidino-2-phenylindole (DAPI) (Sigma Aldrich)

Triton X-100 (Carl Roth GmbH)

Phosphate-buffered saline (PBS) (Gibco)

2.1.2 Buffers and solutions

Nonidet™ P40 (NP-40) lysis buffer: 150 mM NaCl, 50 mM Tris/Cl (pH 8.0), 1% NP-40 in double-distilled water (ddH_2O).

Co-IP lysis buffer: 10 mM Tris/Cl (pH 7.5), 150 mM NaCl, 0.5 mM EDTA, 0.5% NP-40 Substitute in ddH_2O.

Co-IP dilution buffer: 10 mM Tris/Cl (pH 7.5), 150 mM NaCl, 0.5 mM EDTA in ddH_2O.

10XTBS: 176 g NaCl and 48 g Tris were dissolved into 2 L ddH_2O, and adjusted pH to 7.6.

TBS: 100 mL 10XTBS was diluted into 900 mL ddH_2O.

TBST: 500 µL of Tween 20 to 1 L TBS solution

5x sodium dodecyl sulfate (SDS) sample buffer: 1.82 g Tris, 1.5 g SDS, 9 mg BP blue, 1.16 mg DTT were mixed with 4.5 mL glycerol, add ddH_2O to 15 mL.

25xTris-Glycine transfer buffer: 36.4 g Tris and 180 g Glycine were dissolved into 1 L ddH2O

Towbin buffer: 80 mL 25xTris-Glycine transfer buffer, 720 mL ddH2O and 200 mL methanol

LB medium: 10 g NaCl, 5 g yeast extract powder, 10 g Trypton, added ddH_2O to 1L and autoclaved to sterilize.

10% Glycerol stock (for preparation of competent *E. coli* bacteria): 2 mL glycerol, 18 mL 100 mM $CaCl_2$, sterilized with a 0.22 μm filter.

YPD medium: Yeast extract 5 g, Bacto peptone 10 g, add ddH_2O to 450 mL. The mixture was then autoclaved to sterilize it. Subsequently, 50 mL of 20% sterile glucose medium was added.

SORB medium: 100 mM Lithiumacetate, 10 mM Tris/Cl (pH 8.0), EDTA-NaOH 1mM, Sorbitol 1M in ddH_2O to 250 mL and adjusted pH to 8.0. Then the medium was filtered to sterilize.

2.1.3 Plasmids

Table 1. Information of the plasmids

Plasmid	Reference
pLenti CMV/TO Puro DEST (670-1)	Addgene # 17293
pGL3-ELAM-Luc	Addgene plasmid #13029
pGL3-p125-Luc	As described [75]
pCG1-SARS-CoV-2 Nsp3 a.a.1-1363	As described [76]
pDONR223-SARS-CoV-Nsp3 and pDONR223-SARS-CoV-2-Nsp3 full length	As described [77]
Plasimids for ISGylation assay (ISG15-myc, Ube1L, UbcH8, and Herc5)	As described [75]
RCHY1 fused to GFP/RFP/HA/myc tag	As described [42]
pDONR223-p53 and pDONR223-p63	From a human cDNA library of genes cloned into pDONR223 vectors as described [74].
pDEST-GFP-ct- p63(p63-GFP)	This study
pDONR207-RCHY1-RING-deletion	This study
pDEST-HA-nt-RCHY1-RING-deletion (HA-RCHY1-RING-del)	This study
pDONR207-ubiquitin-K48R	This study
pDONR207-ubiquitin-K63R	This study
pDEST-myc-nt-ubiquitin-K48R(myc-ubi-K48R)	This study
pDEST-myc-nt-ubiquitin-K63R(myc-ubi-K63R)	This study
pDONR207-SARS-CoV-2-Nsp13	This study
pDEST-RFP-nt-SARS-CoV-2-Nsp13	This study
pDEST-HA-YFP^c–SARS-CoV-2 Nsp13	This study
pGBKT7g-SARS-CoV-2 Nsp13	This study
pGBKCg-RCHY1	This study
pGADT7g-RCHY1	This study
pDEST-N2H-N2-RCHY1(N2-RCHY1)	This study
pLenti-cmvTO-puro-dest-p53(pLenti-p53 OV)	This study
pLenti-cmvTO-puro-dest-p63(pLenti-p53 OV)	This study

2.1.4 Primers

Table 2. Information of the primers

Primer name	Sequence (5′–3′)
β-actin qPCR F	TCC TGA GCG CAA GTA CTC CG
β-actin qPCR R	CTG ATC CAC ATC TGC TGG AAG G
β-actin qPCR probe	6-FAM-ATC GGC GGC TCC ATC CTG-BHQ1
RCHY1 qPCR F	CCG CTT GTG TCA TGA TAA CAA TG
RCHY1 qPCR R	CAT TCT TCA CAA GTC TGT TGG
RCHY1 qPCR probe	6-FAM-CTA GAT CGC TTT AAA GTG AAG G-BHQ1
TNFα qPCR F	CTC TTC TGC CTG CTG CAC TTT G
TNFα qPCR R	ATG GGC TAC AGG CTT GTC ACT C
TNFα qPCR probe	6-FAM-CAG AGG GAA GAG TTC CCC AG-BHQ1
OC43 qPCR F	AGC GAT GAG GCT ATT CCG AC
OC43 qPCR R	AGA TCT GGA ATT AGG AGC AGA C
OC43 qPCR probe	FAM-TCC GCC TGG CAC GGT ACT CCC T-BHQ1
NL63 qPCR F	CTT CTG GTG ACG CTA GTA CAG CTT AT
NL63 qPCR R	AGA CGT CGT TGT AGA TCC CTA ACA T
NL63 qPCR probe	FAM-CAG GTT GCT TAG TGT CCC ATC AGA TTC AT-TAMRA
SARS-CoV-2 qPCR F	GAC CCC AAA ATC AGC GAA AT
SARS-CoV-2 qPCR R	TCT GGT TAC TGC CAG TTG AAT CTG
SARS-CoV-2 qPCR probe	ACC CCG CAT TAC GTT TGG TGG ACC
RCHY1RINGdel F	ATG CAC TCT GCT TTA GAT ATG ACC
RCHY1RINGdel R	ATT CTG TCG GGA CAC ATT TTC
ubiK48R-F	CTG GGA GAC AGC TGG AAG ATG
ubiK48R-R	CAA AGA TCA ACC TCT GCT GGT C
ubiK63R-F	TCC AGA GAG AGT CCA CCC TG
ubiK63R-R	TGT TGT AGT CAG ACA GGG TGC
SARS-CoV-2 Nsp3-PLpro att F	GGG GAC AAG TTT GTA CAA AAA AGC AGG CTC CGC CAT GGA AGT GAG GAC TAT TAA GGT GTT TAC AAC
SARS-CoV-2 Nsp3-PLpro att R	GGG GAC CAC TTT GTA CAA GAA AGC TGG GTC TCM ATA AGT AAC TGG TTT TAT GGT TGT TGT GTA ACT G
SARS-CoV-2 Nsp3-SUD att F	GGG GAC AAG TTT GTA CAA AAA AGC AGG CTC CGC CAT GAA AAT CAA AGC TTG TGT TGA AGA AGT TAC
SARS-CoV-2 Nsp3-SUD att R	GGG GAC CAC TTT GTA CAA GAA AGC TGG GTC TCM AGA AAG AAG TGT CTT AAG ATT GTC AAA GG
SARS-CoV-2 Nsp13 att F	GGG GAC AAG TTT GTA CAA AAA AGC AGG CTC CGC CAT GGC TGT GGG GCT TGT GTT CTT TG
SARS-CoV-2 Nsp13 att R	GGG GAC CAC TTT GTA CAA GAA AGC TGG GTC TCM TTG TAA AGT TGC CAC ATT CCT ACG TG

2.1.5 Antibodies

Table 3. Information of the antibodies

target	Cat. number, company	dilution	source
anti-p53	sc-125, Santa Cruz	1:700	mouse
anti-p63	sc-25268, Santa Cruz	1:500	mouse
anti-SUD (Nsp3)	7g 9-1-1, mouse serum (lab-made) [78, 79]	1:5	mouse
anti-vincullin	V9264, Sigma	1:1000	mouse
anti-beta-actin	A3854, Sigma	1:100 000	mouse
anti-RFP	MA5-15257, Invitrogen	1:1000	mouse
anti-GFP	A6455, Invitrogen	1:1000-1500	rabbit
anti-HA	Clone 3F10, Roche	1:1000	rat
anti-rabbit	P0217, DAKO	1:1000	pig
anti-mouse	A9917, sigma	1:10 000	goat
anti-rat	A9037, sigma	1:5000	goat
anti-myc	ProteinTech, 16286-1-AP	1:1500	rabbit
anti-puromy-cin	MABE341, Millipore	1:10000	rat
anti-SARS2 N(condensed)	21H2-1-1, (labmade, produced by Larissa Hansbauer, Elisabeth Kremmer, and Dr. Luca Zinzula)	1:500	rat
Anti-OC43 N	MAB9012, Merckmillipore	1:1000	mouse

2.2 Methods

2.2.1 Cell culture

The maintenance of HEK 293, HEK 293T and Huh7 cells was conducted in Dulbecco's modified Eagle medium (DMEM, Gibco), with the addition of 10% (v/v) fetal bovine serum (FBS) and 1% (v/v) penicillin/streptomycin. BEAS-2B-ACE2 cells [80] were cultured in DMEM/F-12 (Gibco) containing 10% FBS, 1% penicillin/streptomycin (P/S) and 1% N-2-Hydroxyethylpiperazine-N-2-Ethane Sulfonic Acid (HEPES). All cells were cultured in a 5% carbon dioxide atmosphere at 37 degrees, and were routinely examined for the presence of mycoplasma.

Cells were passaged by Trypsin-EDTA (Thermo Fisher Scientific) when they reached the confluency of 80%-95%.

2.2.2 Cell transfection

Transient DNA transfections were performed using Lipofectamine 3000 (Thermo Fisher Scientific) (Table 4) when the cell confluency was 60%-80%.

Table 4. Reagents for DNA transfection by Lipofectamine 3000 (for 6-well plate as an example)

Reagent A	**Volume**
Opti-MEM	125 µL
Plasmid DNA	2.5 µg (The volume is calculated according to plasmid concentration)
P3000 reagent	5 µL
Reagent B	**Volume**
Opti-MEM	125 µL
Lipofectamine 3000	5 µL

In order to prepare Reagent A, the plasmid DNA was added to Opti-MEM initially. Subsequently, the P3000 reagent was added to the previously prepared reagent A, with the purpose of enhancing transfection efficiency. The two reagents, A and B, were combined and subsequently incubated for 20 minutes at room temperature and added into the cells and mixed by shaking the plate gently.

Large amount of transient DNA transfections were performed by 25 KD polyethylenimine (PEI) when the cell confluency was 80%-90%. Before the transfection, the cell

growth medium was replaced from 10% FBS+1%P/S to 5%FBS without P/S to increase the transfection efficiency.

Table 5. Reagents for DNA transfection by PEI (for 10 cm petri-dish as an example)

Reagent	Volume
Opti-MEM	3 mL
Plasmid DNA	24 µg
PEI	24 µL

For the preparation with the reagent, the Opti-MEM was mixed with plasmid DNA and incubated at room temperature for 5 minutes. Following this, the PEI was added to the reagent and this mixture was incubated for a further 15 minutes. Finally, the reagent mixture was added to the cells and mixed by shaking the dish gently.

2.2.3 Plasmid construction

For the cloning SARS-CoV-2-Nsp13/SUD/PLpro related constructs, first the SARS-CoV-2 gene was amplified by PCR using related gateway primers (Table 2) and SARS-CoV-2 genome DNA as a template. Then the PCR product was cloned into pDONR207 vector to generate pDONR207-Nsp13/SUD/PLpro by BP reaction: PCR product (150 ng) 2 µL, pDONR207 vector (150 ng) 2 µL, BP clonase enzyme 1 µL, 25 °C overnight. 0.5 µL proteinase K was added to enhance the transformation efficiency.

pDONR207-Nsp13/SUD/PLpro was further cloned into pGBKT7g, pDEST-RFP or pDEST-HA-YFP^{c} destination vectors via LR reaction: pDONR207-Nsp13/SUD/PLpro (150 ng) 1 µL, pDEST plasmid (150 ng) 1 µL, LR clonase enzyme 0.5 µL, 25 °C overnight.

For the cloning of pLenti CMV/TO Puro DEST-p53 and pLenti CMV/TO Puro DEST-p63. The pDONR223-p53 and pDONR223-p63 were cloned into the destination vector pLenti CMV/TO Puro DEST (gateway compatible) by LR reaction.

2.2.4 Transformation

50 µL of competent *E. coli* was thawed on ice for 30 minutes. Then 5 µL of the BP or LR reaction was added into competent *E. coli* and incubated on ice for another 30 minutes. Thereafter, 5 µL of the BP or LR reaction was added to the competent *E. coli* and the mixture was incubated on ice for a further 30 minutes. The mixture was then subjected to heat shock at 42°C for 15 seconds, after which it was returned to ice for

2 minutes. 500 µL of LB medium was added to the mixture. This mixture was then subjected to incubation on a shaker at 37°C for a period of one hour. Following this, the mixture was streaked onto an LB agar plate with antibiotics, in order to select colonies that had been successfully transformed.

2.2.5 Isolation of plasmid DNA

The colonies were picked up from LB agar plates and then incubated with 4 mL LB medium containing the respective selection antibiotic at 37 °C for a duration of 16-20 hours in a shaking incubator at 200 rpm. After the incubation, the *E. coli* bacteria pellets were precipitated by centrifuging at 10,000xg for 3 minutes. The plasmids were isolated by Metabion mi-Plasmid Miniprep Kit according to the standard protocol from the manufacturer. The plasmid DNA was eluted in 100 µL autoclaved Ampuwa water. For the plasmids cloned by gateway cloning, they were digested by BsrGI at 37 °C for one hour. For the plasmids cloned by other methods, the selection of specific digestion enzymes was determined by the multiple cloning sites on the plasmids. Subsequently, the DNA fragments were subjected to agarose gel electrophoresis to separate DNA fragments based on their size. This analysis was then used to determine the size of the fragments in relation to their respective gene sizes, as referenced in the National Center for Biotechnology Information (NCBI) database. The correct plasmids were preserved for future experiments.

2.2.6 Yeast-two-hybrid

The genes of the virus SARS-CoV-2, or RCHY1, were cloned into the yeast two-hybrid bait vector pGBKT7g, which expresses leucine (Leu), or into the prey vector pGADT7g, which expresses tryptophan (Trp) by gateway cloning. The expression of the reporter protein histidine (His) is observed in cases of interaction between RCHY1 and SARS-CoV-2 candidate proteins. (Figure 7).

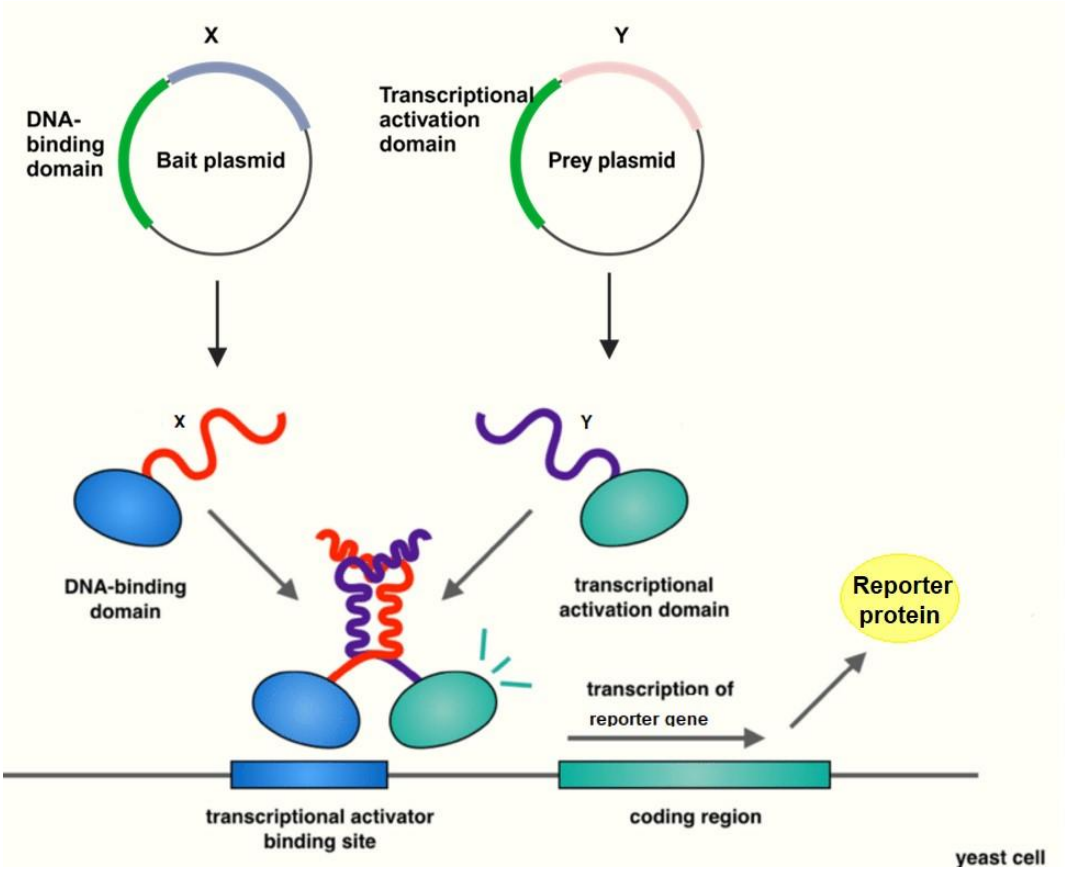

Figure 7. Schematic diagram of yeast-two-hybrid system. Gene X and gene Y are cloned in bait plasmid (includes DNA-binding domain) and prey plasmid (prey plasmid), respectively. The interaction of the protein X and Y mediates the transcription of the reporter gene to express the reporter protein. Figure modified from [81].

Different SARS-CoV-2 OFRs and domains that had been previously cloned into pGBKT7g were subjected to individual mixing with Polyethylene glycol (PEG), with the volume ratio set at 1:100, in a 96-well plate. This mixture was then named "SARS-CoV-2 gene format".
RCHY1 cloned into pGADT7g, or an empty vector was then mixed with different pGBKT7g-SARS-CoV-2 OFRs and domains. This was subsequently transformed into competent yeast cells, PJ69–7A strain (Table 6), which carries the reporter gene HIS3 (express His) under the control of GAL4 upstream activating sequences and is optimized for strong, specific detection of protein–protein interactions [82].

Table 6. Procedure of yeast transformation

Reagent and step	Temperature
1. Mix pGADT7g-RCHY1 with competent yeast cells (volume ratio, plasmid: competent yeast=1:20). This mixture should then be added to a clean 96-well plate, with 5 µL being added to each well.	RT
2. Take 25 µL "SARS-CoV-2 gene format" and mix with the mixture from step 1 using a multi-channel	RT

pipette. The mixture should then be left to incubate for 30 minutes.	
3. Heat shock for 10 minutes	42 °C
4. Add double dropout medium (without Leu and Trp) in another clean deep 96-well plate (1.3 ml per well). Then transfer the mixture from step 3 to this plate.	RT
5. The plate should then be covered with aluminum foil and the mixture should be left to incubate in the shaker at 200 rpm for four days. The orange pellets will be observed if the transformation is successful.	30°C

Subsequently, the mixture was transferred on one double dropout plate (without Leu and Trp) and two triple dropout plates (without Leu, Trp, and His) by a specially made "stamp" (Figure 8) and incubated at 30°C for 3-4 days. The success of the transformation process was determined by the yeast growth on the double dropout plate. The interactions between RCHY1 and SARS-CoV-2 proteins were determined by yeast growth on the triple dropout plates.

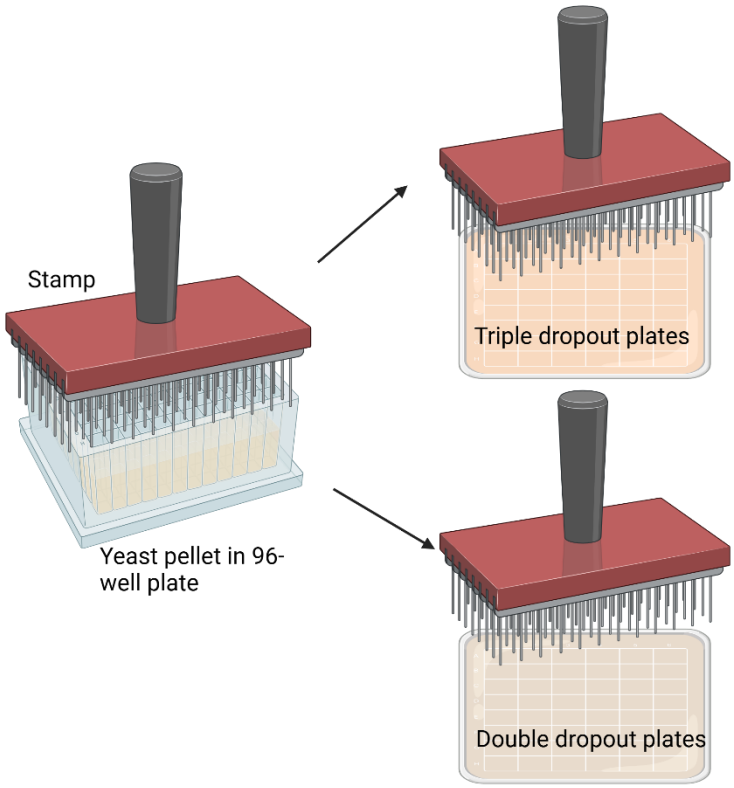

Figure 8. Stamp of yeast-two-hybrid assay. The stamping process was performed in quadruplicate. The stamp was immersed in a 96-well plate containing a yeast culture and then transferred to double or triple dropout plates for a few seconds to transfer the mixture (Created by BioRender).

2.2.7 Co-immunoprecipitation (co-IP)

Twenty-four to forty-eight hours after the transfection, the cells were washed by cold PBS twice and lysed by 200 µL co-IP lysis buffer for 30 minutes on ice. Subsequently,

the lysates were centrifuged at 20,000xg for 10 minutes at 4°C. The supernatant was transferred to a pre-cooled tube and 300 µL co-IP dilution buffer was added.

This mixture was incubated with 25 µL GFP/RFP/myc-trap agarose beads (Proteintech) or HA-trap agarose beads (ThermoFisher Scientific) by way of repeated rotation at 4°C for one hour. Then the beads underwent a centrifugation process at 2,500 xg at 4**°**C for two minutes and were washed by 500 µL Co-IP dilution buffer twice. Last, the remaining supernatant was removed and 35 µL 5xSDS sample buffer was added. The samples were subjected to heating at 95°C for 10 minutes, followed by centrifugation at 2,500 xg at 4°C for two minutes. The protein interaction will be analyzed by Western blot (Figure 9).

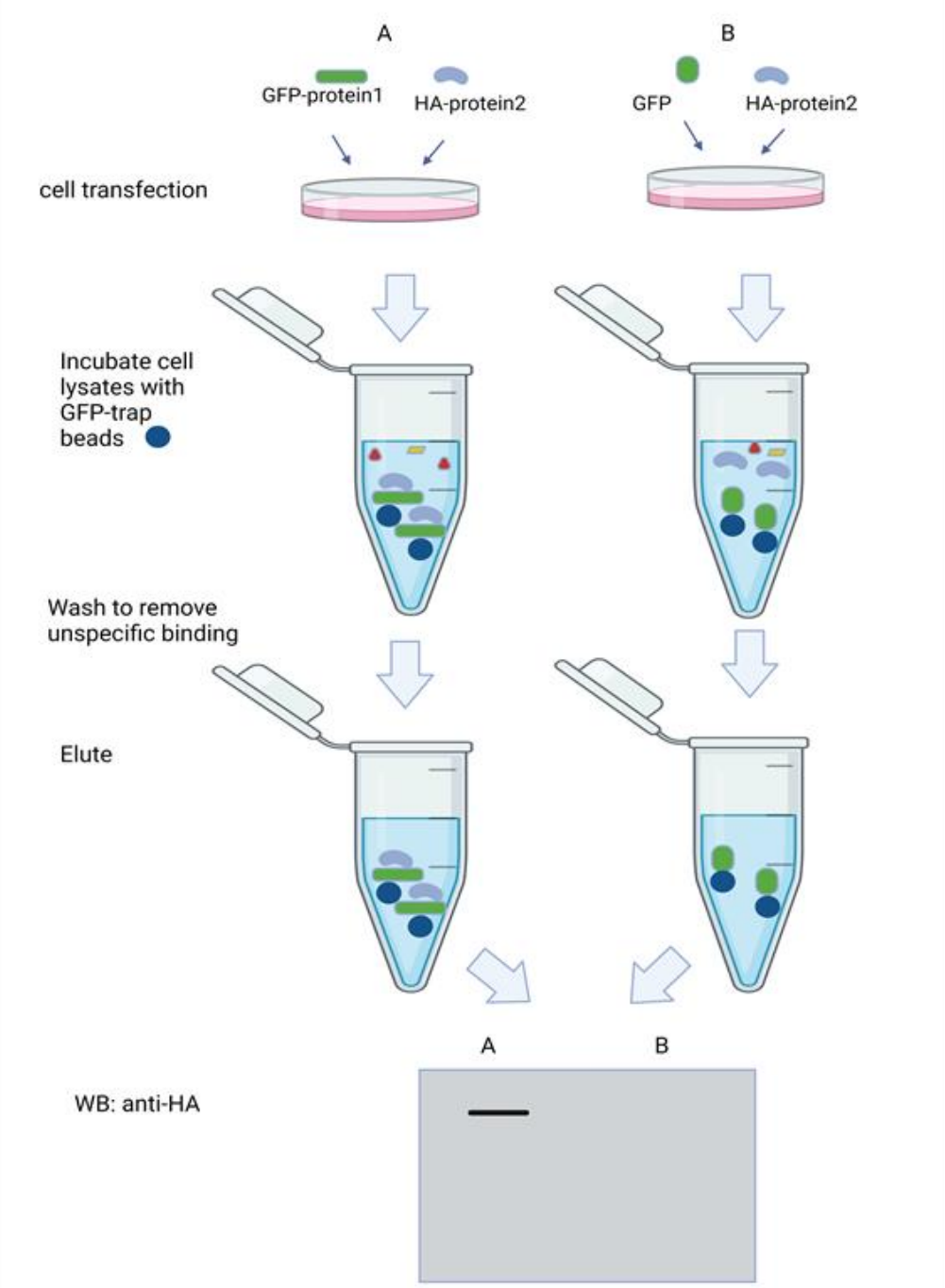

Figure 9. Flow chart of co-IP. (GFP trap as an example). Cells are transfected with plasmid 1 encoding protein 1 fused to GFP tag, and plasmid 2 encoding protein 2 fused to HA tag. If protein 1 and 2 interact with each other, HA-protein 2 can bind to GFP-trap indirectly. As a result, the band for HA-protein 2 is visible by Western Blot using anti-HA antibody (Created by BioRender).

2.2.8 Western blot

The cells were washed with cold PBS and lysed by NP-40 lysis buffer (50 µl for one well of a 12-well plate) for 15 minutes. Then the lysates were centrifuged at 20,000xg for 10 minutes at 4°C. The supernatant was transferred into another tube including

5xSDS buffer and boiled at 95°C for 5 minutes.15-20 µL protein samples were loaded into 12% or 14% sodium dodecyl sulfate polyacrylamide (SDS-PAGE) gel (Thermo Fisher Scientific) and were subjected to separation at 125 V for a duration of 60-80 minutes. Subsequently, the protein was transferred onto nitrocellulose membranes using a wet transfer system with Towbin buffer. After one hour, the membrane was blocked by 5% milk in TBS at room temperature for another one hour. Then the membranes were incubated with the primary antibodies at 4°C overnight. Following this, the membranes were washed with TBST three times and incubated with the secondary antibodies at room temperature for one hour. The membranes were finally subjected to three further washes with TBST, after which they were covered by SuperSignal™ West Pico PLUS Chemiluminescence Substrate (ThermoFisher Scientific) and imaged using the Gel Doc system (Bio-Rad).

The images of Western blot were analyzed by Image Lab and the band intensities were quantified by ImageJ.

2.2.9 *In vivo* ubiquitination assay

The *in vivo* ubiquitination assay was performed as described [42]. In summary, plasmids encoding ubiquitin fused to HA or myc tags were transfected into HEK293 cells together with plasmids that expressed target proteins. The cells were treated with 10 µM MG132 at 37°C for 4 hours before being harvested. At 48 hours post-transfection, the cells were lysed using co-IP lysis buffer and then followed by protein purification using GFP or RFP Trap beads. The ubiquitination levels of the target proteins were then assessed by Western blot using anti-HA or anti-myc antibodies.

2.2.10 Ribopuromycylation assay

The ribopuromycylation assay was a method to monitor total protein synthesis [83].

In summary, HEK293 cells were co-transfected with the GFP-fused RCHY1, along with pCG1-SARS-CoV-2 Nsp3 a.a.1-1363 or a control vector. Twenty-four hours after transfection, the cells were treated with 3 µM puromycin for 2 h at 37°C to label all newly produced proteins with puromycin (Figure 10). Thereafter, the cells were harvested and the GFP-RCHY1 was purified by GFP-trap. The newly generated RCHY1 was analyzed by Western blot via anti-puromycin antibody.

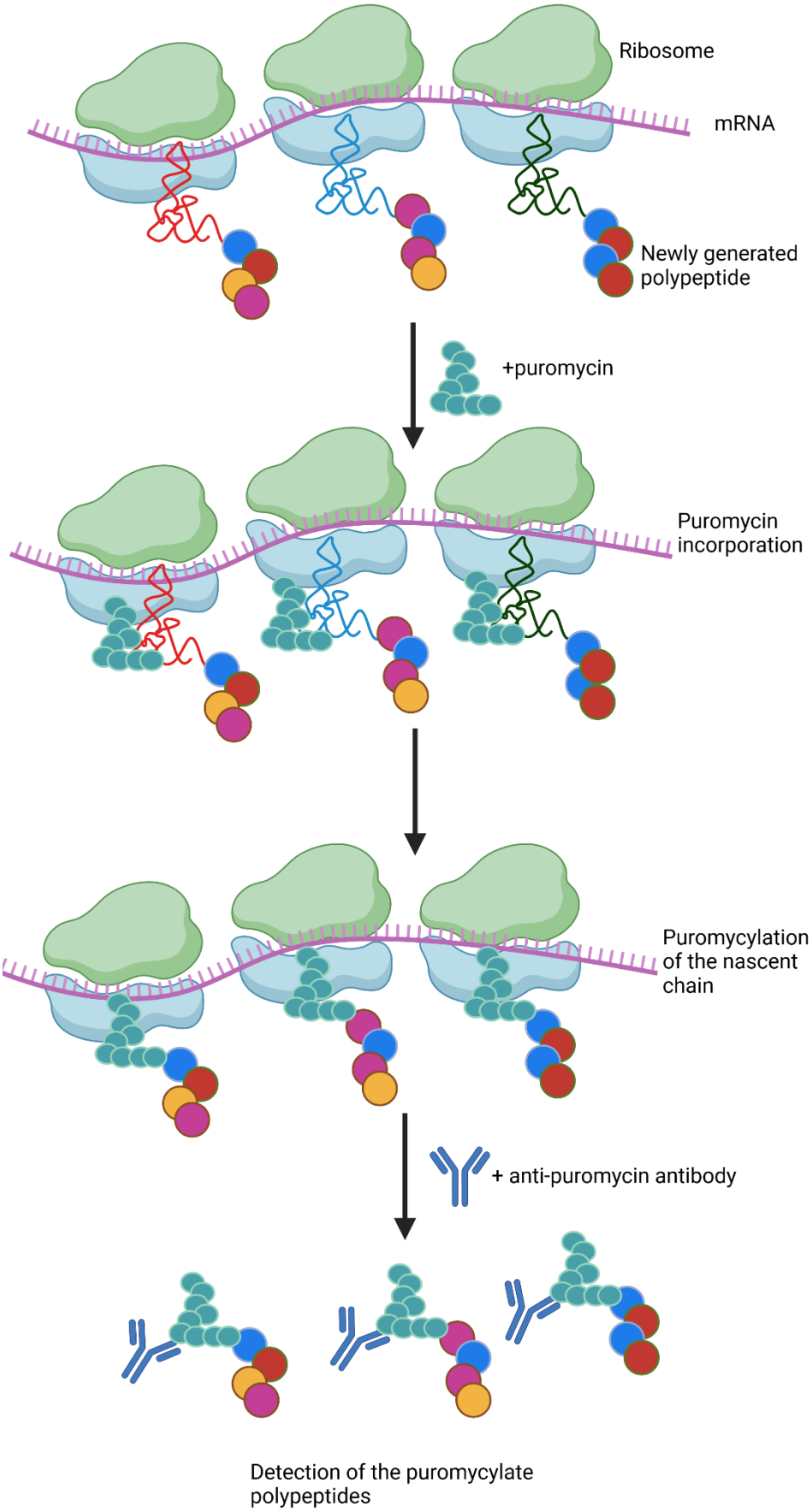

Figure 10. Schematic diagram of RiboPuromycylation assay. Created by BioRender.

2.2.11 Cycloheximide (CHX) chase assay

The CHX chase assay is a method of observing intracellular protein degradation and determining the half-life of a given protein. Following the inhibition of protein synthesis by CHX, a decrease in the level of intracellular proteins is observed, resulting from degradation through the proteasome or lysosome system [84]. The total protein is harvested at different time points, thus enabling the measurement of the rate of protein degradation (Figure 11).

The HEK293 cells were co-transfected with the GFP-fused RCHY1 together with pCG1-SARS-CoV-2 Nsp3 a.a.1-1363 or a control vector. Twenty-four hours after transfection, cells were treated with CHX (100 µg/mL) and the protein was harvested at 2 hours, 4 hours, or 6 hours after the treatment. The expression levels of GFP-RCHY1 were analyzed by Western blot.

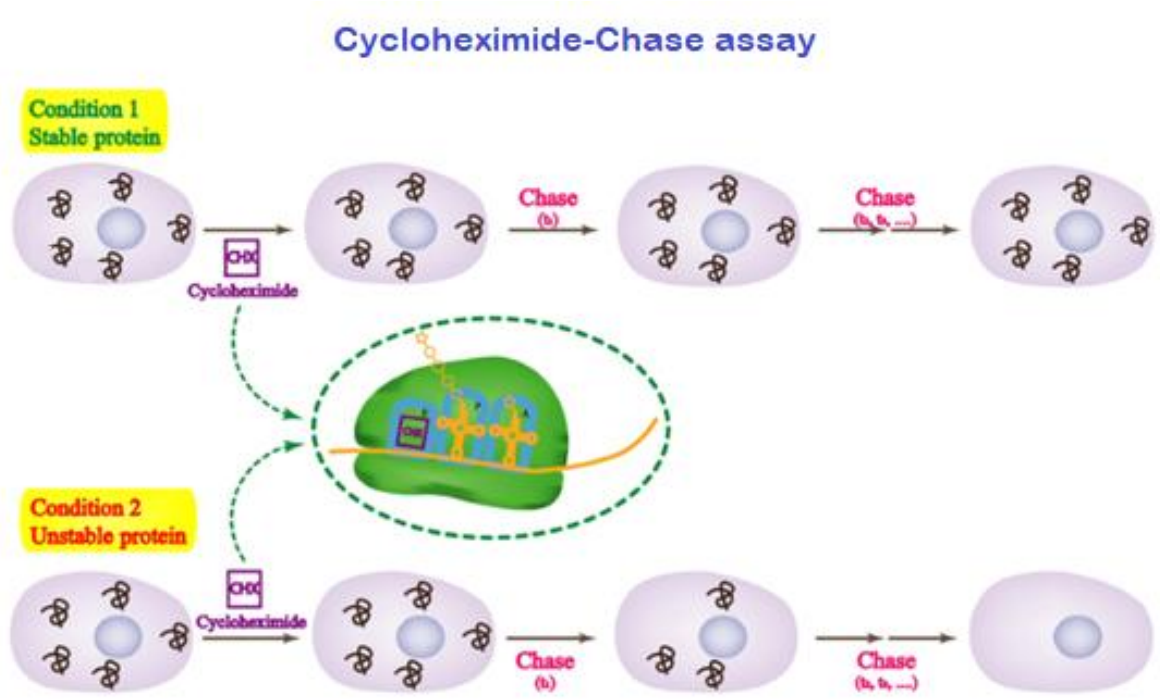

Figure 11. Schematic diagram of CHX chase assay. The cells are treated with the global protein translation inhibitor CHX to terminate protein translation and the protein samples are harvested at different time points after the treatment. The subsequent procedure involves the examination of the reduction in the levels of a target protein 'chase' via Western blot. Figure modified from [85].

2.2.12 RNA isolation and quantitative polymerase chain reaction (qPCR)

Total RNA was isolated from cells seeded in a 24-well plate using the Bioline ISOLATE II RNA Mini Kit. For probe-based qPCR, the mRNA levels of the target genes were quantified using Luna Probe One-Step RT-qPCR 4x Mix with UDG (New England Biolabs). All the qPCRs were run by the Lightcycler System (Roche) according to the

program in Table 7. The relative mRNA levels of the target genes were then normalized to those of β-actin.

Table 7. qPCR program for One step RT-qPCR

Temperature	Time	Cycles
30 °C	5 min	1
55 °C	10 min	1
95 °C	1 min	1
95 °C	10 s	45
60 °C	1 min	

2.2.13 Site-directed mutagenesis

pDONR207-ubiquitin-K48R, pDONR207-ubiquitin-K63R, pDONR207-RCHY1-without RING domain (pDONR207-RCHY1-RING-del) were generated by Q5® Site-Directed Mutagenesis Kit (New England Biolabs). Specific primers (Table 2) were designed to substitute one nucleotide or delete a region of the plasmid DNA. 12.5 µL Q5 Hot Start High-Fidelity 2X Master Mix, 1.25 µL 10 µM Forward Primer, 1.25 µL 10 µM Reverse Primer, 1 µL Template DNA (1–25 ng/µl) and 9 µL Nuclease-free water were added into the reaction. The program of the PCR cycler was set as indicated in Table 8.

Table 8. PCR cycling conditions for site-directed mutagenesis reaction

Temperature	Time	Cycles
98 °C	30 s	1
98 °C	10 s	25
50-72 °C (according to the annealing temperature of the primers)	30 s	
72 °C	30 s/kb	
72 °C	2 min	1
4 °C	∞	

Subsequently, the PCR product was subjected to a Kinase-Ligase-DpnI (KLD) reaction, which facilitated the circularization of the PCR template and the removal of the template DNA: PCR product 1 µL, 2X KLD Reaction Buffer 5 µL, 10X KLD Enzyme Mix 1

µL, Nuclease-free Water 3 µL, incubated at room temperature for 5 minutes. Then 5 µl of KLD was mixed to competent *E. Coli* for transformation.

2.2.14 Luciferase assay

For the Renilla luciferase assay, HEK293 cells were seeded in 96-well plates or 48-well plates and then subjected to transfection using the plasmids fused to RL reporter [73]. Twenty-four hours after transfection, cells were lysed by the lysis buffer of Renilla luciferase assay system (Promega) and the luciferase activities were measured according to the manufacturer's instructions.

For the Firefly luciferase assay, HEK293 cells seeded in 96-well plates were transfected with pGL3-ELAM-luc [86] which carries Firefly luciferase signals. Twenty-four hours after transfection, cells were lysed by lysis buffer and the luciferase signals were measured by the Firefly luciferase system (Promega).

For the NanoBiT luciferase assay, the N-terminal and C-terminal fragments of Nanoluc are fused to the N-terminus of the target protein in the NanoLuc two-hybrid (N2H) N1 and N2 vectors (pDEST-N2H-N1 and pDEST-N2H-N2) [87]. In situations where two target proteins interact with each other, the Nanoluc luciferase signals are generated and can be measured by the microplate reader (Figure 12).

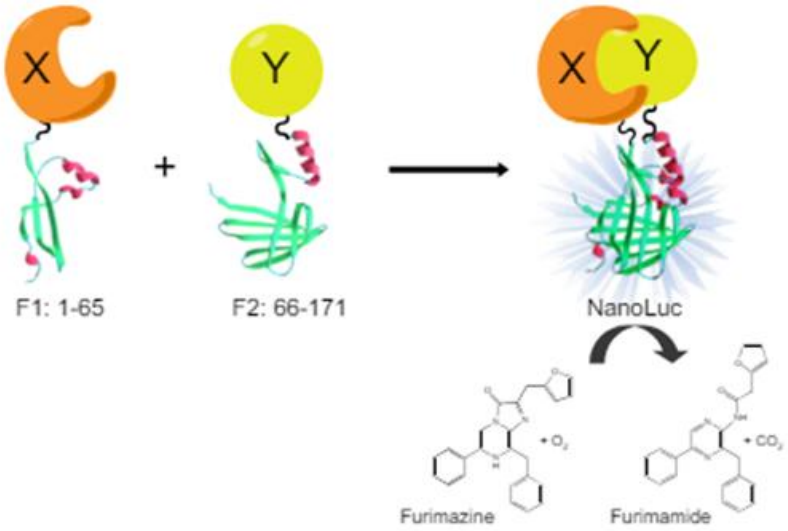

Figure 12. Schematic figure of the mechanism of NanoLuc two-hybrid assay. Figure from [87].

HEK 293 cells were transiently transfected with the respective N2H plasmids in a 96-well plate. Twenty-four hours after transfection, the cells were lysed with 20 µl NP-40 lysis buffer, and then mixed with 20 µl substrate containing 0.5% Nano-Glo® Luciferase Assay Substrate (Promega) in 1x Nano-Glo® Blotting Buffer (Promega) for the measurement.

For the cell viability assay, BEAS-2B-ACE2 cells seeded in 96-well black and clear bottom plates (Corning) were treated with inhibitors or DMSO control. Forty-eight hours after the treatment, cells were equilibrated at room temperature for 30 minutes. Then 50 µl of the supernatant was removed and 50 µl of CellTiter-Glo® 2.0 Reagent (Promega) was added for the measurement. All the luciferase signals were measured using a CLARIOstar microplate reader (BMG LABTECH).

2.2.15 HCoV infection assay

Human coronaviruses (HCoVs) NL63 and OC43 were diluted using serum-free DMEM, after which the cells were infected at a multiplicity of infection (MOI) of 0.05 for HCoV-NL63 or 0.1 for HCoV-OC43. Two hours post-infection, the cells were washed twice with DPBS, after which they were supplied with a growth medium. Forty-eight hours after infection, the cells were harvested for RNA isolation and quantitative PCR (qPCR). The viral RNA was quantified by qPCR using virus-specific primers and probes.

The cells were also infected with attenuated SARS-CoV-2 sCPD9 in this study. sCPD9 was generated through codon pair deoptimization (CPD), a process which has been demonstrated to result in the rapid and highly efficient attenuation of RNA viruses without altering the amino acid sequence of the encoded proteins [88, 89]. The cells were infected with sCPD9 virus at a MOI of 0.0001 (for BEAS-2B-ACE2 cells) or 0.0004 (for Huh7 cells). Two hours post-infection, the cells were washed with DPBS twice, after which a complete growth medium was added. At 72 hours post-infection (h.p.i.), the cells were harvested for RNA isolation and qPCR. The quantification of viral RNA was performed using specific nucleocapsid primers and probes for SARS-CoV-2 (Table 2).

In the case of SARS-CoV-2-GFP infection, the BEAS-2B-ACE2 cells were infected with a MOI of 1 for the integrated SARS-CoV-2-GFP. The GFP signals were measured at 4-hour intervals up to 24 h.p.i. The cell confluency was measured in a manner consistent with the previous description [90].

2.2.16 Preparation of competent yeast cells (*S. cerevisiae* strain PJ69–7A)

Five to six yeast colonies were selected and cultivated in 50 mL YPD medium at 30°C, 200 rpm overnight. Then the overnight culture was replenished with an additional 150 mL of YPD medium and continued to be incubated in the shaker at 30°C. The optical density at 600 nm (OD_{600}) value was measured frequently until it reached 0.5-0.7. The yeast pellet was collected by a centrifugation at 1,000xg for 5 minutes at room temperature. The pellet was then washed by 40 mL sterile water once and 20 mL SORB medium once. Following this, the yeast pellet was centrifuged at 1,000xg for 5 minutes at room temperature and resuspended in 1.44 mL SORB medium. To increase the

transformation efficiency, 160 µL denatured Salmon sperm DNA was added. The competent yeast cells were then aliquoted in 1.5 mL centrifuge tubes and stored in a -80 °C freezer.

2.2.17 Preparation of competent *E. coli* bacteria

The *E. coli* bacteria (DH5α, DB3.1 or Stbl3 strain) single colony was picked up and incubated in 20 mL LB at 37°C, 200 rpm overnight. Following this, the overnight culture was added into 300 mL LB in a larger flask and incubated at 37°C, 220 rpm until the OD_{600} was 0.35. Then the culture was transferred from the flask to a centrifuge bottle and incubated on ice for 10 minutes. Subsequently, the bacteria were precipitated by centrifugation at 6,000x rpm at 4°C for 10 minutes. The supernatant was discarded and the bacterial pellet was washed by 60 mL $CaCl_2$. Then the bacteria were precipitated again by centrifugation at 4,000x rpm, at 4°C for 10 minutes. The supernatant was discarded and the pellet was resuspended in 60 mL $CaCl_2$ and incubated on ice for 1 hour. Finally, the competent bacteria pellet was collected by centrifugation and resuspended in 6 mL 10% glycerol, after which it was aliquoted in 1.5 mL centrifuge tubes. The aliquots were frozen in liquid nitrogen immediately and then stored in a -80 °C freezer.

2.2.18 Establishment of stable cell lines overexpressing p53 or p63

The HEK293T cells were seeded into 6 well plates and co-transfected with 1333 ng pLenti-CMV-p53 or pLenti-cmv-p63, 1333 ng psPAX2, and 1333 ng pCMV-VSV-G through PEI. Three days after transfection, the cell culture medium was harvested and subjected to a centrifugation process at 10,000xg for 10 minutes to remove cell pellets. The resulting lentivirus-containing supernatant was either stored at -80°C freezer or used immediately to infect BEAS-2B-ACE2 or Huh7 cells in a 12-well plate. Following a 3-day infection period, cells were selected using growth medium containing 2 µg/ml puromycin (for BEAS-2B-ACE2 cells) or 4 µg/ml puromycin (for Huh7 cells) for 5 to 7 days. The surviving cells were then harvested for Western blot analysis to assess the expression levels of the target proteins. The cells that overexpressed the target protein successfully were preserved in liquid nitrogen. The details of the cell lines constructed in this study are in Table 9.

Table 9. Stable cell lines constructed in this study.

Name	Target	Cell line
BEAS-2B-ACE2 pLenti-CMV control	None (CMV control)	BEAS-2B-ACE2
BEAS-2B-ACE2 pLenti-p53-OV	p53 (overexpression)	BEAS-2B-ACE2
BEAS-2B-ACE2 pLenti-p63-OV	p63 (overexpression)	BEAS-2B-ACE2

Huh7 pLenti-CMV control	None (CMV control)	Huh7
Huh7 pLenti-p63-OV	p63 (overexpression)	Huh7

2.2.19 Fluorescence microscopy

HEK293 cells were seeded in a 24-well plate and transfected with RFP and GFP-tagged expression plasmids. Cells were fixed with 4% PFA for 15 minutes at room temperature. This was followed by washing with PBS and the permeabilisation in 0.1% Triton X-100 in PBS for a further 15 minutes. The cells were then washed with PBS again and stained with DAPI diluted 1:1000 in PBS for 10 minutes in the dark. Then the cells were washed with PBS and observed using Leica DM4000 B with 10x objective. Three fields were randomly selected and the fluorescence intensity was quantified by Image J.

2.2.20 Molecular docking

The protein structure of SARS-CoV-2-Nsp13 (PDB ID 6ZSL) was obtained from RCSB Protein Data Bank (https://www.rcsb.org/) and the structures of SUD and RCHY1 (AF-Q96PM5-F1) were predicted or obtained from AlphaFold2 (https://alphafold.ebi.ac.uk/). Then the structure of SUD and RCHY1 were uploaded to HDOCK Server [91] to predict the protein-protein interactions. The top 10 binding models predicted by HDOCK Server were downloaded and analyzed. The binding model that was consistent with co-IP results with the highest confidence score was analyzed and labeled by PyMol.

2.2.21 Statistical analysis

Statistical analysis was performed using one- or two-way analysis of variance (ANOVA) for multiple comparisons or Student's t-test for two-group comparisons. All data plots were generated using GraphPad Prism 10. Data are presented as mean ± standard deviation. Statistical significance was defined as $P < 0.05$. The following symbols were used to denote statistical significance: *$P < 0.05$, **$P < 0.01$, ***$P < 0.001$, and NS not significant.

3. Results

3.1 RCHY1 interacts with Nsp3 and Nsp13

3.1.1 RCHY1 interacts with SUD and Nsp13 in yeast

To investigate viral-host interactions, yeast 2-hybrid (Y2H) assays were performed using SARS-CoV-2 viral genes as bait to screen a human cDNA library. As a result, an E3 ubiquitin ligase, RCHY1, was discovered as an interacting partner for the SARS-CoV-2 SUD domain of Nsp3 (Figure 13A) and SARS-CoV-2 Nsp13 (Figure 13B), and there was no unspecific binding between RCHY1 and empty vector (Figure 13C).

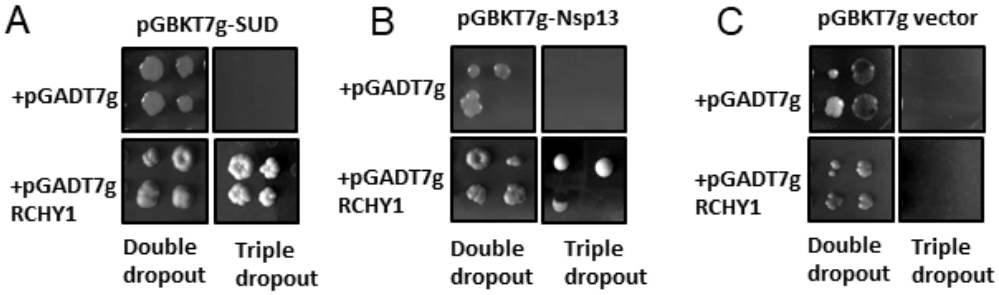

Figure 13. RCHY1 interacts with SARS-CoV-2 SUD and Nsp13 in yeast two-hybrid assay. The pGADT7g vector expressing RCHY1 or the empty control vector was co-transformed into yeast PJ69-7A competent cells together with the pGBKT7g vector encoding SARS-CoV-2 genes. Successful transformation was validated by the proliferation of yeast colonies on double dropout agar plates. The presence of yeast growth on triple dropout agar plates further indicated interactions between SUD and RCHY1 (A), as well as Nsp13 and RCHY1 (B). The presence of unspecific binding was not detected (C).

3.1.2 RCHY1 interacts with SUD and Nsp13 in human cells

To verify these interactions in human cells, GFP trap-based co-IP was performed using Human Embryonic Kidney (HEK) 293 cells transfected with pDEST-GFP control or pDEST-GFP-RCHY1 together with SARS-CoV-2 SUD. As shown in Figure 14, GFP-RCHY1 interacts with SUD, whereas no non-specific binding of SARS-CoV-2 SUD to the empty GFP vector has been observed.

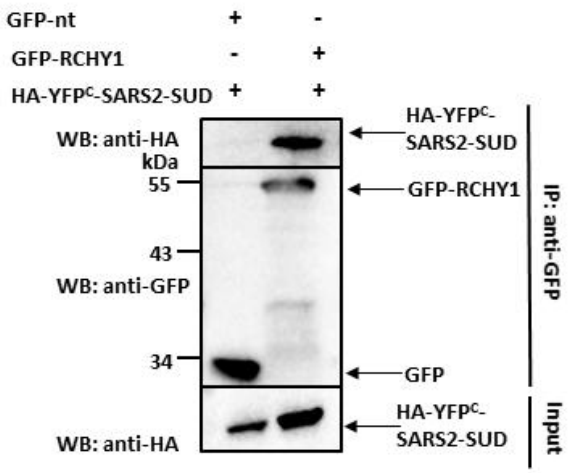

Figure 14. Interaction between RCHY1 and the SUD domain of SARS-CoV-2 Nsp3 in a co-IP assay. As indicated, plasmids expressing HA-YFP^{c}-SARS-CoV-2 SUD and GFP or GFP-RCHY1 were transfected into HEK293 cells using Lipofectamine 3000 in a 6-well plate. Twenty-four hours post-transfection, the cells were harvested for co-IP with GFP-trap (Chromotek) in accordance with its standard protocol. Immunoprecipitation and input samples were analyzed by Western blot using anti-GFP and anti-SARS-CoV-2 SUD antibodies. The cells were harvested 24 h later for a GFP trap-based pulldown assay. SARS2: SARS-CoV-2. HA-YFP^{c}-SARS2-SUD: the HA-YFP^{c} (C-terminus of Yellow fluorescent protein) tag is expressed at the N-terminus of SARS2-SUD. GFP-RCHY1: GFP tag is expressed at N-terminus of RCHY1.

Furthermore, the interaction between RCHY1 and another SARS-CoV-2 non-structural protein, Nsp13, was validated through co-IP in HEK293 cells (Figure 15).

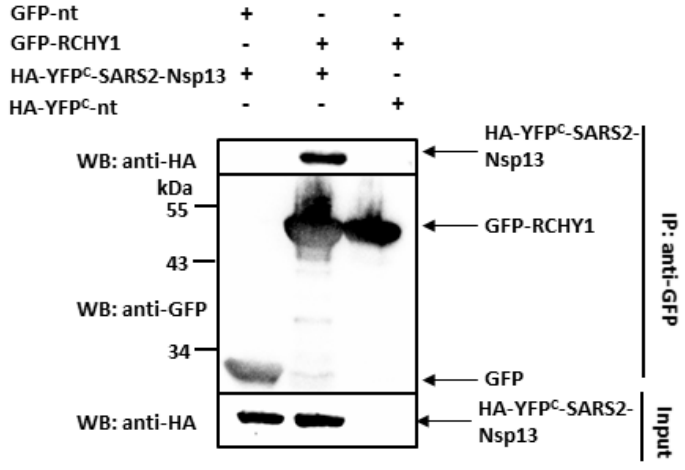

Figure 15. Interaction between RCHY1 and SARS-CoV-2 Nsp13 in a co-IP assay. Plasmids constructed as pDEST-GFP, pDEST-GFP-RCHY1, pDEST-HA-YFP^{c}–nt, and pDEST-HA-YFP^{c}–SARS-CoV-2 Nsp13 were co-transfected into HEK293 cells as indicated using PEI in a 6-well plate. The cells were harvested 48 hours after transfection for a GFP-trap-based co-IP assay.

3.1.3 RCHY1 interacts with the PLpro domain of Nsp3 *in vivo*

The PLpro is another domain adjacent to SUD in Nsp3 (Figure 2). It has been reported that the PLpro domain of SARS-CoV and SARS-CoV-2 share 82.9% amino acid sequence identity [25]. In addition, our previous research has shown that SARS-CoV PLpro interacts with RCHY1 [42]. Therefore, whether SARS-CoV-2 PLpro interacts with RCHY1 has been explored. As demonstrated in Figure 16, the SARS-CoV-2 PLpro is able to bind to RCHY1.

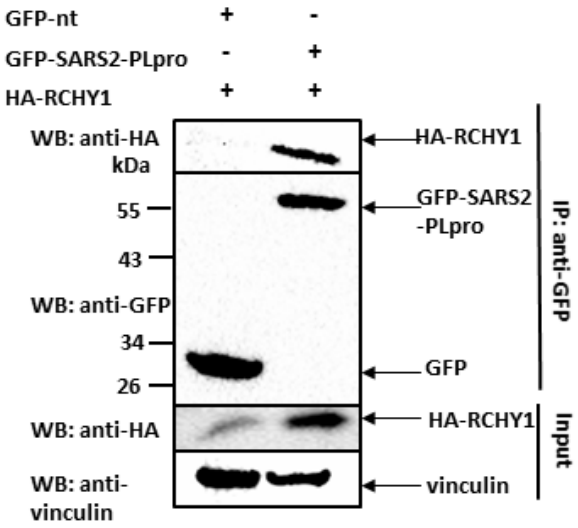

Figure 16. Interaction between RCHY1 and the PLpro domain of SARS-CoV-2 Nsp3. HEK 293 cells were co-transfected with the indicated combinations of expression plasmids. After 24 hours, the cells were harvested and subjected to co-IP.

3.1.4 RCHY1 interacts with Nsp3 full length *in vivo*

As SUD is a domain of Nsp3, whether Nsp3 interacts with RCHY1 has been investigated. The co-IP assay was performed in HEK293 cells transfected with SARS-CoV-2 Nsp3 large fragment amino acid 1-1363 (a.a.1-1363), which contains both SUD and PLpro, together with GFP-RCHY1 or GFP empty vector. There is a clear interaction with Nsp3 a.a.1-1363 and RCHY1 (Figure 17A). Moreover, a Nanoluc Two-Hybrid (N2H) assay [87] detected the interaction between RCHY1 and full-length SARS (SARS-CoV) as well as SARS2 (SARS-CoV-2) Nsp3. Notably, the interaction between RCHY1 and SARS2-Nsp3 appears to be more robust in comparison to that with SARS-CoV Nsp3, as measured by the NanoLuc signals (Figure 17B).

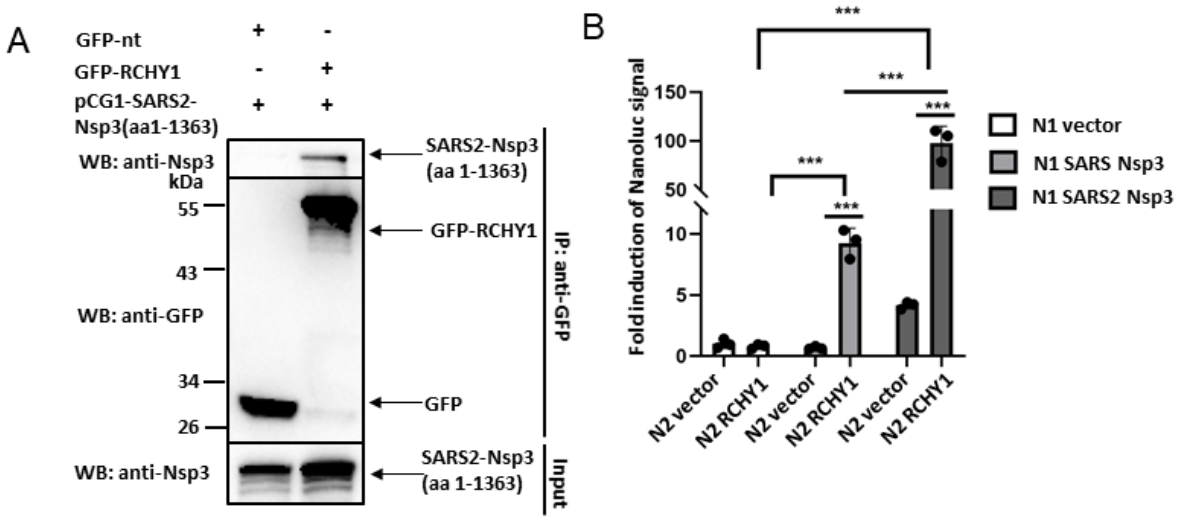

Figure 17. SARS-CoV-2 Nsp3 targets RCHY1. (**A**) Interaction between RCHY1 and SARS-CoV-2 Nsp3 (a.a.1-1363) in co-IP assay. HEK293 cells were co-transfected with plasmids pDEST-GFP-nt or pDEST-GFP-RCHY1 and pCG1-SARS-CoV-2 Nsp3 (a.a.1-1363). The cells were harvested 24 h later for a GFP trap-based pulldown assay. (**B**) Binding of RCHY1 to full-length SARS-CoV Nsp3 and SARS-CoV-2 Nsp3 in an N2H assay. The indicated N2H plasmids were transfected into HEK293 cells split in a 96-well plate. Twenty-four hours post-transfection, the cells were lysed with NP-40 lysis buffer and the Nanoluc signals were measured. Normalization of the signals from each group to the N1+N2 vector group was performed. The mean values and standard deviation presented in the figure were calculated based on three biological repeats (n = 3). The statistical analysis was performed using a two-way analysis of variance (2-way ANOVA). *** P < 0.001. SARS: SARS-CoV. SARS2: SARS-CoV-2.

3.2 RCHY1 residues 95-144 mediate the interaction between Nsp3 and Nsp13

3.2.1 RCHY1 residues 95-144 bind to SUD

Following the confirmation of the domains of Nsp3 responsible for the interaction, the domain of RCHY1 that mediates the interaction has been also identified. RCHY1 belongs to the RING domain-containing family of ubiquitin ligases and contains 261 amino acid residues. The N-terminus of RCHY1, comprising residues 1–94, contains a CHY zinc finger domain. The C-terminus, comprising residues 145-261, contains a RING finger domain that confers ubiquitin ligase activity [92]. The middle region, residues 95-144, has been shown to be responsible for binding to SARS-CoV SUD, and the residues 120-137 have been identified as being required for binding to p53 [38, 42]. In order to examine whether RCHY1 residues 95-144 are also crucial for binding to SARS-CoV-2 SUD, a co-IP assay was performed using RCHY1 full-length and different truncations (Figure 18A). As shown in Figure 18B, the full length of RCHY1 interacts with SUD as a positive control. In addition, all the three truncations bind to SARS-CoV-2-SUD. Therefore, the common region, residues 95–144, is likely to be essential for binding to SARS-CoV-2-SUD.

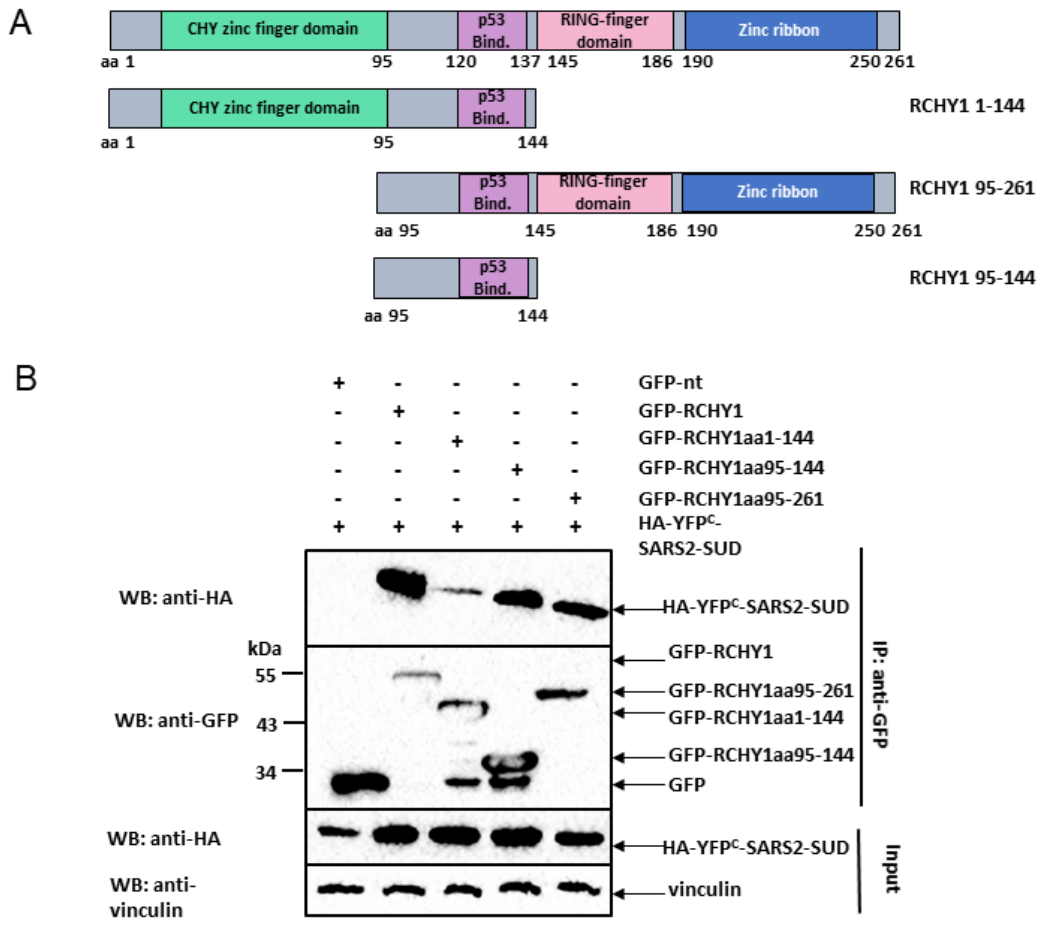

Figure 18. RCHY1 a.a.95-144 interacts with SARS-CoV-2 SUD. (**A**) Schematic representation of RCHY1 full length and different fragments. (**B**) Interaction between SARS-COV-2 SUD and different RCHY1 truncations. HEK293 cells were co-transfected with indicated plasmids by PEI in a 6-well plate. The cells were harvested 48 hours post-transfection followed by GFP-trap based co-IP.

A binding model was predicted based on the co-IP results. In this model, the structures of RCHY1 and SUD are represented as a transparent surface, with the residues mediating the interactions highlighted in the rod representation (Figure 19). The close-up view has shown that RCHY1 Glu114 binds to SUD Gln292. RCHY1 Asn129 interacts with SUD Ser290. At the C-terminal of RCHY1, Arg195 mediates the interaction with SUD Ile71. RCHY1 Arg198 binds to SUD Thr261. RCHY1 Asp201 and Asp202 interact with SUD Ser263 and Lys75 correspondingly.

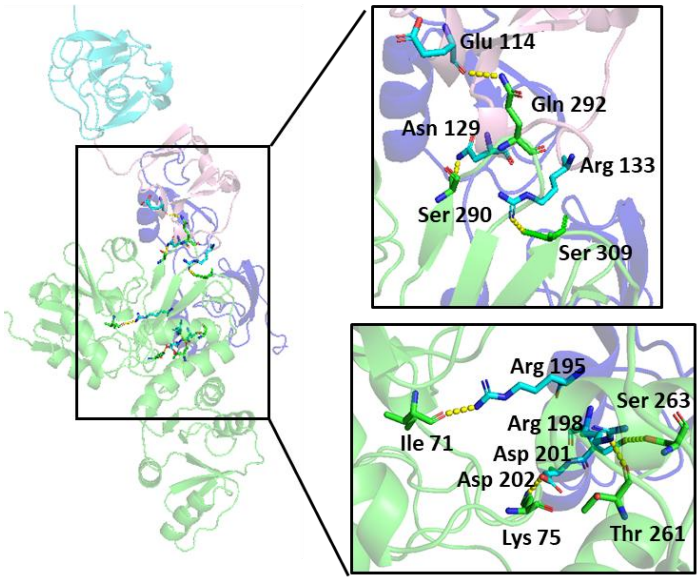

Figure 19. Binding model of RCHY1 and SARS-CoV-2 SUD. Green: SARS2-SUD, cyan: RCHY1 N- terminal, pink: RCHY1 RING domain. Dark blue: RCHY1 C-terminal Right: a close-up view of the interaction complex, the residues responsible for the interaction were labeled as sticks (green sticks: SUD, cyan sticks: RCHY1, yellow dotted line: hydrogen bond). Binding affinity: -208.15 kcal/mol.

3.2.2 RCHY1 residues 95-144 interact with Nsp13 a.a.1-259 and Nsp13 a.a.260-601

SARS-CoV-2 Nsp13 was divided into two distinct fragments. The N-terminal fragment, spanning amino acids 1–259, includes the Zinc Binding Domain (ZBD), which coordinates three structural zinc ions, and the stalk domain, which is essential for helicase activity [93]. The C-terminal fragment, spanning amino acids 260–601, comprises two "RecA-like" helicase subdomains, 1A and 2A, responsible for nucleotide binding and hydrolysis [28] (Figure 20A). It has been observed that RCHY1 is sufficient to pull down both fragments of Nsp13 (Figures 20B and 20C), thus suggesting that Nsp13 has multiple binding sites for RCHY1.

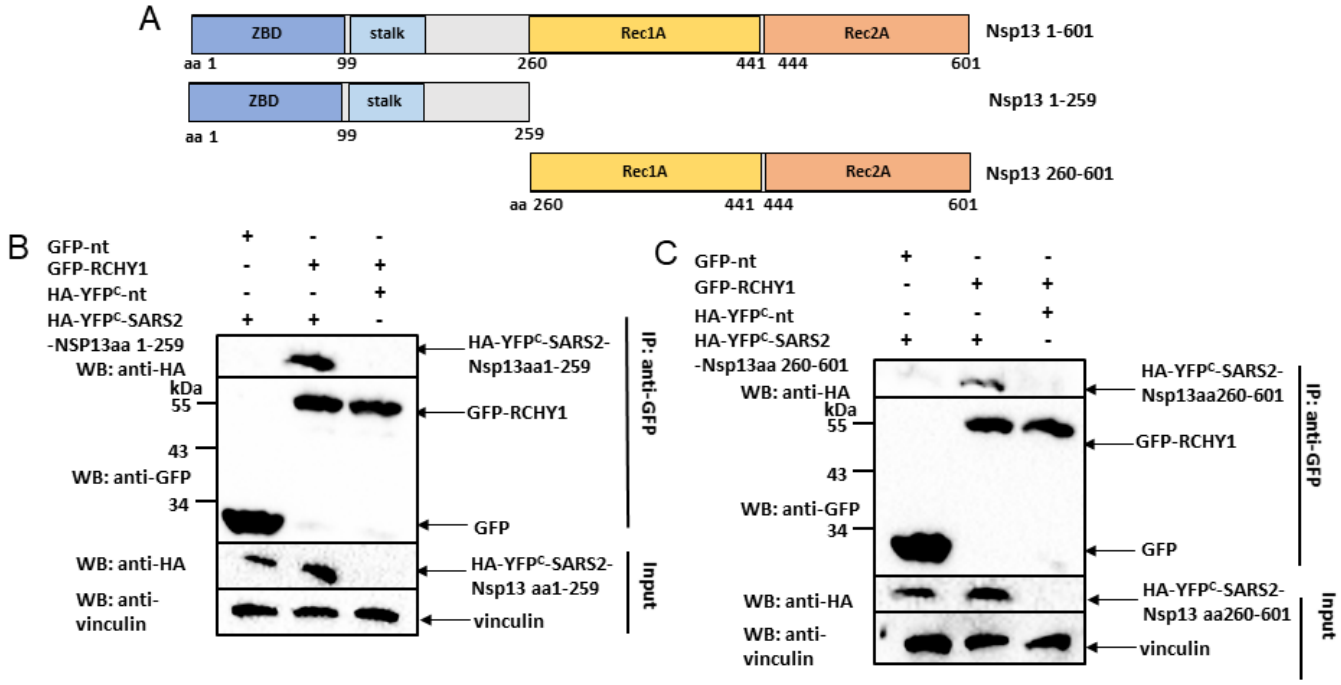

Figure 20. RCHY1 interacts with Nsp13 a.a.1-259 and Nsp13 a.a.260-601. (A) Schematic of Nsp13 full length and truncations. **(B)** Interaction between RCHY1 and SARS-CoV-2 Nsp13 a.a.1-259 in co-IP assay. Plasmids expressing HA-YFP^C tagged SARS-CoV-2 Nsp13 a.a.1-259 or an empty vector, as well as GFP or a GFP-RCHY1 fusion, were transfected into HEK293 cells in 6-well plates. The cells were then harvested 48 hours post-transfection, and a co-IP assay was performed as described previously. (**C**) Interaction between RCHY1 and SARS-CoV-2 Nsp13 a.a.260-601. The indicated plasmids were transfected into HEK293 cells cultured in a 6-well plate. After 48 hours, the cells were lysed for co-IP assay.

Further co-IP assay with truncated RCHY1 has revealed that residues 95–144 of RCHY1 bind to SARS2-Nsp13 a.a. 1- 259 (Figure 21A). Additionally, different fragments of RCHY1 have exhibited a weak interaction with Nsp13 a.a. 260–601, whereas the full-length RCHY1 protein displays a strong binding affinity for this region (Figure 21B). These findings suggest that multiple regions of RCHY1 are required for effective binding to Nsp13 a.a.260–601.

Together, these data have suggested that RCHY1 a.a. 95–144 are critical for the interaction with both Nsp3 and Nsp13.

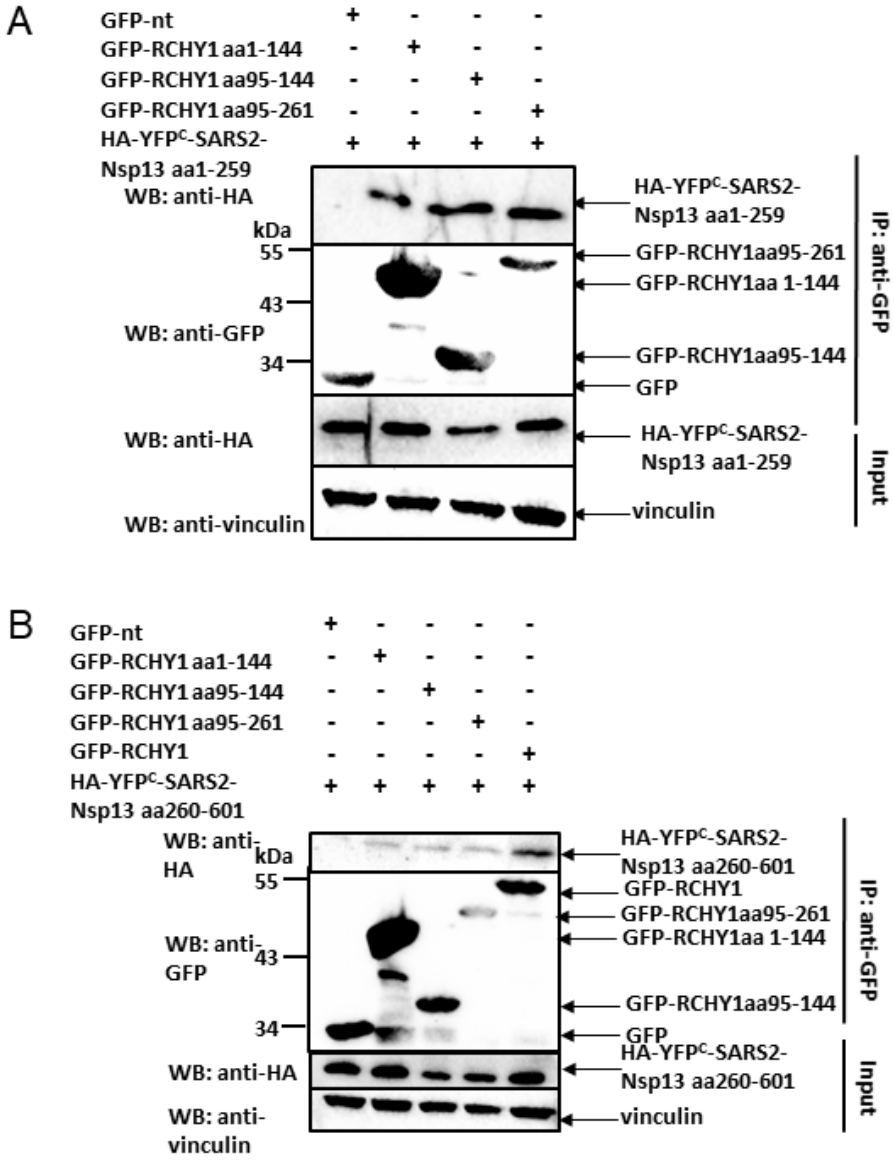

Figure 21. The interactions between RCHY1 truncations and Nsp13 a.a.1-259 or Nsp13 a.a.260-601. (**A**) Interaction between different RCHY1 truncations and Nsp13 a.a.1-259. HEK293 cells were co-transfected with plasmids expressing GFP fused RCHY1 full length, different RCHY1 truncations or empty vector together with HA-YFP^C-SARS-CoV-2 Nsp13 a.a.1-259 in a 6-well plate. The cells were harvested 48 hours later for the co-IP assay. (**B**) Interaction between different RCHY1 truncations and Nsp13 a.a.260-601. HEK293 cells were co-transfected with indicated plasmids. Forty-eight hours after transfection, cells were harvested for co-IP assay.

3.3 Nsp3 but not Nsp13 increases RCHY1 protein expression

3.3.1 Nsp3 stimulates RCHY1 protein expression

In order to investigate the effect of the interaction between RCHY1 and Nsp3, Nsp3 a.a.1-1363 was co-transfected together with RCHY1 or an empty vector in HEK293 cells. Due to the consistently low expression levels of the full-length Nsp3 in cellular

assays, the pCG1 SARS-CoV-2 Nsp3 a.a.1-1363 ectopically expressing Nsp3 a.a.1-1363 was used as an alternative for the tests. Western blot analysis indicated that the protein expression of RCHY1 was stimulated in the presence of Nsp3 a.a.1-1363 (Figure 22A). Moreover, Renilla luciferase reporter assay showed that the presence of Nsp3 a.a.1-1363 significantly enhanced the luciferase activity of the luciferase-fused RCHY1 (RL-RCHY1), rather than the luciferase control (Figure 22B). This finding suggests that the stimulation is due to RCHY1 rather than luciferase.

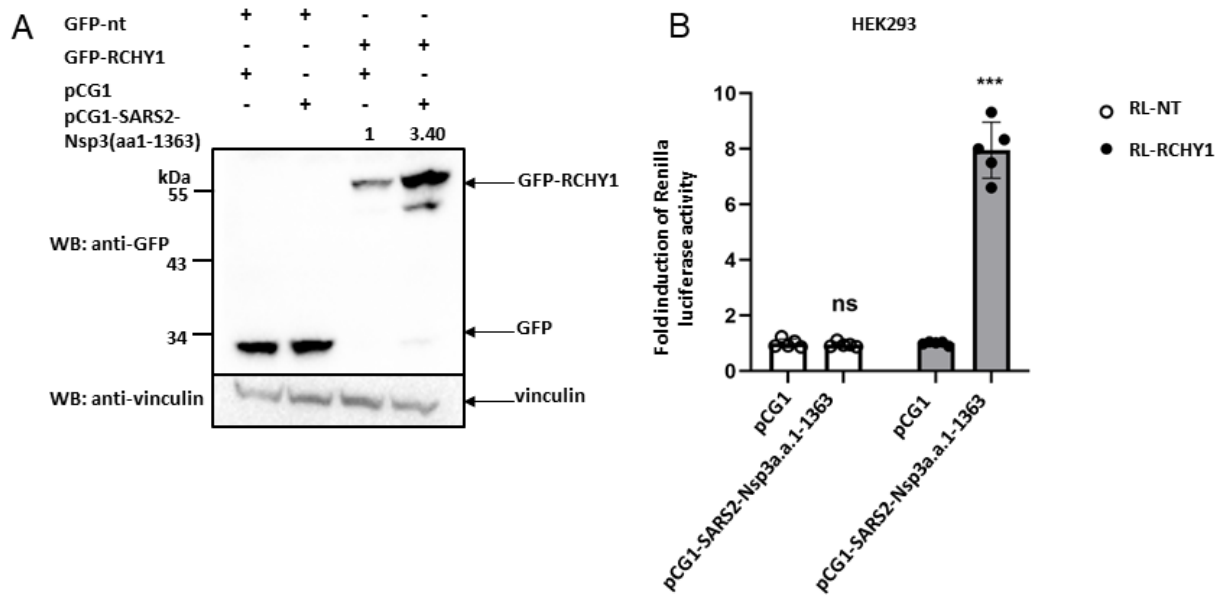

Figure 22. Nsp3 enhances RCHY1 protein expression. (**A**) Western blot analysis revealed an increase in RCHY1 caused by SARS-CoV-2-Nsp3 a.a.1–1363. The indicated plasmids were transfected into HEK293 cells seeded in a 12-well plate. After a 24-hour period, cell lysates were collected and analysed by Western blot using anti-GFP and anti-vinculin antibodies. (**B**) Nsp3 enhances the luciferase activity of RCHY1 fused to the Renilla luciferase reporter. HEK293 cells were transfected with pcDNA3 luciferase-fused RCHY1 (RL-RCHY1) or empty vector RL-NT and pCG1 empty vector or SARS-CoV-2-Nsp3 a.a.1–1363 plasmids in a 96-well plate. The cells were harvested 24 hours post-transfection and luciferase activity was measured using the Renilla Luciferase Assay System (Promega). The Renilla luciferase signals of each group were then normalized to the pCG1+RL-NT group. The mean values and standard deviations presented in the figure were calculated based on five independent biological repeats (n = 5; mean ± SD). The statistical analysis was performed using a two-way analysis of variance (ANOVA). ns: not significant; ***: $P < 0.001$. The band intensities were quantified by ImageJ.

In addition, the fluorescence microscopy revealed that the expression level of the RCHY1-RFP fusion was very low when it was co-transfected with GFP empty vector, due to the short half-life of RCHY1 of 3-4 hours [94]. However, both SUD and PLpro enhanced the signals of the RCHY1-RFP fusion significantly (Figure 23A). SUD can be divided into three subdomains: SUD-N terminal (SUD-N), the middle domain of SUD (SUD-M), and SUD-C terminal (SUD-C). Our laboratory has previously reported that

SUD-N interacts with human protein translation stimulator Paip1 to increase viral protein synthesis [73]. SUD-NM subdomain interacts with DNA and RNA G-quadruplexes which regulate the transcription of multiple human genes and mRNA metabolism [95]. To further explore which domain of SUD is responsible for RCHY1 enhancement, the fluorescence signals of RCHY1-RFP co-transfected with different SUD domains were observed. As demonstrated in Figure 23B, all these subdomains, including only SUD-N or SUD-M domain alone can stimulate RCHY1 expression.

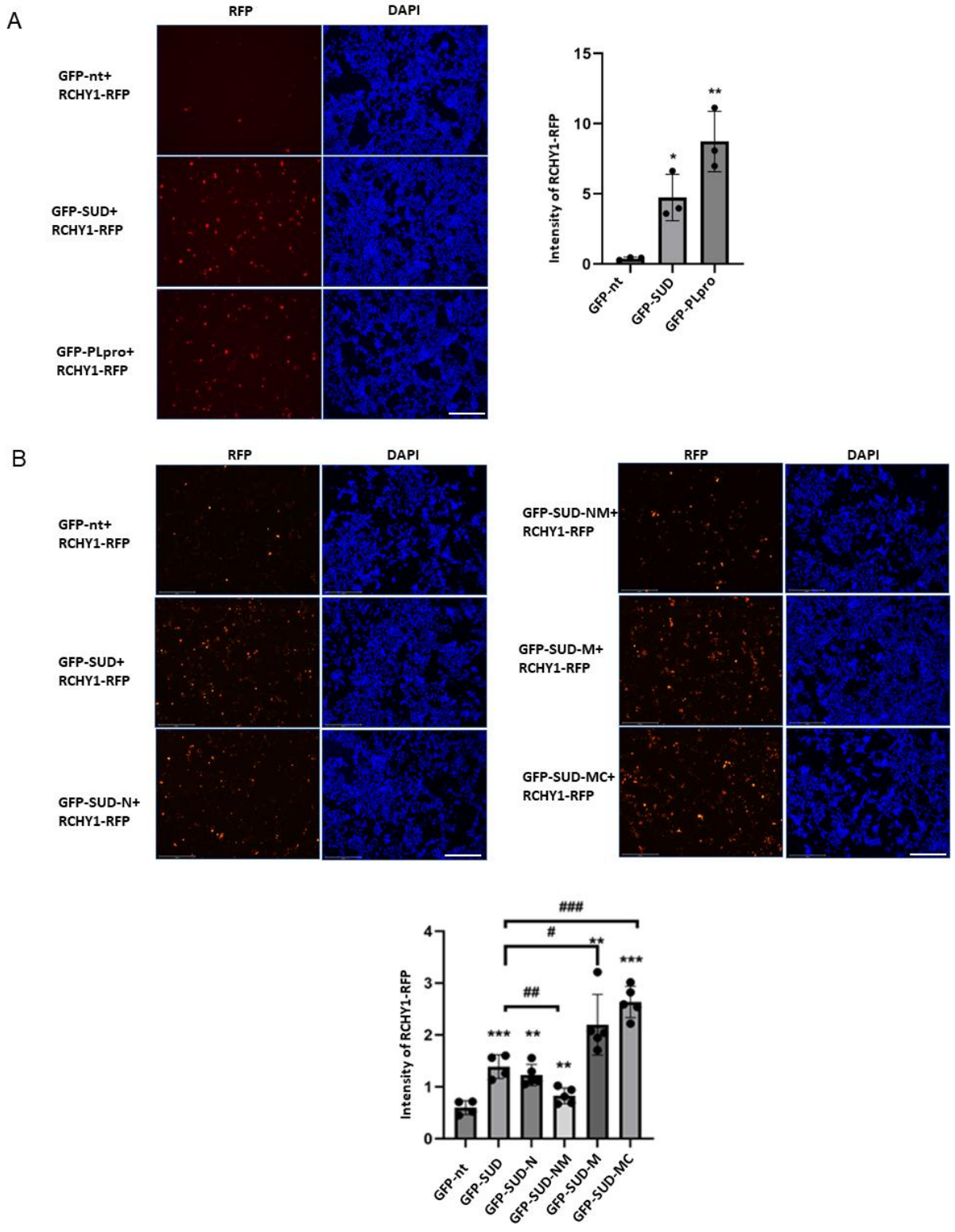

Figure 23. Fluorescence microscopy analysis of RCHY1 induction caused by SUD and PLpro domains. (**A**) Left: RFP-fused RCHY1 (RCHY1-RFP) was co-transfected with GFP-empty vector (GFP-nt) or GFP-fused SUD or PLpro into HEK293 cells in a 24-well plate. Twenty-four hours after transfection, the cells were fixed with 4% PFA and stained with DAPI. Images were captured using a Leica DM4000 B fluorescence microscope with a 10x objective. Right: Three images were randomly selected for each group and the intensities of RFP signals were quantified using ImageJ software. RFP fluorescence intensities of each group were then

normalized to the empty vector group. Statistical analysis was performed using one-way analysis of variance (1-way ANOVA). (mean ± SD, * P < 0.05, ** P < 0.01). Scale bar: 275 μm. (**B**) HEK293 cells were co-transfected with RCHY1-RFP and GFP-fused SUD domains (SUD, SUD-N, SUD-NM, SUD-M, SUD-MC) or GFP empty vector. The cells were fixed with 4%PFA and stained with DAPI 24 hours after transfection. The quantification was performed as described in (A). Statistical analysis was performed using 1-way ANOVA. (mean ± SD, # P < 0.05, ## P < 0.01, ###P < 0.001, **P < 0.01, ***P < 0.001). Scale bar: 275 μm.

3.3.2 Nsp13 does not alter RCHY1 protein level

To explore if the interaction between RCHY1 and Nsp13 also influences RCHY1 protein expression, HEK293 cells were transfected with plasmids expressing RCHY1 fused to GFP tag or the GFP control together with Nsp13 fused to HA-YFP^{c} tag or HA-YFP^{c} control. The expression of RCHY1 was not affected by the full length of Nsp13 (Figure 24A). The presence of Nsp13 also did not affect the RCHY1 substrate p53. Additionally, this result was confirmed with RCHY1 or Nsp13 fused to different tags. As shown in Figure 24B, RFP-tagged Nsp13 did not influence the expression of HA-tagged RCHY1, which is consistent with the result in Figure 24A. In conclusion, the SUD and PLpro domains contribute to the upregulation of RCHY1 by SARS-CoV-2 Nsp3, whereas Nsp13 does not influence RCHY1 expression.

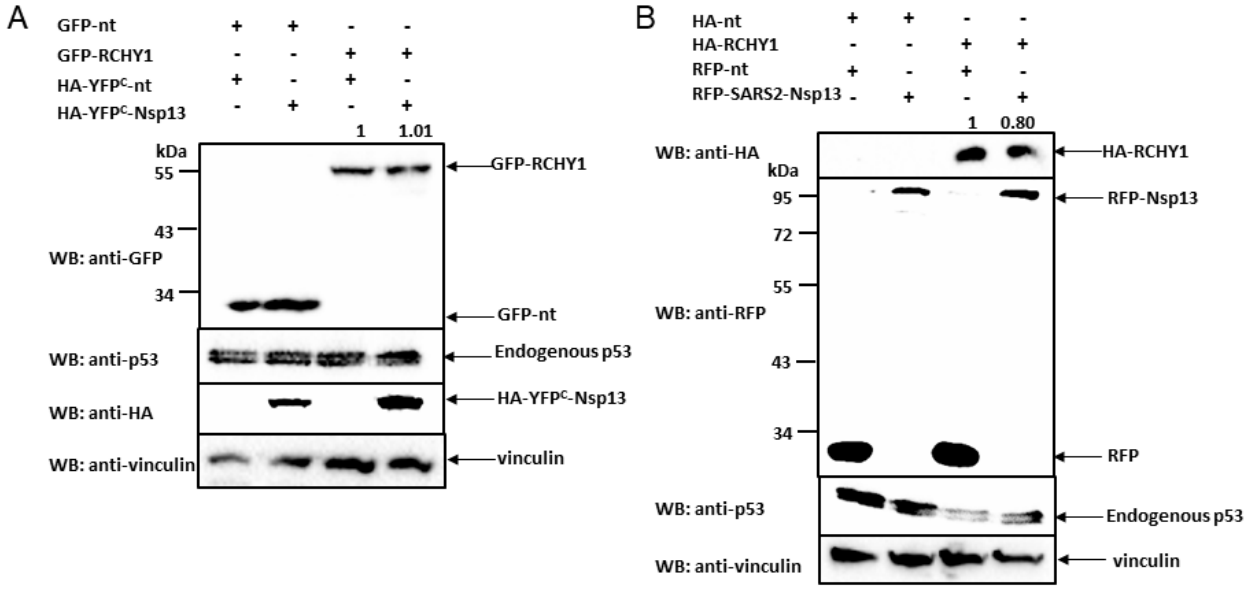

Figure 24. Unchanged RCHY1 protein level in the presence of SARS-CoV-2 Nsp13. (**A**) and (**B**) Indicated plasmids were transfected into HEK293 cells. Forty-eight hours after transfection, the cells were harvested for Western blot analysis using anti-p53, anti-vinculin, anti-HA, anti-GFP (A) or anti-RFP (B) antibodies. The band intensities were quantified by ImageJ and shown as 1, 1.01, 1 and 0.80.

3.4 Nsp3 reduces RCHY1 protein degradation and increases RCHY1 protein translation

3.4.1 Nsp3 does not influence RCHY1 at transcription level

In order to gain further insight into the molecular mechanism by which Nsp3 increases RCHY1 expression, an analysis was performed of the mRNA levels of endogenous RCHY1 in the presence of Nsp3. Figure 25A showed that the mRNA levels of RCHY1 remained unaffected despite the robust protein expression of Nsp3 (Figure 25B). Therefore, it is most likely that Nsp3 regulates RCHY1 at the translational or post-translational level.

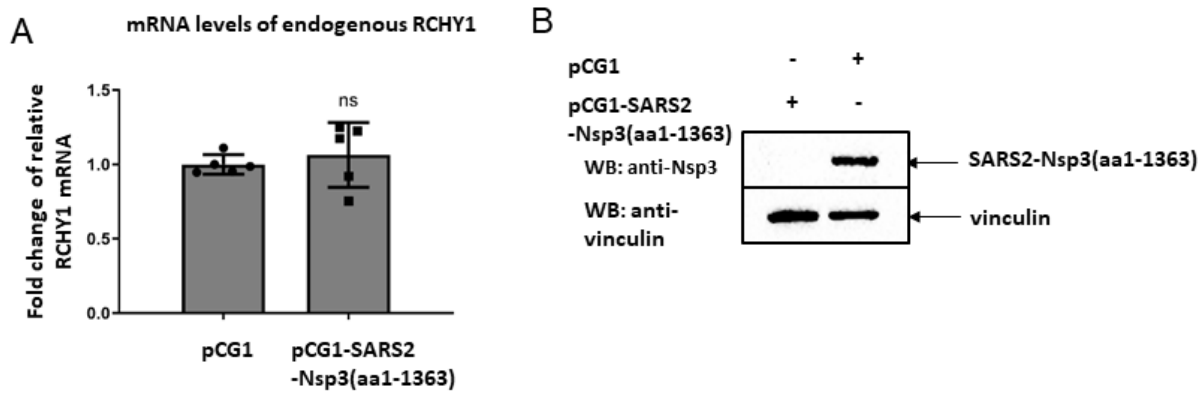

Figure 25. Unchanged RCHY1 mRNA levels in the presence of Nsp3 a.a.1-1363. (**A**) qPCR analysis of the endogenous RCHY1 mRNA levels. HEK293 cells were transiently transfected with the indicated plasmids in 24-well plates. The cells were harvested 24 hours after transfection to isolate total RNA. Probe-based qPCR was then performed to detect the endogenous mRNA level of RCHY1 (normalized to actin-β, n=5, mean ± SD). The statistical analysis was performed using Student's t-test, ns: not significant. (**B**) The detection of SARS-CoV-2-Nsp3 a.a.1-1363 expression by Western blot. HEK293 cells cultured in a 24-well plate were subjected to transfection with pCG1 SARS-CoV-2 Nsp3 a.a.1-1363 or control plasmids, and the cells were harvested 24 hours post-transfection. The expression of Nsp3 was confirmed by Western blot using an anti-Nsp3 antibody.

3.4.2 Nsp3 enhances RCHY1 protein translation

To explore if Nsp3 influences RCHY1 protein translation, a ribopuromycylation assay [83], combined with GFP-trap based protein purification was performed to evaluate the protein synthesis of RCHY1. Puromycin has been shown to incorporate into peptide chains during the process of translation, resulting in the release of elongating polypeptides from ribosomes [96]. Therefore, the incorporation of puromycin-labelled GFP-RCHY1 polypeptides following puromycin treatment and subsequent purification of GFP-RCHY1 polypeptides using GFP-traps served as a method for the assessment of GFP-RCHY1 during the process of translation. Interestingly, it was observed that Nsp3 did not increase the total protein levels, but there were more puromycin-labeled GFP-

RCHY1 polypeptides (Figure 26). This indicates that Nsp3 stimulates RCHY1 protein translation.

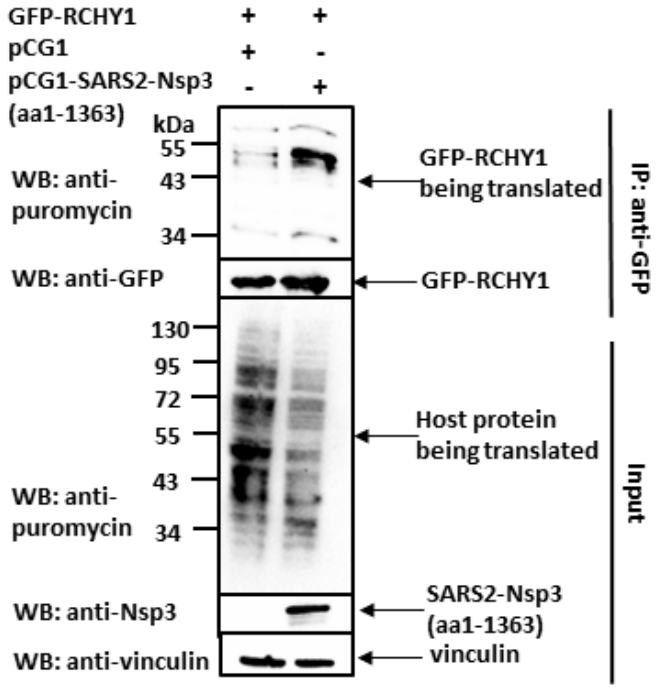

Figure 26. Nsp3 stimulates RCHY1 protein expression in a ribopuromycylation assay. HEK293 cells cultured in a 6-well plate were transfected with the indicated plasmids. Following a 24-hour incubation at 37°C, the cells were treated with 3 µM puromycin for a further 2 hours. Then the cells were harvested and purified by GFP trap. The expression of newly synthesised RCHY1 was then determined by Western blot analysis using an anti-puromycin antibody.

3.4.3 Nsp3 inhibits RCHY1 protein degradation

Subsequently, an investigation was conducted to determine whether Nsp3 influences the degradation of RCHY1 protein. For this purpose, a cycloheximide (CHX) chase assay was performed. Nsp3 was found to prolong the half-life of RCHY1 and stabilize it, thereby suggesting that Nsp3 disrupts the degradation process of RCHY1 (Figure 27).

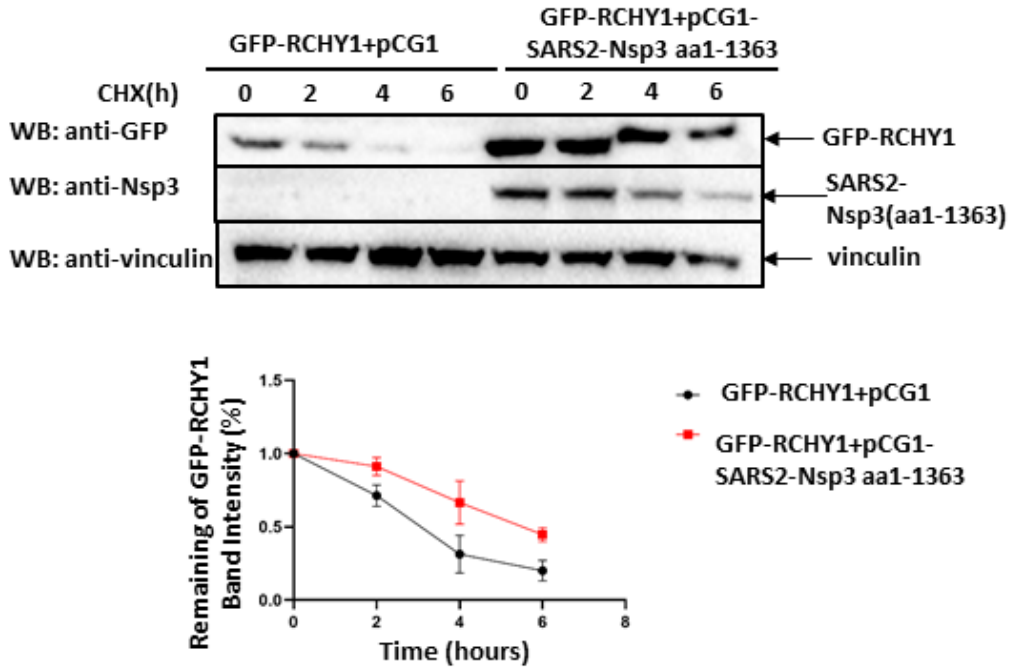

Figure 27. Nsp3 prolonged RCHY1 half-life in a CHX chase assay. The indicated plasmids were co-transfected into HEK293 cells cultured in a 12-well plate. After 24 hours, the cells were treated with CHX at a final concentration of 100 μg/ml. The cells were then harvested at various time points after CHX treatment for Western blot analysis. The band intensity of GFP-RCHY1 was normalized to the stable endogenous protein vinculin.

Proteasomal degradation is tightly linked to ubiquitination. Therefore, an *in vivo* ubiquitination assay was conducted to determine whether Nsp3 influences the ubiquitination status of RCHY1. As shown in Figure 28, Nsp3 decreased RCHY1 ubiquitination level significantly.

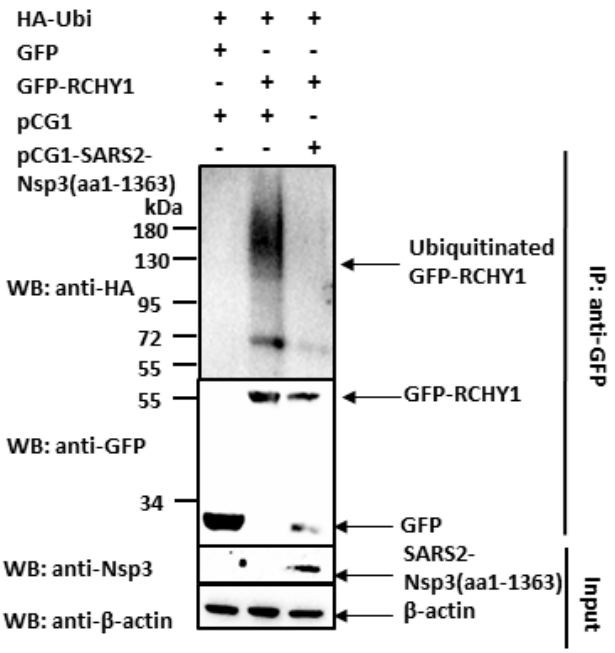

Figure 28. Reduction of RCHY1 ubiquitination by SARS-CoV-2-Nsp3 a.a.1-1363 in an *in vivo* ubiquitination assay. Plasmids expressing HA-tagged ubiquitin, GFP or GFP-RCHY1 fusion, and pCG1 empty vector or pCG1–SARS-CoV-2 Nsp3 a.a.1-1363 were co-transfected into HEK293 cells cultured in a 6-well plate. Following a 48-hour transfection period, the cells were treated with 10 μM MG132 for a further 4 hours at 37°C. Then, the cells were lysed and purified by GFP trap. The level of RCHY1 ubiquitination was detected by Western blot using anti-HA antibodies.

To explore which domain of Nsp3 is responsible for RCHY1 deubiquitination, *in vivo* ubiquitination assay was performed with the SUD domain only. As shown in Figure 29A, the SUD domain alone did not influence RCHY1 ubiquitination level. Since the PLpro domain of Nsp3 is known to possess deubiquitinating (DUB) activity [97], it was speculated that the PLpro domain is responsible for the deubiquitination of RCHY1. To investigate this, an *in vivo* ubiquitination assay was performed using both wild-type (wt) PLpro and a catalytic mutant (ca) in which the cysteine at position 111 was replaced with alanine. This substitution aimed to abolish PLpro enzyme activity [75]. Western blot analysis revealed that while the wild-type PLpro exhibited deubiquitination activity, this function was abolished in the catalytic mutant, as evidenced by the ubiquitination levels of the host proteins (Figure 29B). Furthermore, the RCHY1 protein purified from myc-trap revealed that RCHY1 was deubiquitinated by PLpro wt (lane 2). However, the catalytic mutant version restored and even increased the ubiquitination level of RCHY1 (lane 3). Interestingly, the mutation in the catalytic domain did not affect the binding affinity between RCHY1 and PLpro (Figure 29B).

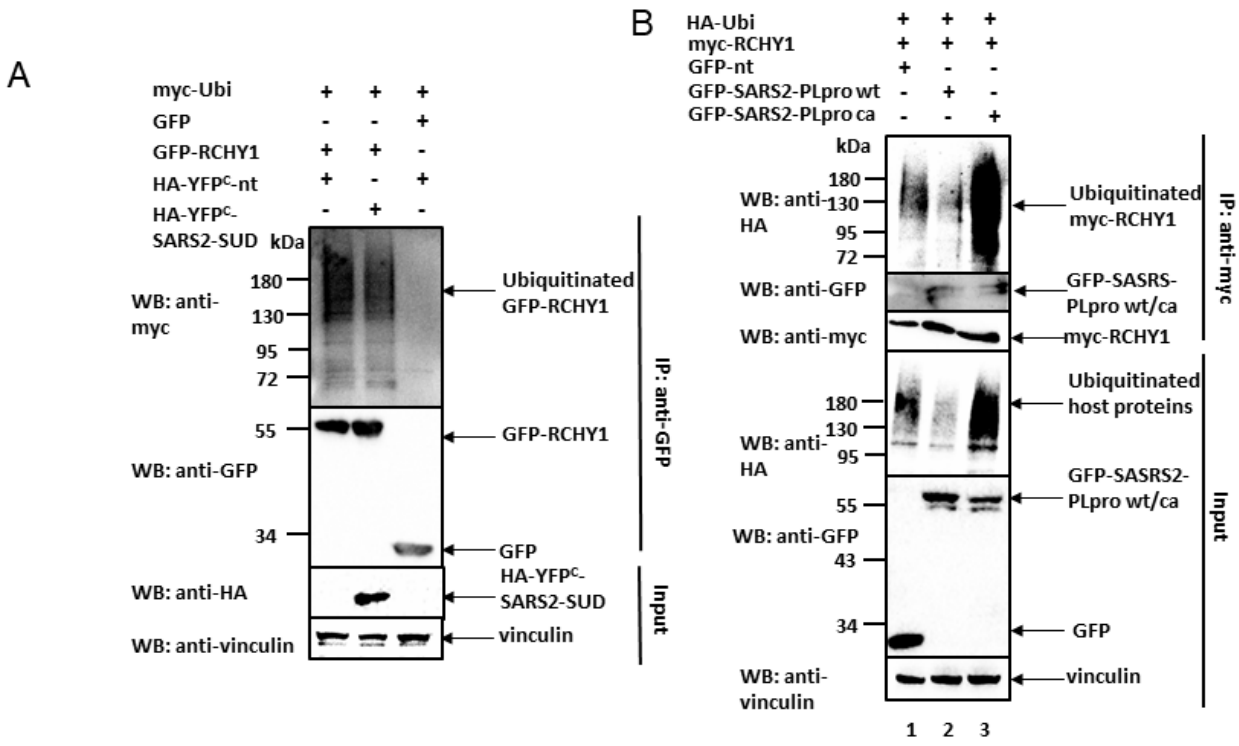

Figure 29. The deubiquitination of RCHY1 is dependent on the enzyme activity of PLpro. (**A**) Unaltered RCHY1 ubiquitination level in the presence of the SUD domain of SARS-CoV-2 Nsp3. The indicated plasmids were co-transfected into HEK293 cells, which were cultured in a 6-well plate. After 48 hours, the cells were treated with 10 µM MG132 for 4 hours at 37°C. This was followed by purification of the myc-trap, and the ubiquitination level of RCHY1 was analysed by performing a Western blot on the myc-eluted samples using an anti-HA antibody. (**B**) Decrease of RCHY1 ubiquitination by PLpro domain of SARS-CoV-2 Nsp3. HEK293 cells were cultured in a 6-well plate and co-transfected with HA-ubiquitin, myc-RCHY1, GFP-SARS-CoV-2 PLpro wt or GFP-SARS-CoV-2 PLpro ca by PEI. Following a 48-hour incubation period, the cells were treated with 10 µM MG132 for a further 4 hours. The *in vivo* ubiquitination assay was performed as (A). wt: wild type. ca: catalytic mutant, which abolishes the enzymatic activity of PLpro.

Furthermore, Western blot analysis revealed that RCHY1 expression was upregulated by wild-type PLpro. In contrast, mutation of the PLpro catalytic domain abolished this PLpro-induced RCHY1 enhancement (Figure 30). Therefore, SARS-CoV-2 PLpro targets RCHY1 and deubiquitinates RCHY1. SARS-CoV-2 Nsp3 enhances RCHY1 expression by promoting its protein translation while simultaneously reducing RCHY1 polyubiquitination and subsequent proteasomal degradation.

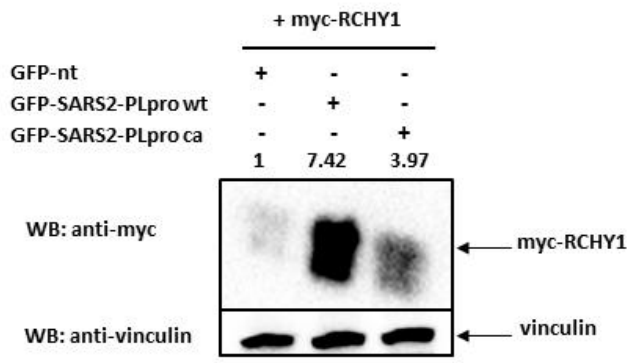

Figure 30. PLpro increases RCHY1 protein level, which is partially dependent on its enzyme activity. Plasmids expressing myc–RCHY1 and expressing GFP or GFP-SARS-CoV-2 PLpro wt or GFP-SARS-CoV-2 PLpro ca were used to transfect HEK293 cells in a 12-well plate. Forty-eight hours post-transfection, the cells were harvested for Western blot analysis using anti-myc and anti-vinculin antibodies. wt: wild type. ca: catalytic mutant, which abolishes the enzymatic activity of PLpro. The band intensities were quantified by ImageJ.

3.5 RCHY1 is a substrate of Nsp3 for deISGylation

Furthermore, it has been demonstrated that PLpro is capable of deISGylating activity [25, 26]. The efficiency of Nsp3 or PLpro in deconjugating ISG15 from RCHY1 was assessed using a deISGylation assay combined with GFP or HA-trap based co-IP. In the deISGylation assays, the ISG15-conjugation machinery consisting of ISG15, UbcH8, UbeII, and Herc5 [75] was applied to the ISGylation of GFP- or HA-RCHY1 in the absence and presence of Nsp3 or PLpro. First, it was observed that Nsp3 significantly decreased the ISGylation level of RCHY1 (Figure 31A). A deISGylation assay was then performed using both PLpro wt and ca. As shown in Figure 31B, PLpro wt deISGylated RCHY1 to a large extent, whereas the catalytic mutant abolished the deISGylation effect exerted by the wild-type PLpro. Taken together, these findings suggest that RCHY1 serves as a substrate of Nsp3, and the reduction of RCHY1 ubiquitination and ISGylation by Nsp3 is specifically mediated through its PLpro domain.

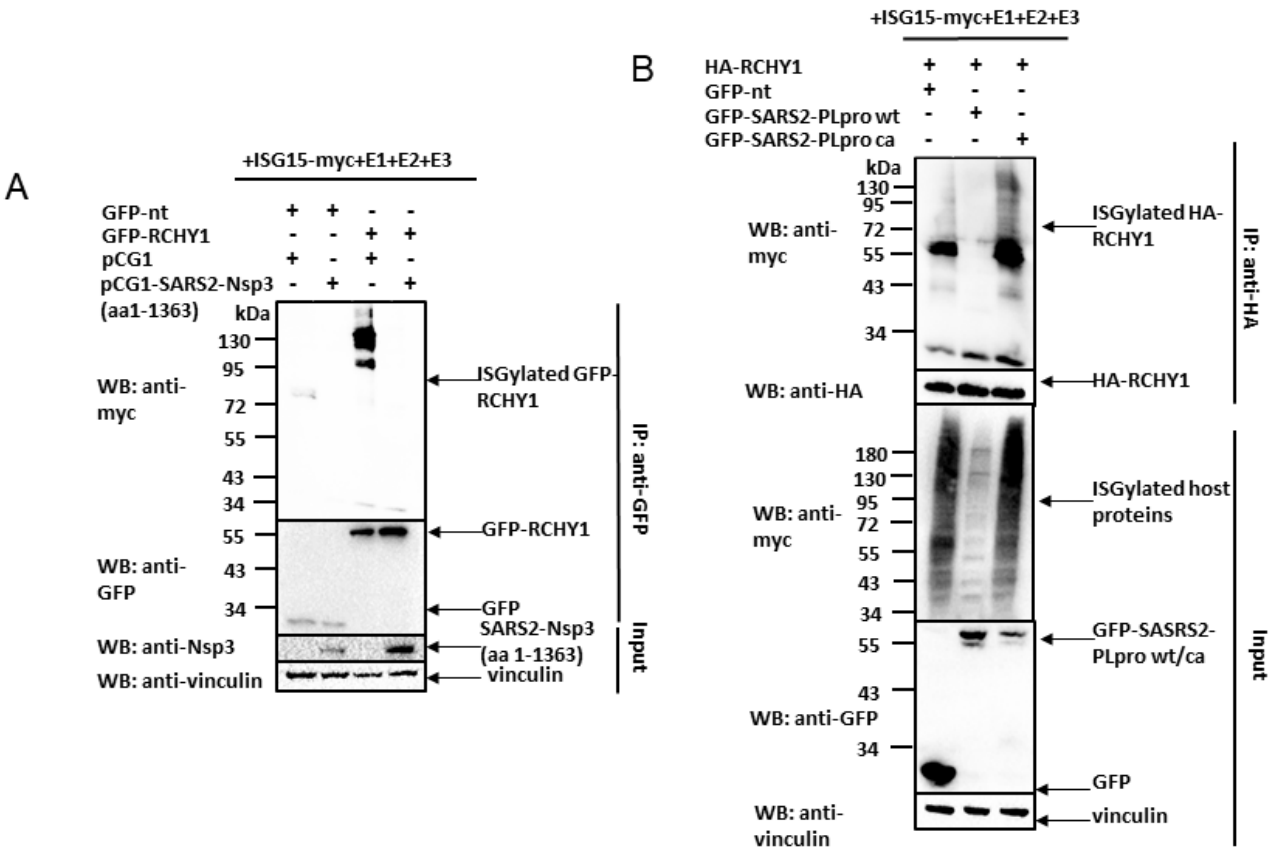

Figure 31. Nsp3 delSGylates RCHY1 via the PLpro domain. (**A**) Reduction of RCHY1 ISGylation by SARS-CoV-2 Nsp3 a.a.1-1363. HEK293 cells were co-transfected with ISG15-myc, pUbe1L (E1), pUbcH8 (E2), Herc5 (E3), GFP-RCHY1 or GFP empty vector and pCG1-SARS-CoV-2 Nsp3 a.a.1-1363 or pCG1 empty vector using PEI in 6-well plates. At 48 hours post-transfection, cells were harvested and purified by GFP trapping. The ISGylation level of RCHY1 was analysed by Western blot of the GFP eluate samples with anti-myc antibody. (**B**) Reduction of RCHY1 ISGylation by the PLpro domain HEK293 cells were co-transfected with the indicated plasmids in a 6-well plate. Forty-eight hours post-transfection, cells were harvested and purified by HA-trap (Thermofisher Pierce™). The ISGylation level of RCHY1 was analysed by Western blot of HA eluate samples with anti-myc antibody. wt: wild type. ca: catalytic mutant that abolishes the enzymatic activity of PLpro.

3.6 Nsp3 decreases and delSGylates RCHY1 substrates p53 and p63

3.6.1 Nsp3 reduces the expression of endogenous p53 and p63

RCHY1 can function as an E3 ubiquitin ligase by affecting target proteins such as p53 [38]. To investigate the impact of Nsp3-induced upregulation of RCHY1, the levels of endogenous p53 protein were assessed. The overexpression of Nsp3 led to a noticeable increase of RCHY1 protein level. Nsp3 slightly decreased the expression of endogenous p53 (Figure 32, lane 2 versus lane 1). When co-expressed with RCHY1, this reduction in p53 expression was further enhanced (lane 4 versus lane 2), suggesting

that Nsp3 can also enhance RCHY1-mediated p53 degradation only through endogenous RCHY1.

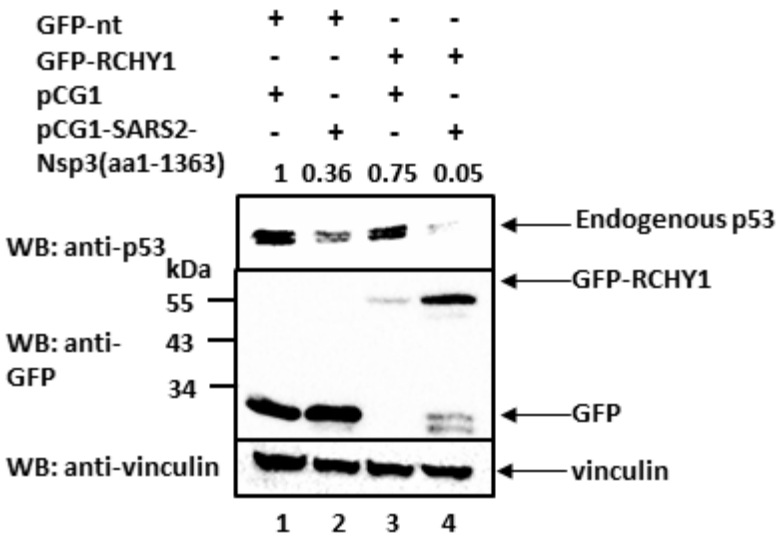

Figure 32. Decrease of RCHY1 substrate, p53 by SARS-CoV-2 Nsp3 a.a.1-1363. HEK293 cells were co-transfected with GFP-RCHY1 or GFP-nt, and pCG1 or pCG1-SARS-CoV-2 Nsp3 a.a.1-1363 plasmids, in a 12-well plate. Cells were harvested 48h post-transfection for Western blot analysis using anti-p53, anti-GFP and anti-vinculin antibodies. The band intensities were quantified by ImageJ.

To confirm that Nsp3 enhances RCHY1 and consequently downregulates p53 during SARS-CoV-2 infection, the endogenous expression levels of RCHY1 and p53 in human ACE2 transgenic bronchial epithelial cells (BEAS-2B-ACE2) were examined. These cells were either infected with SARS-CoV-2 or maintained as a non-infected control group. As shown in Figure 33A, SARS-CoV-2 infection led to the decrease of endogenous p53, implying that Nsp3 causes p53 reduction via endogenous RCHY1 during SARS-CoV-2 infection in human bronchial epithelial cells. Notably, infection with HCoV-OC43 lacking the SUD domain did not affect the expression of endogenous p53 (Figure 33B), suggesting that RCHY1-induced p53 degradation enhanced by Nsp3 may be specific to SARS-related viruses. Unfortunately, endogenous RCHY1 expression in BEAS-2B cells was insufficient for detection by different anti-RCHY1 antibodies.

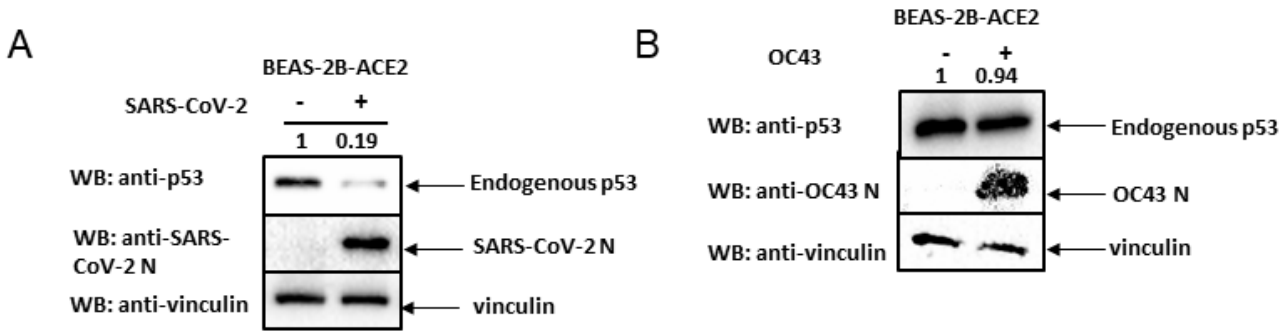

Figure 33. SARS-CoV-2 but not HCoV-OC43 infection reduces endogenous p53 expression. (**A**) Reduction of p53 by SARS-CoV-2 infection in BEAS-2B-ACE2 cells (a collaboration with Dr. Zhe Ma and Dr. Gregor Ebert in S3 laboratory). BEAS-2B-ACE2 cells were infected with SARS-CoV-2 (Wuhan strain) (MOI=1). Cells were harvested 48 hours post infection (h.p.i.) for Western blot analysis using anti-SARS-CoV-2 nucleocapsid (anti-N), anti-p53 or anti-vinculin antibodies. (**B**) Endogenous p53 protein levels remained unchanged in BEAS-2B-ACE2 cells infected with HCoV-OC43. Cells were infected with HCoV-OC43 (MOI = 0.1) and harvested 48 h.p.i. for Western blot analysis using anti-OC43 nucleocapsid (anti-OC43 N), anti-p53, and anti-vinculin antibodies. The band intensities were quantified by ImageJ.

Furthermore, p63 is another substrate of RCHY1. Full-length p63 was decreased in the presence of both Nsp3 and RCHY1 (Figure 34).

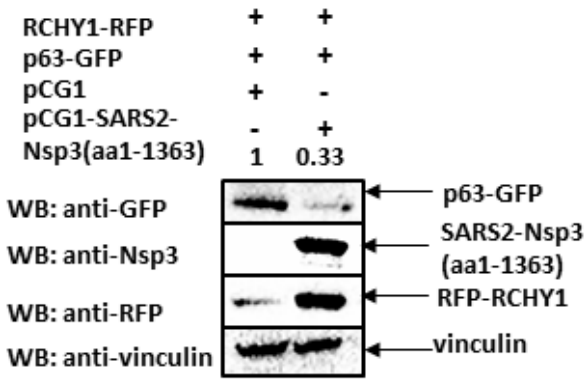

Figure 34. SARS-CoV-2 Nsp3 a.a. 1–1363 induces a decrease in p63 levels. HEK293 cells were transfected with the indicated plasmids and lysed 48 hours post-transfection for Western blot analysis using anti-Nsp3, anti-GFP, anti-RFP, and anti-vinculin antibodies. The band intensities were quantified by ImageJ.

3.6.2 Nsp3 delSGylates p53 and p63

The interaction between p53 and SARS-CoV-2 Nsp3 start (a.a.1-412) in yeast two-hybrid screening was also observed (Figure 35A). Since p53 and p63 are homologous proteins [98], whether they bind to Nsp3 in human cells was investigated. The co-IP assay reveals that both p53 and p63 interact with SARS-CoV-2 Nsp3 (a.a.1–1363) (Figure 35B).

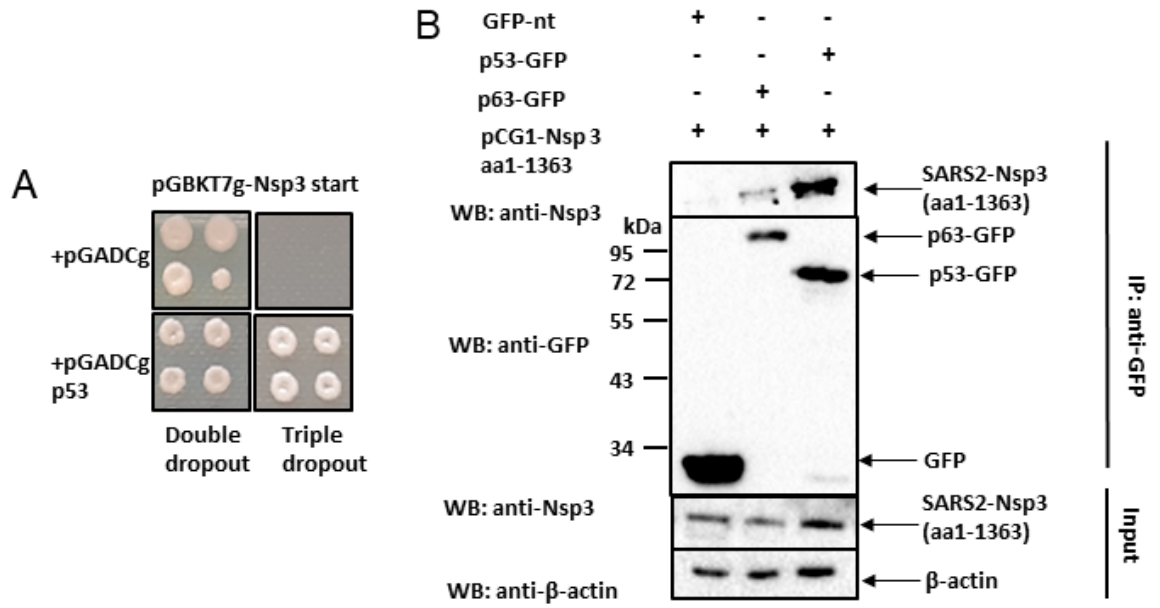

Figure 35. Nsp3 interacts with p53 and p63. (**A**) Interaction between pGADTCg-p53 and the pGBKT7g-Nsp3 start (a.a.1-412) in yeast two-hybrid assay. (**B**) Interaction between p53, p63 and SARS-CoV-2 Nsp3 in co-IP assay. HEK293 cells were transfected with plasmids as indicated in a 6-well plate. Cells were harvested 48 hours post-transfection for GFP-trap-based co-IP assay.

The PLpro domain in Nsp3 carries catalytic activity for deubiquitylation and deISGylation of host proteins [25, 75]. Therefore, whether p53 and p63 could be substrates of Nsp3 was investigated. Figure 36A revealed that Nsp3 decreased the ISGylation level of p53 largely. This effect was dependent on the enzyme activity of the PLpro domain (Figure 36B, lane 2 versus lane 3).

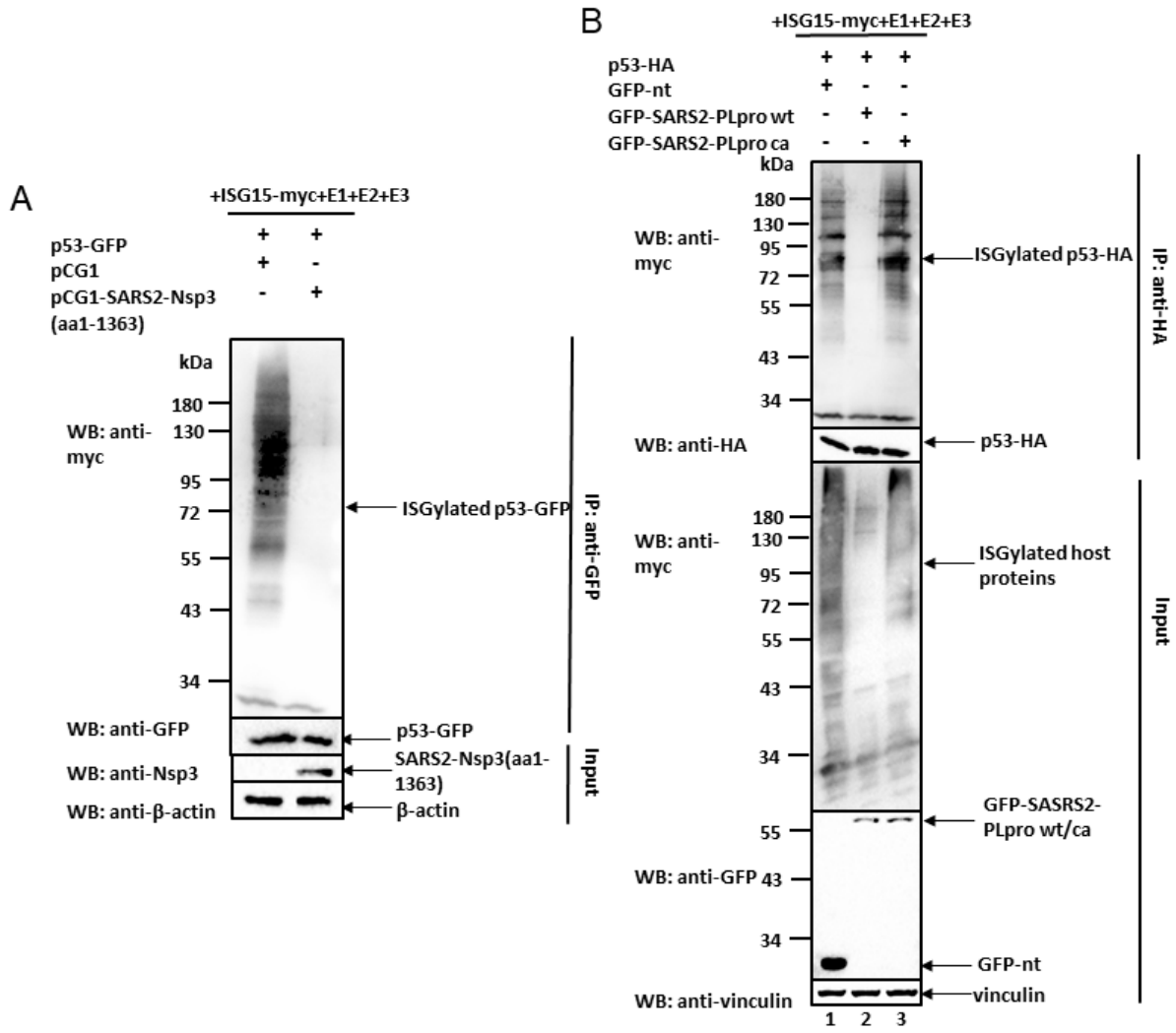

Figure 36. Reduction of p53 ISGylation by SARS-CoV-2 Nsp3. (**A**) Plasmids expressing ISG15-myc, pUbe1L (E1), pUbcH8 (E2), Herc5 (E3), p53-GFP and pCG1-SARS-CoV-2 Nsp3 a.a.1-1363 or pCG1 empty vector were co-transfected into HEK293 cells cultured in a 6-well plate. Forty-eight hours after transfection, cells were harvested and purified by GFP trapping. The level of ISGylation of p53 was determined by Western blot of the GFP-eluted samples using an anti-myc antibody. (**B**) Reduction of p53 ISGylation by the PLpro domain. The indicated plasmids were co-transfected into HEK293 cells cultured in a 6-well plate. 48 h after transfection, cells were harvested and purified by HA-trap (Thermofisher Pierce™). The ISGylation level of p53 was analyzed by Western blot of the HA eluate samples with anti-myc antibody. wt: wild type. ca: catalytic mutant, which abolishes the enzymatic activity of PLpro.

In addition, the deISGylation of p63 was observed in the presence of Nsp3 (Figure 37A), This effect was abolished when the catalytic domain of PLpro was mutated (Figure 37B, lane 3 versus lane 2).

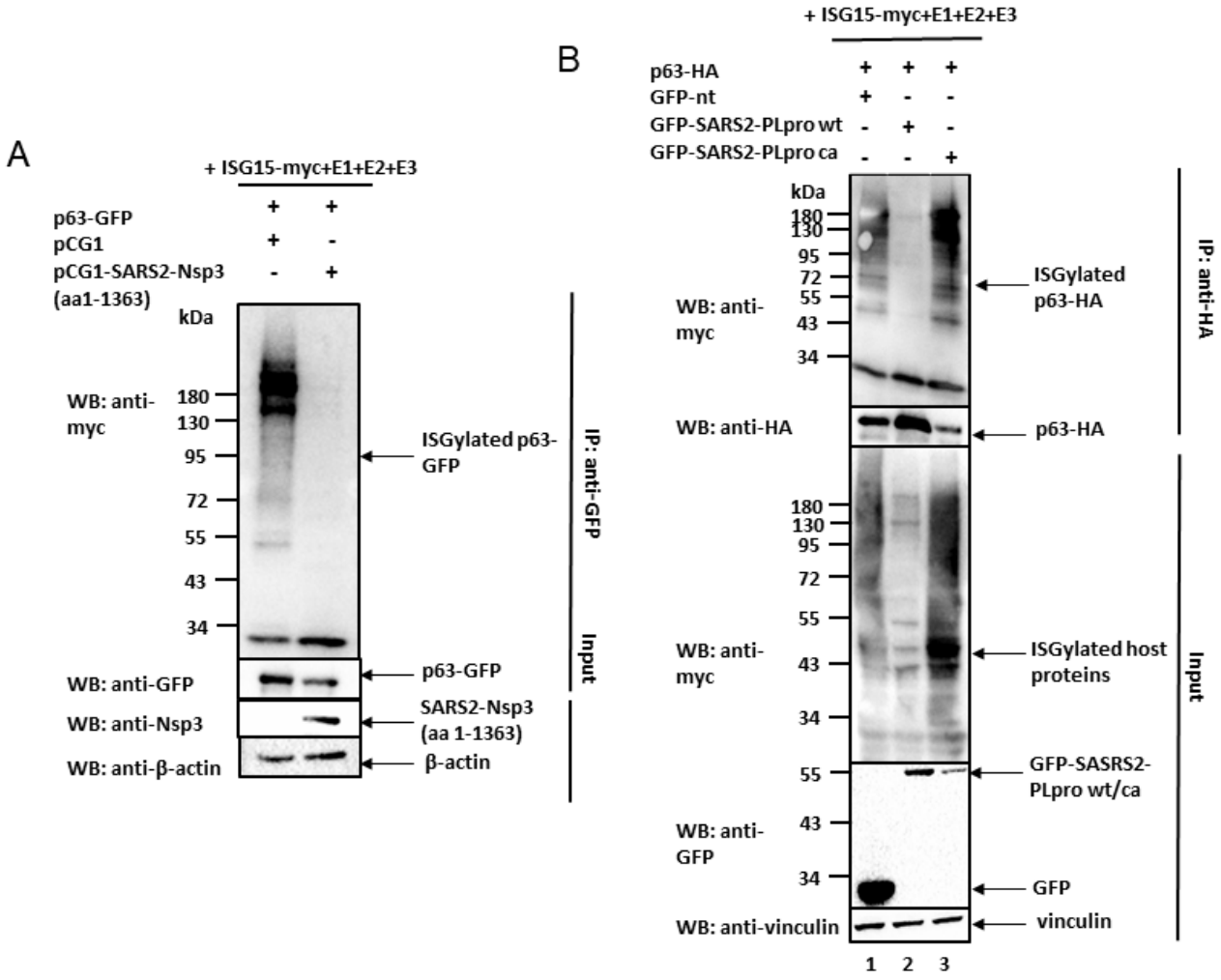

Figure 37. Reduction of p63 ISGylation by SARS-CoV-2 Nsp3. (**A**) Indicated plasmids were co-transfected into HEK293 cells cultured in a 6-well plate. Forty-eight hours after transfection, cells were harvested and purified by GFP trap. The ISGylation level of p63 was evaluated as described in Figure 36(A). (**B**) Reduction of p63 ISGylation by the PLpro domain.

3.6.3 Nsp3 does not deubiquitinate p53 and p63

To explore if p53 and p63 are the substrates for Nsp3 for ubiquitination, the *in vivo* ubiquitination assay was performed. As shown in Figure 38A, Nsp3 did not significantly alter the level of p53 ubiquitination. For p63, expression of Nsp3 alone caused a marked reduction in p63-GFP (Figure 38B, lane 2 versus lane 1), suggesting that p63 deubiquitination by Nsp3 is unlikely. Furthermore, the *in vivo* ubiquitination did not show that p63 was a substrate of Nsp3 for ubiquitination when the band intensity of ubiquitinated p63-GFP was normalized to the band intensity of p63-GFP due to the strongly reduced expression of p63-GFP caused by Nsp3 (Figure 38C). Nsp3 reduced p63-GFP probably through endogenous RCHY1. Therefore, p53 and p63 are substrates of PLpro only for deISGylation, but not for deubiquitination.

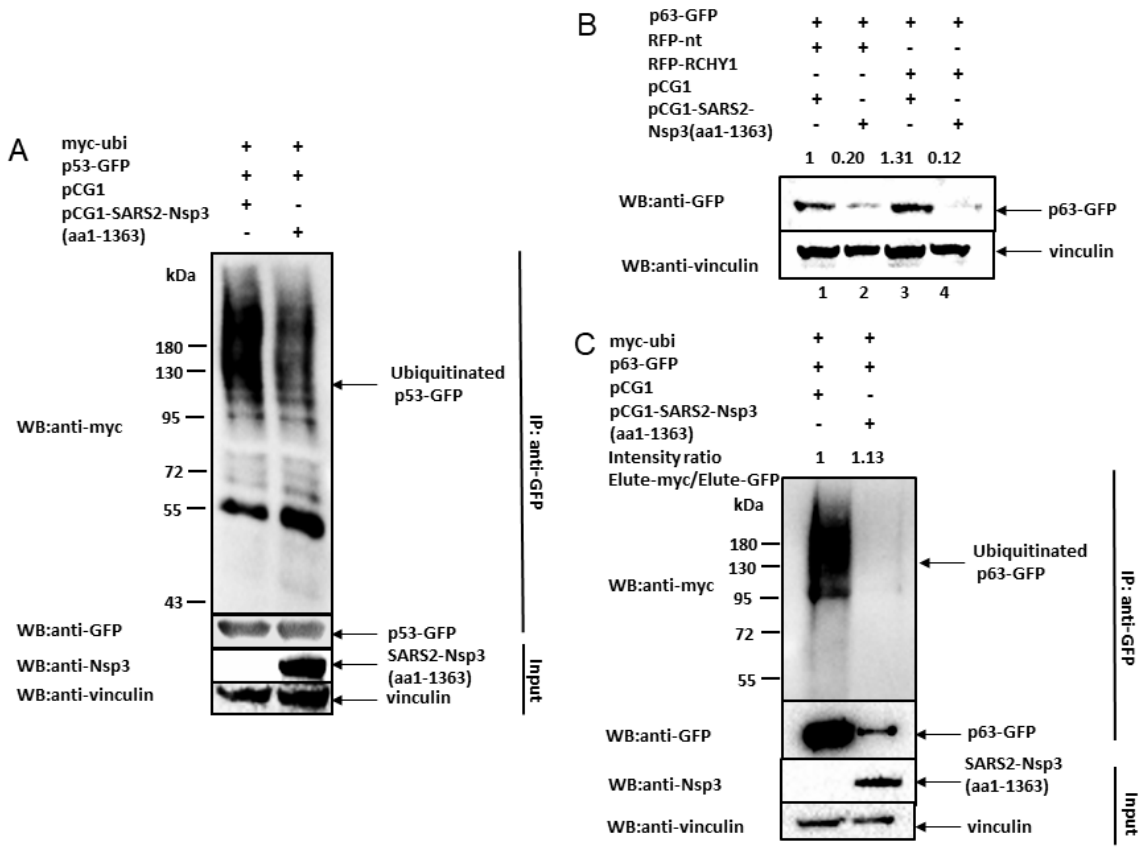

Figure 38. Nsp3 does not mediate the deubiquitination of p53 or p63. (**A**) Unaltered ubiquitination level of p53 in the presence of SARS-CoV-2 Nsp3. HEK293 cells were transfected with indicated plasmids. The cells were harvested for co-IP 48 hours after transfection. The *in vivo* ubiquitination assay was performed as described previously. (**B**) Reduction of p63-GFP by SARS-CoV-2 Nsp3 in the presence or absence of RCHY1. HEK293 cells were transfected with indicated plasmids and harvested 48 hours after transfection for Western blot analysis. (**C**) The ubiquitination level of p63 remained unchanged in the presence of SARS-CoV-2 Nsp3. HEK293 cells were transfected with the indicated plasmids. Forty-eight hours after transfection, the cells were harvested for co-IP and *in vivo* ubiquitination assay. The band intensities were quantified by ImageJ.

3.7 P53 and p63 are antiviral restriction factors for human coronaviruses

3.7.1 P53 inhibits HCoVs replication in BEAS-2B-ACE2 cells

To explore how SARS-CoV-2 benefits from the reduction of p53 and p63 induced by Nsp3, the effect of p53 and p63 on human coronavirus replication including SARS-CoV-2 was investigated. BEAS-2B-ACE2 cells stably overexpressing p53 (BEAS-2B-ACE2 pLenti-p53-OV) or control cells (BEAS-2B-ACE2 pLenti-CMV control) were infected with live attenuated SARS-CoV-2 virus sCPD9 [88, 89].

Overexpression of endogenous p53 was detected by Western blot (Figure 39A). As shown in Figure 39B, the overexpression of p53 resulted in a reduction of attenuated

SARS-CoV-2 replication to less than 10%. Further Western blot analysis indicated that overexpression of p53 results in an undetectable level of SARS-CoV-2 nucleocapsid protein in the infected cells due to the large suppression of virus replication (Figure 39C). BEAS-2B-ACE2 pLenti-p53-OV and BEAS-2B-ACE2 pLenti-CMV control were challenged with SARS-CoV-2 virus fused to GFP protein [90]. Overexpression of p53 significantly suppressed SARS-CoV-2 replication 24 h.p.i. (Figure 39D, left). The cell confluence between these cell lines was comparable (Figure 39D, right). In order to determine whether p53 exerts an influence on the replication of human coronaviruses other than SARS-CoV-2, an experiment was conducted in which BEAS-2B-ACE2 pLenti-p53-OV and control cells were infected with two mild human coronaviruses, HCoV-NL63 and HCoV-OC43. qPCR analysis demonstrated that the replications of both HCoV-NL63 and HCoV-OC43 were inhibited to less than 50% by the over-expression of p53 (Figures 39 E, F).

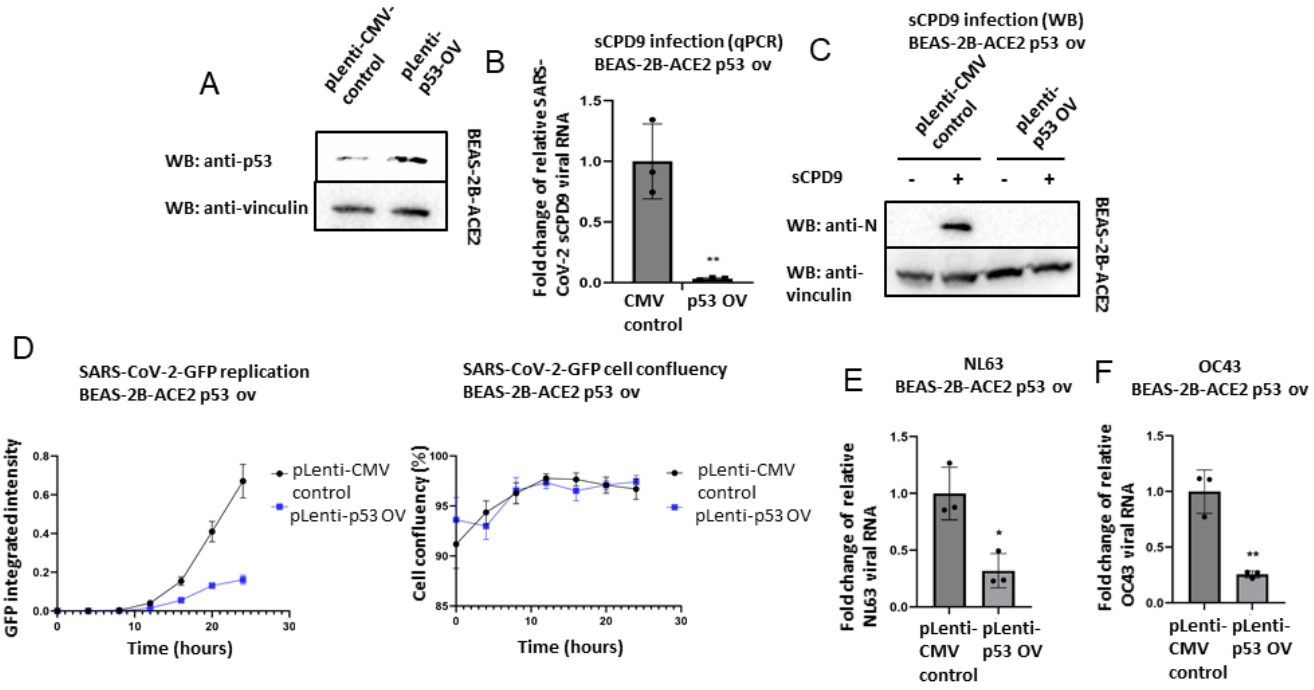

Figure 39. P53 functions as a restriction factor that inhibits human coronavirus replication. (**A**) Western blot detection of p53 overexpression in BEAS-2B-ACE2 cells. (**B**) sCPD9 replication in BEAS-2B-ACE2 pLenti-p53-OV cells by qPCR assay. BEAS-2B-ACE2 pLenti-p53-OV and control cell lines were infected with attenuated SARS-CoV-2 virus sCPD9 (MOI: 0.0001). Cells were harvested 72 h.p.i. for RNA isolation followed by qPCR using SARS-CoV-2 virus nucleocapsid-specific probes and primers. (**C**) sCPD9 replication in BEAS-2B-ACE2 pLenti-p53-OV cells by Western blot analysis. BEAS-2B-ACE2 pLenti-p53-OV and control cell lines were infected with attenuated SARS-CoV-2 virus sCPD9 as described in (B). Cells were harvested at 72 h.p.i. for Western blot analysis. Anti-SARS-CoV-2 nucleocapsid (anti-N) or anti-vinculin antibodies were used. (**D**) SARS-CoV-2-GFP replication in BEAS-2B-ACE2 pLenti-p53-OV cells (collaboration with Professor Pichlmair S3 laboratory at TUM). Left: BEAS-2B-ACE2 pLenti-p53-OV and control cell lines were infected with SARS-CoV-2-GFP virus (MOI=1). GFP signal intensity was measured every 4 hours up to 24 h.p.i. to evaluate virus replication. Right: Cell viability of the indicated cell lines was evaluated in parallel with the SARS-CoV-2-GFP infection assay. (**E**) and (**F**) Inhibition of seasonal human coronaviruses

replication in BEAS-2B-ACE2 pLenti-p53-OV cells by qPCR assay. BEAS-2B-ACE2 pLenti-p53-OV and control cells were infected with HCoV-OC43 (MOI=0.1) or HCoV-NL63 (MOI=0.05) in a 24-well plate. Two hours after infection, the cells were washed twice with DPBS and replenished with a fresh growth medium. At 48 h.p.i., total RNA was extracted and followed by qPCR analysis using viral-specific probes and primers (n = 3). Statistical analysis was performed using Student's t-test. (mean ± SD, * P < 0.05, ** P < 0.01).

3.7.2 Effect of p63 on HCoVs replication in BEAS-2B-ACE2 cells

In addition, the effect of p63 on human coronavirus replication was investigated. In BEAS-2B-ACE2 cells, the overexpression of the full-length p63 (Figure 40A) did not inhibit the replication of the attenuated SARS-CoV-2 sCPD9 virus in qPCR (Figure 40B) or Western blot analysis (Figure 40C). Additionally, the overexpression of p63 did not suppress the proliferation of SARS-CoV-2-GFP (Figure 40D) in BEAS-2B-ACE2 cells. Interestingly, the replications of both sCPD9 and SARS-CoV-2-GFP were slightly increased. P63 had a weaker inhibitory effect on HCoV-NL63 (Figure 40E), but it suppressed HCoV-OC43 replication to less than half (Figure 40F).

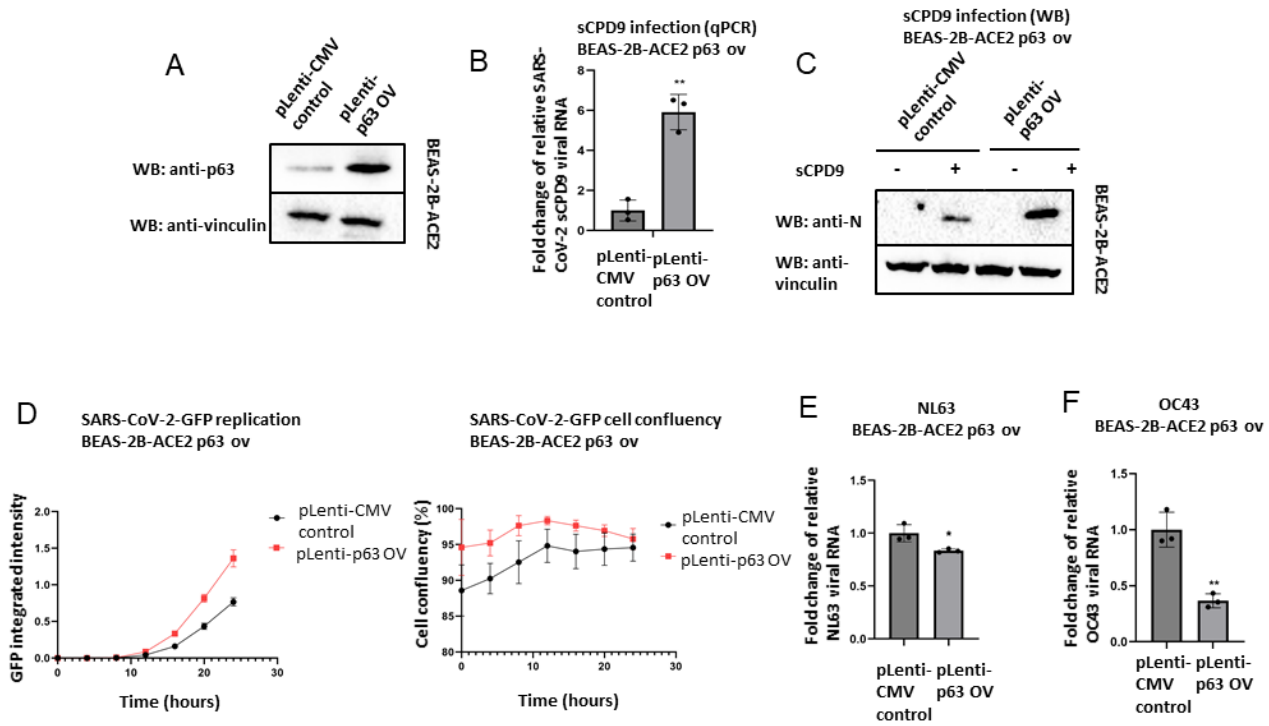

Figure 40. P63 inhibits mild HCoVs, but not SARS-CoV-2 replication in BEAS-2B-ACE2 cells. (**A**) Detection of endogenous p63 in BEAS-2B-ACE2 cells by Western blot assay. Western blot of BEAS-2B-ACE2 pLenti-p63-OV and control cells shows the overexpression of endogenous p63. (**B**) sCPD9 replication in BEAS-2B-ACE2 pLenti-p63-OV cells by qPCR assay. BEAS-2B-ACE2 pLenti-p63-OV and control cell lines were infected with attenuated SARS-CoV-2 virus sCPD9 (MOI: 0.0001) as described previously. Cells were harvested for RNA isolation 72 h.p.i. followed by qPCR using SARS-CoV-2 virus nucleocapsid-specific probes and primers (n=3). Statistical analysis was performed using Student's t-test. (mean ± SD, ** P < 0.01). (**C**) sCPD9 replication in BEAS-2B-ACE2 pLenti-p63-OV cells by Western blot analysis. BEAS-2B-ACE2 pLenti-p63 OV and control cell lines were infected with SARS-CoV-2 virus sCPD9 (MOI: 0.0001). 72 h.p.i., the cells were harvested for Western blot analysis using anti-

SARS-CoV-2 nucleocapsid (anti-N) or anti-vinculin antibodies. (**D**) SARS-CoV-2-GFP replication in BEAS-2B-ACE2 pLenti-p63-OV cells (collaboration with Professor Pichlmair S3 laboratory at TUM). Left: BEAS-2B-ACE2 pLenti-p63-OV and control cell lines were infected with SARS-CoV-2-GFP virus (MOI=1). The intensity of GFP signals was measured every 4 hours until 24 hours after infection. Right: Cell viability of the indicated cell lines was assessed in parallel with the GFP-SARS-CoV-2 infection assay. This experiment was performed in the Pichlmair lab at TUM. (**E**) and (**F**) Detection of replication inhibition of mild human coronaviruses in BEAS-2B-ACE2 pLenti-p63-OV cells by qPCR assay. BEAS-2B-ACE2 pLenti-p63-OV and control cells were infected with HCoV-OC43 (MOI=0.1) or HCoV-NL63 (MOI=0.05) as described previously. Cells were lysed 48 h.p.i. for total RNA extraction followed by qPCR using virus-specific probes and primers (n=3). Statistical analysis was performed using Student's t-test. (mean ± SD, * P < 0.05, ** P < 0.01).

3.7.3 P63 inhibits HCoVs replication in Huh7 cells

To determine whether the effect of p63 on SARS-CoV-2 infection is consistent across different cell lines, hepatocyte-derived carcinoma Huh7 cells were generated stably overexpressing p63 (Figure 41A). Figure 41B and Figure 41C illustrated that the overexpression of p63 inhibited the replication of SARS-CoV-2- derived, attenuated virus sCPD9 in Huh7 cells. Moreover, p63 had an inhibitory effect on the mild coronaviruses HCoV-NL63 (Figure 41D) and HCoV-OC43 (Figure 41E).

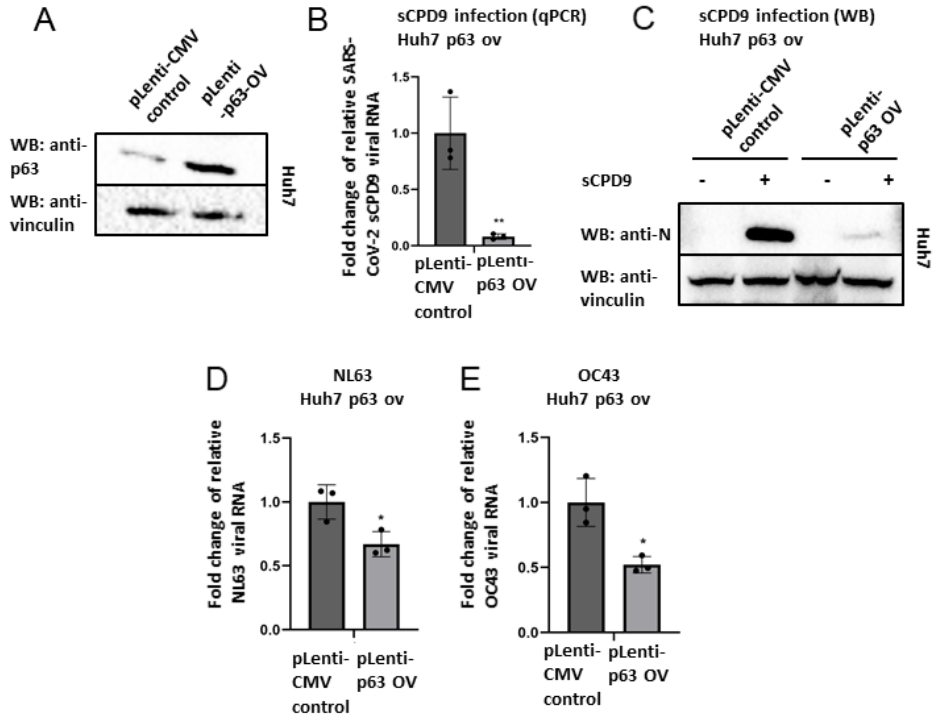

Figure 41. Overexpression of p63 in Huh7 cells suppresses the replication of human coronaviruses. (**A**) Detection of p63 overexpression in Huh7 cells by Western blot analysis. (**B**) sCPD9 replication in Huh7 pLenti-p63-OV cells by qPCR assay. (mean ± SD, Student's t-test, ** P < 0.01). (**C**) sCPD9 replication in Huh7 pLenti-p63-OV cells by Western blot analysis. Huh7 pLenti-p63 OV and control cells were infected with the SARS-CoV-2 virus sCPD9 (MOI: 0.0001). The cells were harvested for Western blot analysis 72 h.p.i., using anti-SARS-CoV-2 nucleocapsid (anti-N) or anti-vinculin antibodies. (**D**) and (**E**) Detection of replication inhibition of mild human coronaviruses in Huh7 pLenti-p63-OV cells by qPCR assays. Huh7 pLenti-p63-

OV and control cells were infected with HCoV-OC43 (MOI=0.1) or HCoV-NL63 (MOI=0.05) as described previously. The cellular RNA was extracted 48 h.p.i. followed by qPCR using viral specific probes and primers (n=3). (mean ± SD, Student's t-test, * P < 0.05, ** P < 0.01).

3.8 RCHY1 targets Nsp13 for polyubiquitination

Our previous Y2H and co-IP results showed that SARS-CoV-2 Nsp13 was another viral protein targeting RCHY1. The absence of catalytical activity of deubiquitination or deISGylation in Nsp13 and the failure of Nsp13 to increase the protein level of RCHY1 (Figure 24) imply entirely different consequences of binding between RCHY1 and Nsp13 compared to binding between RCHY1 and Nsp3. It has been determined that the RCHY1 protein is a substrate of the protease Nsp3; however, it is not a substrate of the RNA helicase Nsp13. A ubiquitinomic analysis reveals that the SARS-CoV-2 Nsp13 protein can be ubiquitinated by host proteins [99]. Given that RCHY1 functions as an E3 ligase capable of targeting multiple host proteins for polyubiquitination, it was investigated whether RCHY1 could also target the SARS-CoV-2 protein Nsp13. The *in vivo* ubiquitination assay combined with RFP-trap based co-IP has demonstrated that RCHY1 induces further ubiquitination of Nsp13 (Figure 42A, lane 2 versus lane 3). Furthermore, the RING finger domain of RCHY1, which possesses E3 ubiquitin ligase activity (RCHY1-RING-del) [38], was deleted. As evidenced in Figure 42B, RCHY1 enhanced the ubiquitination level of Nsp13. However, in the absence of the RING-finger domain, RCHY1 exhibited a partial loss of its capacity to ubiquitinate Nsp13 (compare lanes 2 and 3).

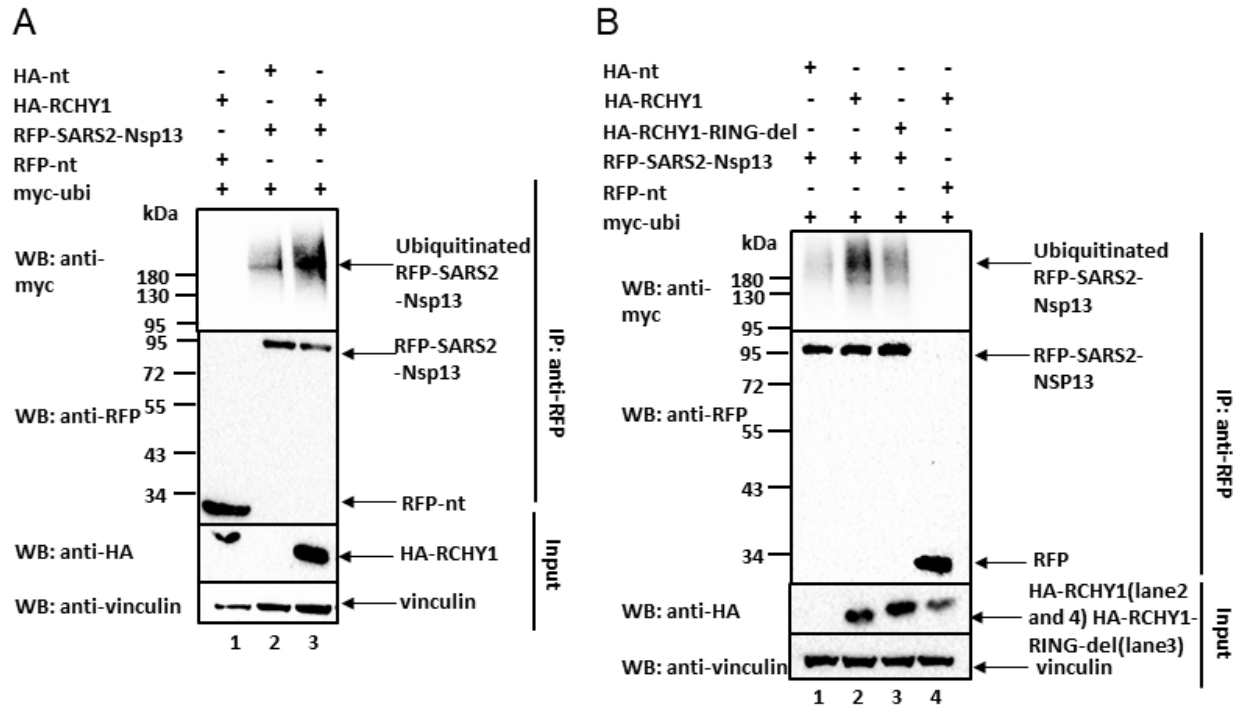

Figure 42. RCHY1 ubiquitinates Nsp13. (**A**) RCHY1 increases the ubiquitination of Nsp13. The indicated plasmids were co-transfected into HEK293 cells. Forty-eight hours after transfection, cells were treated with 10 μM MG132 for 4h. Cells were then lysed and purified by RFP trapping. The ubiquitination level of Nsp13 was analyzed by Western blot on the RFP-eluted samples using an anti-myc antibody**.** (**B**) Reversal of Nsp13-enhanced ubiquitination caused by RCHY1 by the deletion of the RCHY1 catalytic domain. The *in vivo* ubiquitination assay was performed as described in (A). RCHY1-RING-del: RCHY1 without RING finger domain.

Ubiquitin molecules can form polyubiquitin chains by linking through any of the seven lysine residues present in ubiquitin (K6, K11, K27, K29, K33, K48 and K63). It is noteworthy that different linkages can have different functions [100]. K48 and K63 are two common and well-characterized linkage types. In order to investigate the nature of Nsp13 ubiquitination induced by RCHY1, an *in vivo* ubiquitination assay was performed using either wild-type (WT) ubiquitin or ubiquitin variants in which K63 or K48 were substituted with arginine (myc-Ub-K63R, myc-Ub-K48R). The band intensity of ubiquitinated RFP-SARS-CoV-2 Nsp13 was normalized to that of the ubiquitinated endogenous protein due to the variations in ubiquitin variant expression levels. As shown in Figure 43, a reduction in K63-linked ubiquitin chains of Nsp13 was observed in cells transfected with myc-Ub-K63R, but not in cells transfected with myc-Ub-K48R. This result suggests that the ubiquitination of Nsp13 induced by RCHY1 is predominantly of the K63 subtype. In addition, the K48-linked polyubiquitination mediates the target protein degradation [101]. Our previous result has demonstrated that the overexpression of RCHY1 does not result in a reduction of Nsp13 protein levels, which also suggests that the linkage type of Nsp13 ubiquitination caused by RCHY1 should be K63 rather than K48.

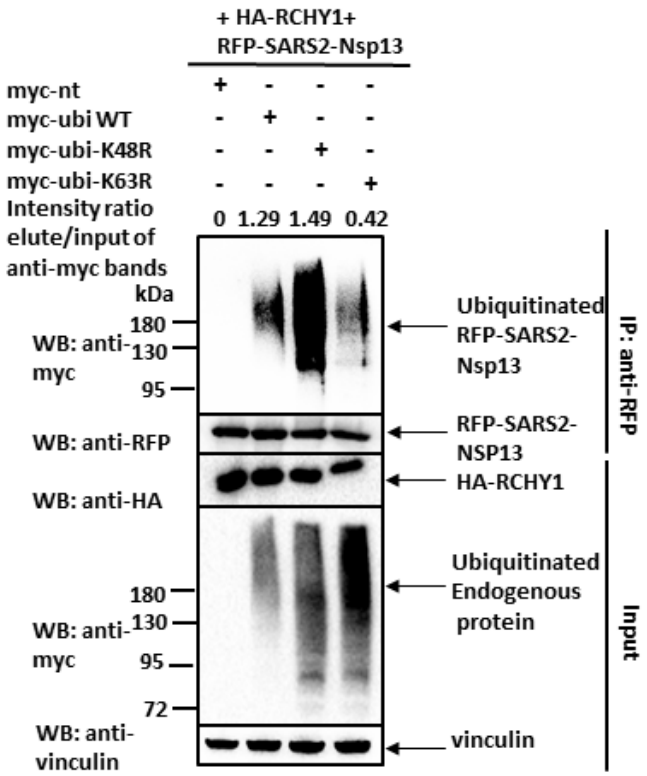

Figure 43. Decrease of Nsp13 ubiquitination by the mutation of K63 to R in ubiquitin. HA-fused RCHY1 and RFP-fused Nsp13 were co-transfected with wild-type ubiquitin or two ubiquitin variants fused to the myc tag. The *in vivo* ubiquitination assay was performed as described previously. The intensity of band quantification was analyzed using ImageJ to calculate the ratio of ubiquitinated RFP-SARS2 Nsp13 to ubiquitinated endogenous protein and ratios were shown as 0, 1.29, 1.49 and 0.42.

In order to verify the hypothesis that modification of Nsp13 with K63 polyubiquitination catalyzed by RCHY1 may favor the virus, a Nsp13-targeting compound, EIS-10700 [70], which clearly disturbed Nsp13 ubiquitination by RCHY1 (Figure 44A), was applied for viral inhibition assay. As a result, the attenuated SARS-CoV-2 sCPD9 viral replication was suppressed by this compound to approximately 25% (Figure 44B), which indicates that K63 ubiquitination of Nsp13 facilitates viral replication. In conclusion, Nsp13 is the substrate of RCHY1 for K63-linked polyubiquitination, which in turn favors viral replication.

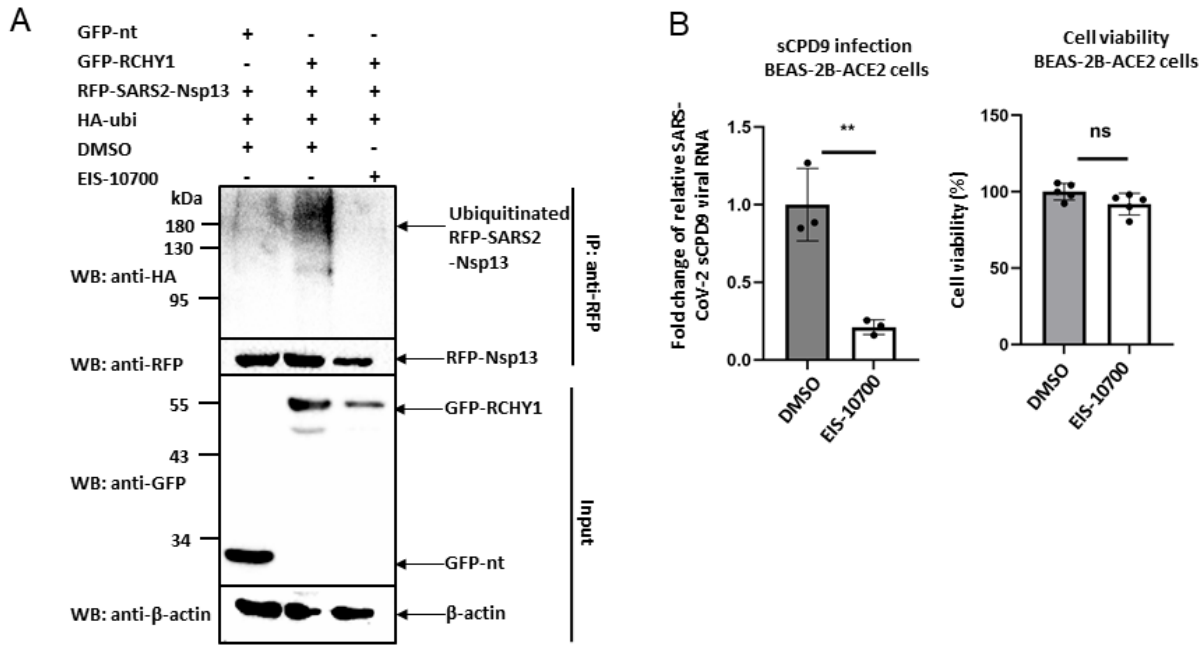

Figure 44. The Nsp13-targeting compound EIS-10700 reduces Nsp13 ubiquitination mediated by RCHY1 and suppresses the replication of the attenuated SARS-CoV-2 virus. (**A**) The indicated plasmids were co-transfected into HEK293 cells cultured in a 6-well plate. Following a 4-hour period of transfection, the cells were treated with 20 μM of the Nsp13-targeting compound EIS-10700 or with the same volume of DMSO. The cells were harvested for an *in vivo* ubiquitination assay 48 hours after the transfection process, as previously described. (**B**) Left: BEAS-2B-ACE2 cells were infected with attenuated SARS-CoV-2 virus sCPD9 (MOI: 0.0001). The cells were washed twice with DPBS 2 h.p.i. and supplied with fresh growth medium containing 20 μM EIS-10700 or DMSO. The cells were harvested for RNA isolation 48 h.p.i., followed by qPCR using specific probes and primers for the SARS-CoV-2 virus nucleocapsid (n=3). Right: the cell viability of BEAS-2B-ACE2 cells treated with 20 μM EIS-10700 or DMSO for 48 hours. (n=5). (mean ± SD, Student's t-test, ** $P < 0.01$, ns: not significant).

3.9 The effect of co-expression of Nsp13 and RCHY1

3.9.1 Co-expression of Nsp13 and RCHY1 does not influence IFN-β signaling

It is reported that Nsp13 can influence type I IFN signaling [102, 103] and NF-κB signaling [104] in the host. To explore if the interaction of Nsp13 and RCHY1 influenced the Nsp13-mediated signaling pathway, a firefly luciferase assay to assess the activation of the IFN-β promoter was performed initially. Figure 45 showed that Nsp13 inhibited IFN-β luciferase reporter activity significantly (bars 1 and 2). However, in the presence of RCHY1, the IFN-β activity remained unchanged (bars 3 and 4).

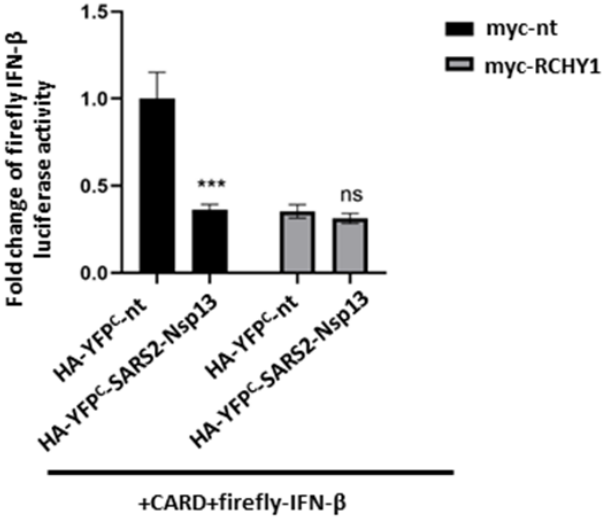

Figure 45. Co-expression of Nsp13 and RCHY1 does not alter IFN-β activity. HEK293 cells were transfected with myc empty vector or myc-fused RCHY1, HA-YFP^c empty vector or HA-YFP^c-fused Nsp13 together with IFN-β-firefly-luc and CARD in a 48-well plate. Twenty-four hours after transfection, cells were harvested for firefly luciferase assay (n=5). (mean ± SD, 2-way ANOVA, *** P < 0.001, ns: not significant).

3.9.2 Nsp13 inhibits NF-κB pathway in the presence of RCHY1

Besides, whether RCHY1 or ubiquitination catalyzed by RCHY1 has an effect on Nsp13-mediated NF-κB inhibition was investigated. As demonstrated in Figure 46A, only in the presence of RCHY1 did Nsp13 significantly reduce the luciferase activity of pELAM firefly luciferase, the reporter of the NF-κB signaling pathway [86]. Additionally, the mRNA level of tumor necrosis factor-alpha (TNFα), the target gene that can be induced by NF-kB signaling pathway [105], was decreased when RCHY1 and Nsp13 were co-transfected (Figure 46B). These results indicate that Nsp13 downregulates the NF-κB pathway only in the presence of RCHY1.

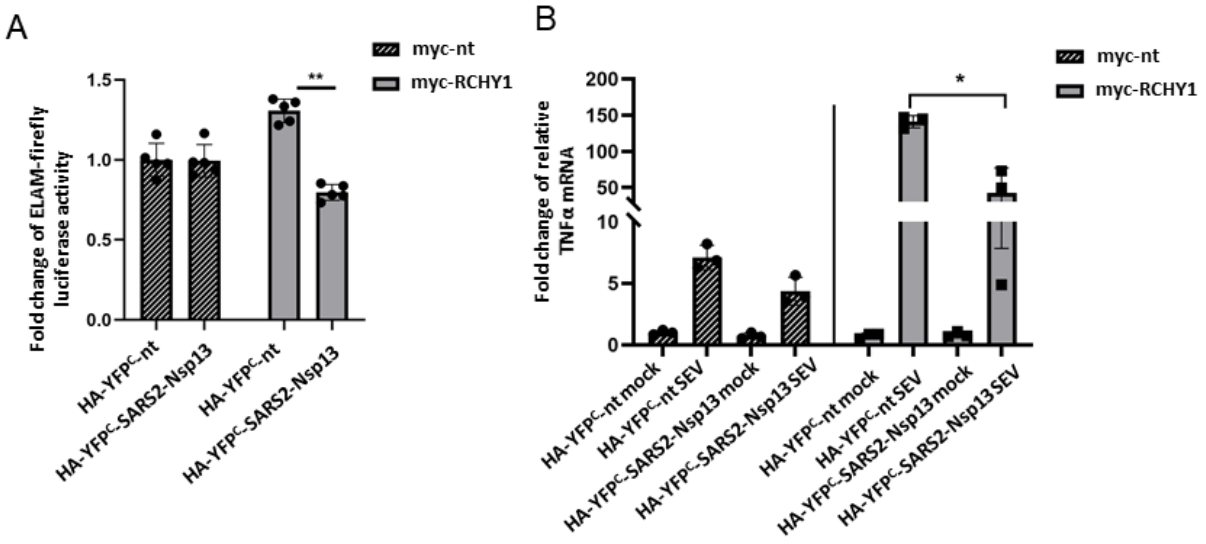

Figure 46. Nsp13 inhibits the NF-κB pathway in the presence of RCHY1. (**A**) Inhibition of NF-κB signaling by co-expression of Nsp13 and RCHY1. To activate NF-κB signaling, the reporter pELAM-firefly luciferase and the plasmid pcmv4-p65 overexpressing p65 were co-transfected with indicated plasmids into HEK293 cells seeded into a 96-well plate. The level of luciferase activity was determined 24 hours post-transfection. The Firefly luciferases of each group were normalized to the HA-YFP^c empty + myc empty vector group (n=5). (**B**) Inhibition of endogenous TNF-α mRNA by co-expression of Nsp13 and RCHY1. HEK293 cells were transfected with indicated plasmids. Three hours after transfection, cells were infected with SEV (50 HAU/ml) to induce the NF-kB pathway. 24 hours after transfection, cells were harvested for RNA isolation followed by qPCR. TNF-α mRNA was normalized to β-actin (n=3). (mean ± SD, 2-way ANOVA, *P < 0.05, **P < 0.01).

3.9.3 The presence of RCHY1 does not influence the subcellular localization of Nsp13

It has been reported that K63 linkage ubiquitination influences the subcellular localization of the target proteins [106, 107]. Therefore, whether the presence of RCHY altered the subcellular localization of Nsp13 was explored. As shown in Figure 47, GFP-Nsp13 was located in both nuclear and cytosol when it was co-expressed with RFP empty vector control. In the presence of RCHY1, the subcellular localization of GFP-Nsp13 remained relatively unchanged compared with the empty vector group.

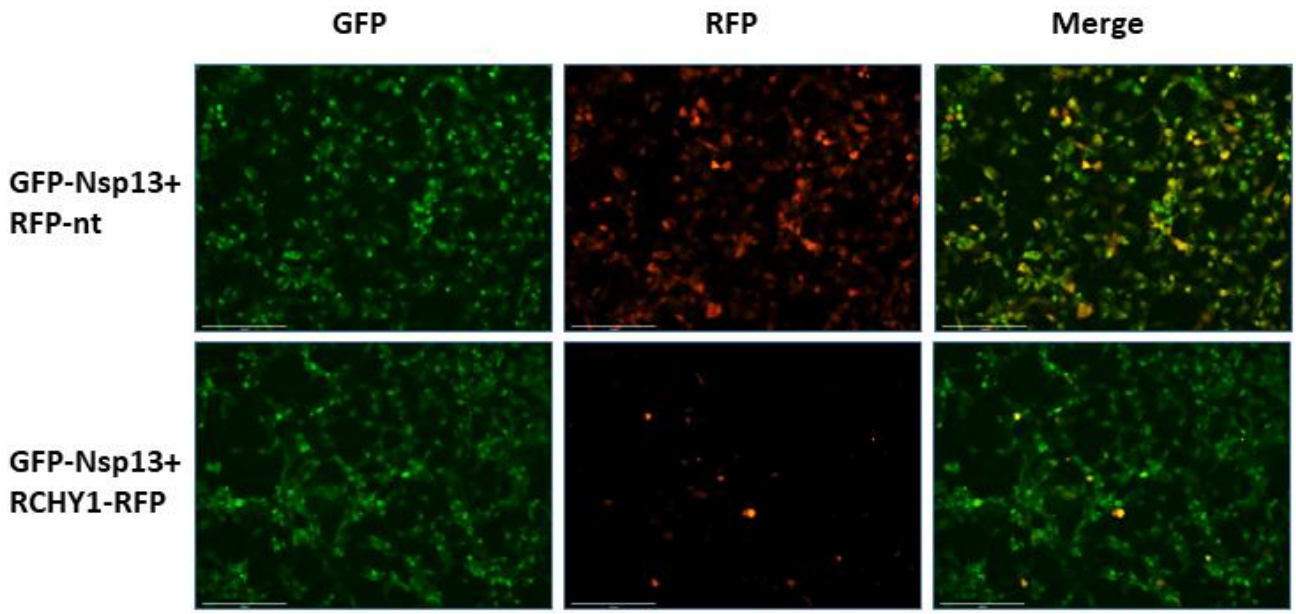

Figure 47. RCHY1 does not alter Nsp13 subcellular localization. HEK293 cells were transfected with plasmids encoding GFP-SARS-CoV-2 Nsp13 together with RFP-nt or RFP-RCHY1. Forty-eight hours after transfection, cells were fixed with 4% PFA for 15 minutes and observed with a fluorescence microscope (Leica DM4000 B, 20xobjective). Scale bar: 150 μm.

4. Discussion

4.1 The mechanism of how Nsp3 stimulates RCHY1 protein expression

In SARS-CoV, the Nsp3 subdomains SUD and PLpro stimulate RCHY1 accumulation [42], but the underlying mechanism remains unknown from our previous study. Here, the mechanism by which SARS-CoV-2 Nsp3 enhances RCHY1 expression is identified. Ribopuromycylation assay suggests that Nsp3 enhances the newly generated RCHY1. In addition, Nsp3 stabilizes RCHY1 in the CHX-chase assay and the PLpro domain of Nsp3 inhibits RCHY1 polyubiquitination for RCHY further degradation. Thus, RCHY1 enhancement occurs through two key aspects: First, Nsp3 increases RCHY1 protein translation. Second, Nsp3 suppresses the degradation of the RCHY1 protein. SUD is absent from catalytic deubiquitination activity but possesses RNA-binding capabilities and forms a complex with PAIP1 and PABP, both of which are crucial for translation initiation, to stimulate translation [73, 95, 108]. It is hypothesized that SUD is attributable to the elevated protein biosynthesis of RCHY1 by recruiting additional translation factors. Therefore, SUD alone also induces RCHY1 expression (Figure 23) without being able to reduce the ubiquitination level of RCHY1 (Figure 29).

In addition, *the in vivo* ubiquitination assay shows that PLpro deubiquitinates RCHY1, which is dependent on its catalytic activity. The mutation in the catalytic domain of PLpro leads to a reduced increase in RCHY1 protein levels (Figure 30). Therefore, the reduction in RCHY1 protein degradation is at least partly due to the deubiquitinating activity of PLpro within Nsp3. A slight increase in the RCHY1 protein level was observed in the PLpro ca group in comparison with the empty vector group. Furthermore, PLpro ca still displays a binding affinity for RCHY1 (Figure 29). Therefore, the binding between PLpro ca and RCHY1 might disturb the interaction of other E3 ligases targeting RCHY1 to decrease RCHY1 protein degradation and stabilize RCHY1.

4.2 The role of p53 and p63 in virus replication

4.2.1 P53

Several studies have shown that p53 functions as a host restriction factor against coronaviruses. Porcine Epidemic Diarrhea Virus (PEDV) is a highly contagious enteric pathogen of the coronavirus family. The PEDV N protein can recruit the E3 ubiquitin ligase COP1, inhibiting COP1 self-ubiquitination and protein degradation. This process enhances COP1-mediated degradation of p53, effectively abolishing p53 activity [109].

The PLP2 domain of non-structural protein 3 from the human coronavirus NL63 stabilizes the E3 ubiquitin ligase MDM2, leading to the degradation of its target, p53. As a result, the p53-mediated innate immune response is inactivated during NL63 infection [110]. In previous research, our laboratory demonstrated the successful inhibition of p53 on SARS-CoV [42]. However, it remains unclear whether p53 functions as an antiviral factor against SARS-CoV-2 and the specific molecular mechanisms involved. This work identifies the interaction between SARS-CoV-2 Nsp3 and RCHY1. As a result, Nsp3 facilitates the increase in RCHY1 protein expression, thereby promoting the degradation of its target, p53. Direct evidence for p53 inhibition of SARS-CoV-2 replication in human bronchial epithelial cells is provided, which is one of the first studies to our knowledge. It would have been desirable to confirm the effect of Nsp3 on p53 in the RCHY1 knockout cell line. Unfortunately, the construction of this cell line was not successful due to the low expression of endogenous RCHY1, which cannot be detected by a variety of RCHY1 antibodies.

The reason why p53 performs antiviral activity is not fully understood. The underlying mechanism is most likely attributable to the function of p53 as a transcription factor, which has been demonstrated to induce the expression of genes involved in host defense responses such as Interferon regulatory factor 7 (IRF7), which can mediate IFN-β expression [111]. In addition, p53 has the ability to induce apoptosis by activation of the pro-apoptotic proteins PUMA and NOXA [112]. The deficiency of the regulation of the apoptotic process has been demonstrated to facilitate viral infection [113]. For instance, Cytomegalovirus protein UL38 plays a pivotal role in the inhibition of apoptosis induced by ER stress during virus infection. UL38 has been shown to suppress the activation of c-Jun N-terminal kinase, and then enhance the expression of anti-apoptotic BCL-2 and decrease pro-apoptotic BH3 indirectly [114, 115]. Therefore, it is hypothesized that the reduction in p53 triggered by SARS-CoV-2 infection can prevent cells from undergoing apoptosis, thereby facilitating virus replication.

4.2.2 P63

In addition to p53, another substrate of RCHY1, full-length p63, was observed to be regulated by Nsp3. Both p63 and p53 are members of the p53 transcription factor family, the DNA binding domains of p63 and p53 share 65% sequence identity [98], indicating that they can bind to similar DNA sequences and regulate overlapping sets of target genes. p63 has the ability to induce cellular senescence and suppress sarcoma development like p53 [62], suggesting that p53 and p63 may have similar functions in cellular progression or tumor development. However, little is known about the role of p63 in virus replication, especially in RNA viruses. This study suggests that p63, like p53, can inhibit mild human coronavirus infection. It has been shown that p63 can target and upregulate the expression of the vitamin D receptor (VDR) [116], which

plays a critical role in regulating anti-inflammatory responses [117], which may explain how p63 suppresses the replication of mild human coronaviruses. The effect of p63 on the SARS-CoV-2 varies between cell lines, and the reason for this is not yet clear.

Unlike p53, p63 exists in multiple isoforms, which can exhibit opposing functions. For instance, ΔNp63, which lacks the N-terminal transactivation domain [118], contributes to cancer development, whereas the full length of p63 (TAp63) functions as a tumor suppressor, similar to p53 [119]. The role of ΔNp63 and TAp63 might also be different in coronaviruses. ΔNp63 was observed to inhibit double-strand RNA sensing and suppress the induction of antiviral interferon regulatory factor 1 (IRF1) signaling [120, 121], which suggests that ΔNp63 might facilitate virus replication. It is important to note that basal cells of the normal human epithelium which include the epidermis, strongly express p63 proteins, predominantly the ΔNp63 isotype. The ratio of ΔNp63 to TAp63 is approximately 100:1 [122]. Therefore, it is hypothesized that the ΔNp63 isotype is more abundant in BEAS-2B cell line which is human epithelial cell, while hepatocytes such as Huh7 cells might express lower levels of ΔNp63. Although the construction of p63 overexpressed cell line was performed using the pLenti CMV plasmid expressing TAp63, the expression level of TAp63 might not be abundant compared with that of ΔNp63 in the BEAS-2B cell line. Given that ΔNp63 and TAp63 exhibit opposing functions, it is important to determine the relative abundance of these isoforms in different cell lines. Furthermore, the observed variations could be due to other factors such as different ACE2 receptor expression and basal RCHY1 levels in different cell lines.

Another explanation might be that although SARS-CoV-2 Nsp3 reduces p63 via RCHY1 from my result, it cannot be excluded the possibility that other SARS-CoV-2 proteins might increase or utilize p63 to facilitate their replication during SARS-CoV-2 infection.

4.3 P53, p63 and RCHY1 are SARS-CoV-2 Nsp3 substrates for deISGylation

A common mechanism by which viral proteases modulate innate immune pathways involves the antagonism of ubiquitin and ubiquitin-like modifications [123, 124]. ISG15, a ubiquitin-like (Ubl) modification, is upregulated in response to viral infection [125]. Furthermore, ISGylation of various proteins associated with antiviral defense, including IRF3 [126], STAT1 [127], and MDA5 [27], has been observed to potentiate immune response signaling.

The removal of ISG15 is facilitated by a limited number of cellular enzymes, allowing this modification to act as a virus-induced danger signal and positively regulate viral infection [26]. Research has shown that the HCMV tegument protein UL26 is critical for evading ISG15-associated antiviral responses by inhibiting protein ISGylation [51].

In addition, OTU domain-containing proteases from Crimean Congo haemorrhagic fever virus (CCHFV) exhibit a function analogous to PLpro, facilitating the reduction of ISGylated proteins. The OTU domain counteracts the protective effect of ISG15 in mice [128]. In SARS-CoV-2, PLpro was reported to significantly reduce the activation of the interferon response, a process dependent on the deISGylation activity of PLpro [25]. Only a limited number of host proteins have been identified as substrates of SARS-CoV-2 PLpro. Our results show that SARS-CoV-2 PLpro deISGylates the host proteins p53 and p63, which have antiviral effects against human coronaviruses. ISGylation of p53 has been demonstrated to enhance p53 transactivity and promote the expression of p53-induced genes, as well as apoptosis [129]. Hence, it is speculated that the deISGylation of p53 caused by SARS-CoV-2 Nsp3 might impair the transcriptional induction of p53-induced genes crucial for host defense. DeISGylation of p63 might have similar consequences in support of the virus. Furthermore, the deISGylation of p53 and p63 can increase their availability for their ubiquitination by RCHY1. In this way, the virus can cause maximal degradation of p53 and p63.

In addition, RCHY1 is identified as the substrate of PLpro in this study, as RCHY1 can be deubiquitinated and deISGylated by PLpro, which is dependent on the activity of the PLpro catalytic domain. Our research is one of the first to show that the human E3 ligase RCHY1 can serve as a direct substrate for SARS-CoV-2 PLpro. The influence of deISGylation of RCHY1 by PLpro remains unclear. Whether this modification affects RCHY1 turnover, the E3 ligase activity of RCHY1, and its regulation of substrates remains unknown and requires further research.

4.4 RCHY1 targets Nsp13 for K63-linked ubiquitination

The role of post-translational modifications in SARS-CoV-2 proteins is of considerable importance but remains largely unknown despite previous research [90]. In this study, the interaction between RCHY1 and another non-structural protein Nsp13 which is an RNA helicase that is highly conserved among SARS viruses [130], was discovered. As a result, RCHY1 increases the level of ubiquitination of Nsp13, a process that depends on the E3 ligase activity of RCHY1. Since RCHY1 does not reduce the protein expression of Nsp13, and considering that K63-linked ubiquitination is typically non-degradative, it is speculated that K63 is the primary linkage type for Nsp13 ubiquitination induced by RCHY1. This was confirmed by an *in vivo* ubiquitination assay using the K63R mutant. K63-linked ubiquitination affects (1) the protein interaction between Nsp13 and other SARS-CoV-2 proteins and (2) the enzyme activity of Nsp13. As Nsp13 is a helicase, to confirm this, Nsp13 and RCHY1 can be purified and the *in vitro* enzyme activity assay can be designed to exclude the disruption of other host proteins in future study. (3) the SARS-CoV-2 virus replication. The envelope protein (E) of Zika

virus (ZIKV) is polyubiquitinated by the human E3 ubiquitin ligase TRIM7 via K63-linked polyubiquitination. This modification enhances ZIKV replication both in cells and *in vivo* [131]. In SARS-CoV-2, the mutation of three specific sites on the spike protein (K310R, K986R, and K1028R), which prevents further ubiquitination, can inhibit spike protein cleavage and reduce the infection of SARS-CoV-2 pseudoviruses [99]. Therefore, it is speculated that RCHY1-induced ubiquitination of Nsp13 may play a role in SARS-CoV-2 replication. The result of this study has demonstrated that the Nsp13-targeting compound disturbing K63-linked ubiquitination of Nsp13 by RCHY1 suppresses SARS-CoV-2 attenuated virus sCPD9 replication, which supports our hypothesis. To confirm this, future work will focus on the identification of the specific lysine sites in Nsp13 that can be ubiquitinated by RCHY1. The subsequent mutagenesis of these sites within the SARS-CoV-2 genome will provide valuable insights into their influence on virus replication and virulence.

4.5 The role of co-expression of Nsp13 and RCHY1 in NF-kB pathway

The NF-κB signaling pathway is crucial for mediating host defense mechanisms against microbial pathogens. To attenuate host inflammatory and immune responses, some viral proteins evolve strategies to suppress the NF-κB pathway and facilitate viral replication [132]. For example, the F317L protein of the African swine fever virus (ASFV) interacts with IκB kinase β (IKKβ) and inhibits its phosphorylation, leading to a subsequent reduction in both the phosphorylation and ubiquitination of IκBα, thereby enhancing its stabilization [133]. In human coronavirus, the membrane (M) protein of SARS-CoV interacts with IKKβ, a key regulatory kinase that triggers NF-κB activation, thereby inhibiting TNFα-induced NF-κB activation, which may facilitate SARS pathogenesis [134]. In addition, SARS-CoV and SARS-CoV-2 PLpro reduce nuclear p65 levels and suppress the NF-kB signaling pathway in A549 cells [25]. The results in this study demonstrate that only in the presence of RCHY1, SARS-CoV-2 Nsp13 can inhibit NF-kB signaling and the downstream target TNFα, which suggests Nsp13 utilizes RCHY1 to further inhibit the NF-κB pathway, thereby antagonizing the host defense.

My findings suggest a novel regulatory mechanism where SARS-CoV-2 Nsp13 inhibits NF-κB signaling through RCHY1, rather than directly targeting IKKβ or p65 as seen in other viral proteins. Unlike the F317L protein of ASFV and SARS-CoV M protein, which interact with IKKβ to prevent its activation, Nsp13 appears to exploit host protein RCHY1 to modulate NF-κB signaling. This suggests that SARS-CoV-2 may have evolved a more complicated mechanism to evade host immunity, potentially offering new insights into viral pathogenesis.

Moreover, these findings give rise to the intriguing possibility that targeting the Nsp13-RCHY1 interaction could serve as a novel therapeutic strategy for COVID-19. Future studies should investigate whether disrupting this interaction can restore NF-κB activation and enhance antiviral immune responses. Additionally, given the role of RCHY1 in protein ubiquitination, further exploration of its broader regulatory network may reveal new insights into viral immune evasion strategies and potential drug targets.

4.6 The relationship between SARS-CoV-2 infection and tumor initiation

It has been demonstrated that oncovirus infection causes 15-20% of human cancers worldwide [135]. Several viruses have been shown to promote tumorigenesis in humans, such as DNA viruses HPV [136], hepatitis B viruses [137], Epstein-Barr virus [138], and RNA virus hepatitis C viruses [139], human T-cell leukemia virus 1 (HTLV-1) [140]. The Tax protein of HTLV-1 has been observed to activate cellular proto-oncogenes, including c-Myc and facilitates the development of adult T-cell leukemia/lymphoma [141].

This study has demonstrated that infection of normal human bronchial epithelial cells BEAS-2B-ACE2 with SARS-CoV-2 results in a decline in the level of tumor suppressor p53. This observation indicates a possible association between SARS-CoV-2 infection and the induction of tumor formation in non-cancerous cells. In addition, the deISGylation of p53 by Nsp3 has been shown to enhance this possibility, given that ISGylation of p53 has been demonstrated to suppress tumourigenesis [129]. It's important to note that RCHY1 has been reported as an oncogene in human non-small cell lung carcinoma cells. The elevated expression of the RCHY1 is significantly associated with a poor survival rate in patients diagnosed with lung cancer [142]. Therefore, it is hypothesized that during SARS-CoV-2 infection, Nsp3 decreases the tumor suppressor p53 via the stimulation of oncogene RCHY1. This mechanism might be similar to how HPV infection suppresses p53. The HPV E6 protein has been observed to bind to the host protein E6-AP to form a complex. This E6-E6-AP complex functions as an E3 ligase, which could target p53 for rapid ubiquitin-dependent degradation [143].

Since SARS-CoV-2 has become a seasonal virus, for patients who are infected with SARS-CoV-2 frequently or with long COVID, the persisting reduction of p53 might increase the risk of lung cancer initiation.

4.7 Conclusion

In conclusion, the results of this work indicate that SARS-CoV-2 Nsp3 increases RCHY1 protein expression not only by increasing RCHY1 translation but also decreasing RCHY1 protein degradation. The enhanced RCHY1 counteracts the antiviral factors p53 and p63. Moreover, the deISGylations of p53 and p63 caused by Nsp3 are speculated to compromise the transcriptional induction of p53 and p63-induced genes which are important for host defense.

In addition, in the context of RCHY1 being increased by Nsp3, another SARS-CoV-2 protein Nsp13 is further ubiquitinated via K63-link by RCHY1. The presence of RCHY1 or K63 ubiquitination of Nsp13 caused by RCHY1, has been demonstrated to inhibit the NF-κB pathway, thereby counteracting the host immune response (Figure 48). Our research contributes to a deeper understanding of the pathogenesis of SARS-CoV-2 and paves the way for the exploration of new therapeutic targets against SARS-CoV-2 infections.

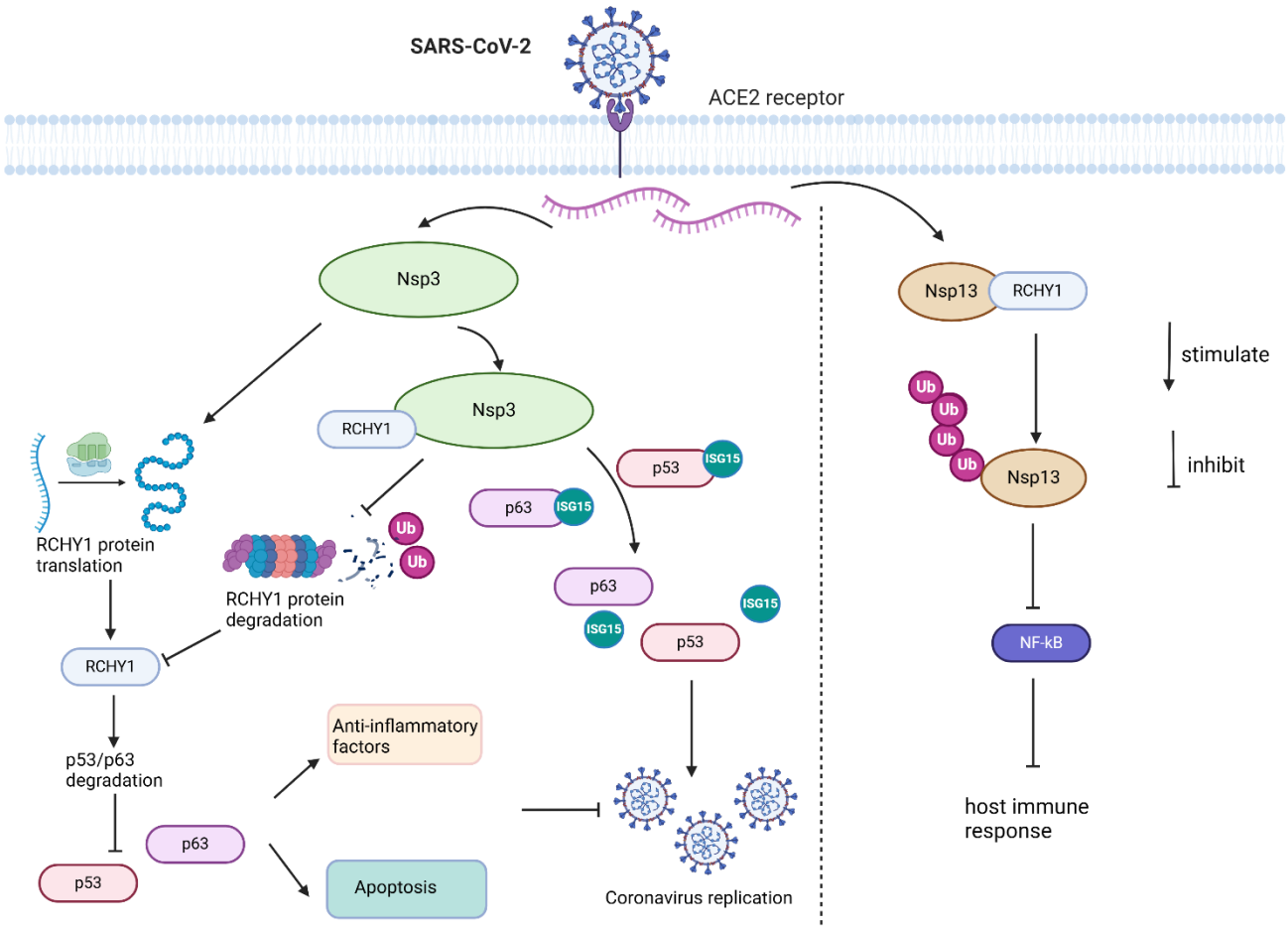

Figure 48. Schematic illustration of how SARS-CoV-2 Nsp3 and Nsp13 exploit RCHY1 to suppress antiviral defense. Left: The signaling model of how Nsp3 counteracts the effects of viral inhibitors p53 and p63. Upon infection with SARS-CoV-2, Nsp3 stimulates RCHY1 protein expression, leading to the degradation of the RCHY1 substrates p53 and p63. These are antiviral factors against coronaviruses. The reduction of these antiviral factors by Nsp3 has been demonstrated to reduce anti-inflammatory factors and apoptosis, thereby facilitating virus replication. In addition, Nsp3 deISGylates p53 and p63, which may also play a role in antagonizing host defenses. The deISGylation of p53 and p63 enhances their availability for RCHY1 to make the mechanism that RCHY1 degrades p53 and p63 optimal. Right: The proposed mechanistic model of how SARS-CoV-2 Nsp13 suppresses the NF-kB pathway. Nsp13 is targeted by RCHY1 for K63-linked ubiquitination and inhibits the NF-kB pathway. (Created with BioRender).

References

1. WHO. Number of COVID-19 deaths reported to WHO. 2025 [updated 2025-03-30; cited 2025 16 April]. Available from: https://data.who.int/dashboards/covid19/deaths?n=o.

2. Pradhevi L, Soegiarto G, Wulandari L, Lusida MA, Saefudin RP, Vincent A. More severe comorbidities, advanced age, and incomplete vaccination increase the risk of COVID-19 mortality. Narra J. 2024;4(2):e949.

3. Robineau O, Zins M, Touvier M, Wiernik E, Lemogne C, de Lamballerie X, Blanché H, Deleuze JF, Saba Villarroel PM, Dorival C, Nicol J, Gomes-Rima R, Correia E, Coeuret-Pellicer M, Druesne-Pecollo N, Esseddik Y, Ribet C, Goldberg M, Severi G, Carrat F. Long-lasting Symptoms After an Acute COVID-19 Infection and Factors Associated With Their Resolution. JAMA Netw Open. 2022;5(11):e2240985.

4. Chan JF, Yuan S, Chu H, Sridhar S, Yuen KY. COVID-19 drug discovery and treatment options. Nat Rev Microbiol. 2024;22(7):391-407.

5. Liu DX, Liang JQ, Fung TS. Human Coronavirus-229E, -OC43, -NL63, and -HKU1 (Coronaviridae). In: Bamford DH, Zuckerman M, editors. Encyclopedia of Virology (Fourth Edition). Oxford: Academic Press; 2021. p. 428-40.

6. Wu F, Zhao S, Yu B, Chen YM, Wang W, Song ZG, Hu Y, Tao ZW, Tian JH, Pei YY, Yuan ML, Zhang YL, Dai FH, Liu Y, Wang QM, Zheng JJ, Xu L, Holmes EC, Zhang YZ. A new coronavirus associated with human respiratory disease in China. Nature. 2020;579(7798):265-9.

7. Kim D, Lee JY, Yang JS, Kim JW, Kim VN, Chang H. The Architecture of SARS-CoV-2 Transcriptome. Cell. 2020;181(4):914-21.e10.

8. Naqvi AAT, Fatima K, Mohammad T, Fatima U, Singh IK, Singh A, Atif SM, Hariprasad G, Hasan GM, Hassan MI. Insights into SARS-CoV-2 genome, structure, evolution, pathogenesis and therapies: Structural genomics approach. Biochim Biophys Acta Mol Basis Dis. 2020;1866(10):165878.

9. McBride R, van Zyl M, Fielding BC. The coronavirus nucleocapsid is a multifunctional protein. Viruses. 2014;6(8):2991-3018.

10. Schoeman D, Fielding BC. Is There a Link Between the Pathogenic Human Coronavirus Envelope Protein and Immunopathology? A Review of the Literature. Front Microbiol. 2020;11:2086.

11. Hassan SS, Choudhury PP, Roy B. SARS-CoV2 envelope protein: non-synonymous mutations and its consequences. Genomics. 2020;112(6):3890-2.

12. Rahman MS, Hoque MN, Islam MR, Akter S, Rubayet Ul Alam ASM, Siddique MA, Saha O, Rahaman MM, Sultana M, Crandall KA, Hossain MA. Epitope-based chimeric peptide vaccine design against S, M and E proteins of SARS-CoV-2, the etiologic agent of COVID-19 pandemic: an in silico approach. PeerJ. 2020;8:e9572.

13. Carvajal JJ, García-Castillo V, Cuellar SV, Campillay-Véliz CP, Salazar-Ardiles C, Avellaneda AM, Muñoz CA, Retamal-Díaz A, Bueno SM, González PA, Kalergis AM, Lay MK. New insights into the pathogenesis of SARS-CoV-2 during and after the COVID-19 pandemic. Front Immunol. 2024;15:1363572.

14. Lei J, Kusov Y, Hilgenfeld R. Nsp3 of coronaviruses: Structures and functions of a large multi-domain protein. Antiviral Res. 2018;149:58-74.

15. Li M, Ye G, Si Y, Shen Z, Liu Z, Shi Y, Xiao S, Fu ZF, Peng G. Structure of the multiple functional domains from coronavirus nonstructural protein 3. Emerg Microbes Infect. 2021;10(1):66-80.

16. Oudshoorn D, Rijs K, Limpens R, Groen K, Koster AJ, Snijder EJ, Kikkert M, Bárcena M. Expression and Cleavage of Middle East Respiratory Syndrome Coronavirus nsp3-4 Polyprotein Induce the Formation of Double-Membrane Vesicles That Mimic Those Associated with Coronaviral RNA Replication. mBio. 2017;8(6).

17. Wolff G, Melia CE, Snijder EJ, Bárcena M. Double-Membrane Vesicles as Platforms for Viral Replication. Trends Microbiol. 2020;28(12):1022-33.

18. Angelini MM, Akhlaghpour M, Neuman BW, Buchmeier MJ. Severe acute respiratory syndrome coronavirus nonstructural proteins 3, 4, and 6 induce double-membrane vesicles. mBio. 2013;4(4).

19. Versteeg GA, Bredenbeek PJ, van den Worm SH, Spaan WJ. Group 2 coronaviruses prevent immediate early interferon induction by protection of viral RNA from host cell recognition. Virology. 2007;361(1):18-26.

20. Zhou H, Perlman S. Mouse hepatitis virus does not induce Beta interferon synthesis and does not inhibit its induction by double-stranded RNA. J Virol. 2007;81(2):568-74.

21. Minkoff JM, tenOever B. Innate immune evasion strategies of SARS-CoV-2. Nat Rev Microbiol. 2023;21(3):178-94.

22. Snijder EJ, Bredenbeek PJ, Dobbe JC, Thiel V, Ziebuhr J, Poon LL, Guan Y, Rozanov M, Spaan WJ, Gorbalenya AE. Unique and conserved features of genome and proteome of SARS-coronavirus, an early split-off from the coronavirus group 2 lineage. J Mol Biol. 2003;331(5):991-1004.

23. Tan J, Vonrhein C, Smart OS, Bricogne G, Bollati M, Kusov Y, Hansen G, Mesters JR, Schmidt CL, Hilgenfeld R. The SARS-unique domain (SUD) of SARS coronavirus contains two macrodomains that bind G-quadruplexes. PLoS Pathog. 2009;5(5):e1000428.

24. Xie S, Song Z, Chen R, Zhang X, Wu S, Chen J, Huang P, Liu H, Yu K, Zhang Y, Tan S, Liu J, Ma X, Zhang H, He X, Pan T. The SARS-unique domain (SUD) of SARS-CoV-2 nsp3 protein inhibits the antiviral immune responses through the NF-κB pathway. J Med Virol. 2024;96(10):e70007.

25. Shin D, Mukherjee R, Grewe D, Bojkova D, Baek K, Bhattacharya A, Schulz L, Widera M, Mehdipour AR, Tascher G, Geurink PP, Wilhelm A, van der Heden van Noort GJ, Ovaa H, Müller S, Knobeloch KP, Rajalingam K, Schulman BA, Cinatl J, Hummer G, Ciesek S, Dikic I. Papain-like protease regulates SARS-CoV-2 viral spread and innate immunity. Nature. 2020;587(7835):657-62.

26. Klemm T, Ebert G, Calleja DJ, Allison CC, Richardson LW, Bernardini JP, Lu BG, Kuchel NW, Grohmann C, Shibata Y, Gan ZY, Cooney JP, Doerflinger M, Au AE, Blackmore TR, van der Heden van Noort GJ, Geurink PP, Ovaa H, Newman J, Riboldi-Tunnicliffe A, Czabotar PE, Mitchell JP, Feltham R, Lechtenberg BC, Lowes KN, Dewson G, Pellegrini M, Lessene G, Komander D. Mechanism and inhibition of the papain-like protease, PLpro, of SARS-CoV-2. Embo j. 2020;39(18):e106275.

27. Liu G, Lee JH, Parker ZM, Acharya D, Chiang JJ, van Gent M, Riedl W, Davis-Gardner ME, Wies E, Chiang C, Gack MU. ISG15-dependent activation of the sensor

MDA5 is antagonized by the SARS-CoV-2 papain-like protease to evade host innate immunity. Nat Microbiol. 2021;6(4):467-78.

28. Newman JA, Douangamath A, Yadzani S, Yosaatmadja Y, Aimon A, Brandão-Neto J, Dunnett L, Gorrie-Stone T, Skyner R, Fearon D, Schapira M, von Delft F, Gileadi O. Structure, mechanism and crystallographic fragment screening of the SARS-CoV-2 NSP13 helicase. Nat Commun. 2021;12(1):4848.

29. Xia H, Cao Z, Xie X, Zhang X, Chen JY, Wang H, Menachery VD, Rajsbaum R, Shi PY. Evasion of Type I Interferon by SARS-CoV-2. Cell Rep. 2020;33(1):108234.

30. Fung SY, Siu KL, Lin H, Chan CP, Yeung ML, Jin DY. SARS-CoV-2 NSP13 helicase suppresses interferon signaling by perturbing JAK1 phosphorylation of STAT1. Cell Biosci. 2022;12(1):36.

31. Fung TS, Liu DX. Post-translational modifications of coronavirus proteins: roles and function. Future Virol. 2018;13(6):405-30.

32. de Bie P, Ciechanover A. Ubiquitination of E3 ligases: self-regulation of the ubiquitin system via proteolytic and non-proteolytic mechanisms. Cell Death Differ. 2011;18(9):1393-402.

33. Dong Y, Chen Y, Ma G, Cao H. The role of E3 ubiquitin ligases in bone homeostasis and related diseases. Acta Pharm Sin B. 2023;13(10):3963-87.

34. Hua F, Hao W, Wang L, Song K, Hasan A, Wu Y, Li K, Lin Z, Sun Y, Li S. Linear ubiquitination mediates coronavirus NSP14-induced NF-κB activation. Cell Commun Signal. 2024;22(1):573.

35. Yu M, Li J, Gao W, Li Z, Zhang W. Multiple E3 ligases act as antiviral factors against SARS-CoV-2 via inducing the ubiquitination and degradation of ORF9b. J Virol. 2024;98(6):e0162423.

36. Freemont PS, Hanson IM, Trowsdale J. A novel cysteine-rich sequence motif. Cell. 1991;64(3):483-4.

37. Bailly V, Lauder S, Prakash S, Prakash L. Yeast DNA repair proteins Rad6 and Rad18 form a heterodimer that has ubiquitin conjugating, DNA binding, and ATP hydrolytic activities. J Biol Chem. 1997;272(37):23360-5.

38. Leng RP, Lin Y, Ma W, Wu H, Lemmers B, Chung S, Parant JM, Lozano G, Hakem R, Benchimol S. Pirh2, a p53-induced ubiquitin-protein ligase, promotes p53 degradation. Cell. 2003;112(6):779-91.

39. Jung YS, Qian Y, Yan W, Chen X. Pirh2 E3 ubiquitin ligase modulates keratinocyte differentiation through p63. J Invest Dermatol. 2013;133(5):1178-87.

40. Logan IR, Gaughan L, McCracken SR, Sapountzi V, Leung HY, Robson CN. Human PIRH2 enhances androgen receptor signaling through inhibition of histone deacetylase 1 and is overexpressed in prostate cancer. Mol Cell Biol. 2006;26(17):6502-10.

41. Mukerjee R, Claudio PP, Chang JR, Del Valle L, Sawaya BE. Transcriptional regulation of HIV-1 gene expression by p53. Cell Cycle. 2010;9(22):4569-78.

42. Ma-Lauer Y, Carbajo-Lozoya J, Hein MY, Müller MA, Deng W, Lei J, Meyer B, Kusov Y, von Brunn B, Bairad DR, Hünten S, Drosten C, Hermeking H, Leonhardt H, Mann M, Hilgenfeld R, von Brunn A. p53 down-regulates SARS coronavirus replication and is targeted by the SARS-unique domain and PLpro via E3 ubiquitin ligase RCHY1. Proc Natl Acad Sci U S A. 2016;113(35):E5192-201.

43. Zhang D, Zhang DE. Interferon-stimulated gene 15 and the protein ISGylation system. J Interferon Cytokine Res. 2011;31(1):119-30.

44. Mustachio LM, Lu Y, Kawakami M, Roszik J, Freemantle SJ, Liu X, Dmitrovsky E. Evidence for the ISG15-Specific Deubiquitinase USP18 as an Antineoplastic Target. Cancer Res. 2018;78(3):587-92.

45. Malakhov MP, Malakhova OA, Kim KI, Ritchie KJ, Zhang DE. UBP43 (USP18) specifically removes ISG15 from conjugated proteins. J Biol Chem. 2002;277(12):9976-81.

46. Basters A, Geurink PP, Röcker A, Witting KF, Tadayon R, Hess S, Semrau MS, Storici P, Ovaa H, Knobeloch KP, Fritz G. Structural basis of the specificity of USP18 toward ISG15. Nat Struct Mol Biol. 2017;24(3):270-8.

47. Zhang M, Li J, Yan H, Huang J, Wang F, Liu T, Zeng L, Zhou F. ISGylation in Innate Antiviral Immunity and Pathogen Defense Responses: A Review. Front Cell Dev Biol. 2021;9:788410.

48. Villarroya-Beltri C, Guerra S, Sánchez-Madrid F. ISGylation - a key to lock the cell gates for preventing the spread of threats. J Cell Sci. 2017;130(18):2961-9.

49. Rodriguez MR, Monte K, Thackray LB, Lenschow DJ. ISG15 functions as an interferon-mediated antiviral effector early in the murine norovirus life cycle. J Virol. 2014;88(16):9277-86.

50. Werneke SW, Schilte C, Rohatgi A, Monte KJ, Michault A, Arenzana-Seisdedos F, Vanlandingham DL, Higgs S, Fontanet A, Albert ML, Lenschow DJ. ISG15 is critical in the control of Chikungunya virus infection independent of UbE1L mediated conjugation. PLoS Pathog. 2011;7(10):e1002322.

51. Kim YJ, Kim ET, Kim YE, Lee MK, Kwon KM, Kim KI, Stamminger T, Ahn JH. Consecutive Inhibition of ISG15 Expression and ISGylation by Cytomegalovirus Regulators. PLoS Pathog. 2016;12(8):e1005850.

52. Zhu J, Liu G, Sayyad Z, Goins CM, Stauffer SR, Gack MU. ISGylation of the SARS-CoV-2 N protein by HERC5 impedes N oligomerization and thereby viral RNA synthesis. J Virol. 2024;98(9):e0086924.

53. Wang H, Guo M, Wei H, Chen Y. Targeting p53 pathways: mechanisms, structures, and advances in therapy. Signal Transduct Target Ther. 2023;8(1):92.

54. Haupt Y, Maya R, Kazaz A, Oren M. Mdm2 promotes the rapid degradation of p53. Nature. 1997;387(6630):296-9.

55. Muñoz-Fontela C, Pazos M, Delgado I, Murk W, Mungamuri SK, Lee SW, García-Sastre A, Moran TM, Aaronson SA. p53 serves as a host antiviral factor that enhances innate and adaptive immune responses to influenza A virus. J Immunol. 2011;187(12):6428-36.

56. Murray-Zmijewski F, Lane DP, Bourdon JC. p53/p63/p73 isoforms: an orchestra of isoforms to harmonise cell differentiation and response to stress. Cell Death Differ. 2006;13(6):962-72.

57. Danilova N, Sakamoto KM, Lin S. p53 family in development. Mech Dev. 2008;125(11-12):919-31.

58. Xu Y, Yang X, Xiong Q, Han J, Zhu Q. The dual role of p63 in cancer. Front Oncol. 2023;13:1116061.

59. Yang A, Walker N, Bronson R, Kaghad M, Oosterwegel M, Bonnin J, Vagner C, Bonnet H, Dikkes P, Sharpe A, McKeon F, Caput D. p73-deficient mice have neurological, pheromonal and inflammatory defects but lack spontaneous tumours. Nature. 2000;404(6773):99-103.

60. Fisher ML, Balinth S, Mills AA. p63-related signaling at a glance. J Cell Sci. 2020;133(17).

61. Flores ER, Sengupta S, Miller JB, Newman JJ, Bronson R, Crowley D, Yang A, McKeon F, Jacks T. Tumor predisposition in mice mutant for p63 and p73: evidence for broader tumor suppressor functions for the p53 family. Cancer Cell. 2005;7(4):363-73.

62. Guo X, Keyes WM, Papazoglu C, Zuber J, Li W, Lowe SW, Vogel H, Mills AA. TAp63 induces senescence and suppresses tumorigenesis in vivo. Nat Cell Biol. 2009;11(12):1451-7.

63. Bankhead A, 3rd, McMaster T, Wang Y, Boonstra PS, Palmbos PL. TP63 isoform expression is linked with distinct clinical outcomes in cancer. EBioMedicine. 2020;51:102561.

64. Kim K, Madak-Erdogan Z, Ventrella R, Katzenellenbogen BS. A MicroRNA196a2* and TP63 circuit regulated by estrogen receptor-α and ERK2 that controls breast cancer proliferation and invasiveness properties. Horm Cancer. 2013;4(2):78-91.

65. Orosz L, Gallyas E, Kemény L, Mándi Y, Facskó A, Megyeri K. Involvement of p63 in the herpes simplex virus-1-induced demise of corneal cells. J Biomed Sci. 2010;17(1):47.

66. Citro S, Bellini A, Medda A, Sabatini ME, Tagliabue M, Chu F, Chiocca S. Human Papilloma Virus Increases ΔNp63α Expression in Head and Neck Squamous Cell Carcinoma. Front Cell Infect Microbiol. 2020;10:143.

67. Kumawat P, Agarwal LK, Sharma K. An Overview of SARS-CoV-2 Potential Targets, Inhibitors, and Computational Insights to Enrich the Promising Treatment Strategies. Curr Microbiol. 2024;81(7):169.

68. Narayanan A, Narwal M, Majowicz SA, Varricchio C, Toner SA, Ballatore C, Brancale A, Murakami KS, Jose J. Identification of SARS-CoV-2 inhibitors targeting Mpro and PLpro using in-cell-protease assay. Commun Biol. 2022;5(1):169.

69. White MA, Lin W, Cheng X. Discovery of COVID-19 Inhibitors Targeting the SARS-CoV-2 Nsp13 Helicase. J Phys Chem Lett. 2020;11(21):9144-51.

70. Menzer WM, Knobloch G, Schomburg A, Lieleg, Corinna, Sennhenn P, inventorsInhibitors of viral helicases binding to a novel allosteric binding site 2024 2024-09-04.

71. Raaben M, Posthuma CC, Verheije MH, te Lintelo EG, Kikkert M, Drijfhout JW, Snijder EJ, Rottier PJ, de Haan CA. The ubiquitin-proteasome system plays an important role during various stages of the coronavirus infection cycle. J Virol. 2010;84(15):7869-79.

72. Lodi G, Gentili V, Casciano F, Romani A, Zauli G, Secchiero P, Zauli E, Simioni C, Beltrami S, Fernandez M, Rizzo R, Voltan R. Cell cycle block by p53 activation reduces SARS-CoV-2 release in infected alveolar basal epithelial A549-hACE2 cells. Front Pharmacol. 2022;13:1018761.

73. Lei J, Ma-Lauer Y, Han Y, Thoms M, Buschauer R, Jores J, Thiel V, Beckmann R, Deng W, Leonhardt H, Hilgenfeld R, von Brunn A. The SARS-unique domain (SUD) of SARS-CoV and SARS-CoV-2 interacts with human Paip1 to enhance viral RNA translation. Embo j. 2021;40(11):e102277.

74. Pfefferle S, Schöpf J, Kögl M, Friedel CC, Müller MA, Carbajo-Lozoya J, Stellberger T, von Dall'Armi E, Herzog P, Kallies S, Niemeyer D, Ditt V, Kuri T, Züst R, Pumpor K, Hilgenfeld R, Schwarz F, Zimmer R, Steffen I, Weber F, Thiel V, Herrler G, Thiel HJ, Schwegmann-Wessels C, Pöhlmann S, Haas J, Drosten C, von Brunn A. The SARS-coronavirus-host interactome: identification of cyclophilins as target for pan-coronavirus inhibitors. PLoS Pathog. 2011;7(10):e1002331.

75. Niemeyer D, Mösbauer K, Klein EM, Sieberg A, Mettelman RC, Mielech AM, Dijkman R, Baker SC, Drosten C, Müller MA. The papain-like protease determines a virulence trait that varies among members of the SARS-coronavirus species. PLoS Pathog. 2018;14(9):e1007296.

76. Hayn M, Hirschenberger M, Koepke L, Nchioua R, Straub JH, Klute S, Hunszinger V, Zech F, Prelli Bozzo C, Aftab W, Christensen MH, Conzelmann C, Müller JA, Srinivasachar Badarinarayan S, Stürzel CM, Forne I, Stenger S, Conzelmann KK, Münch J, Schmidt FI, Sauter D, Imhof A, Kirchhoff F, Sparrer KMJ. Systematic functional analysis of SARS-CoV-2 proteins uncovers viral innate immune antagonists and remaining vulnerabilities. Cell Rep. 2021;35(7):109126.

77. Weller B, Lin CW, Pogoutse O, Sauer M, Marin-de la Rosa N, Strobel A, Young V, Knapp JJ, Rayhan A, Falter C, Kim DK, Roth FP, Falter-Braun P. A resource of human coronavirus protein-coding sequences in a flexible, multipurpose Gateway Entry clone collection. G3 (Bethesda). 2023;13(7).

78. Flaswinkel H, Reth M. Dual role of the tyrosine activation motif of the Ig-alpha protein during signal transduction via the B cell antigen receptor. Embo j. 1994;13(1):83-9.

79. Yeruva S, Kempf E, Egu DT, Flaswinkel H, Kugelmann D, Waschke J. Adrenergic Signaling-Induced Ultrastructural Strengthening of Intercalated Discs via Plakoglobin Is Crucial for Positive Adhesiotropy in Murine Cardiomyocytes. Front Physiol. 2020;11:430.

80. Mathieu C, Touret F, Jacquemin C, Janin YL, Nougairède A, Brailly M, Mazelier M, Décimo D, Vasseur V, Hans A, Valle-Casuso JC, de Lamballerie X, Horvat B, André P, Si-Tahar M, Lotteau V, Vidalain PO. A Bioluminescent 3CL(Pro) Activity Assay to Monitor SARS-CoV-2 Replication and Identify Inhibitors. Viruses. 2021;13(9).

81. Heller GT, Aprile FA, Vendruscolo M. Methods of probing the interactions between small molecules and disordered proteins. Cell Mol Life Sci. 2017;74(17):3225-43.

82. Varikkapulakkal A, Ghosh A, Mishra SK. Broader roles of the ubiquitin-like protein Hub1 indicated by its yeast two-hybrid interactors. MicroPubl Biol. 2022;2022.

83. Schmidt EK, Clavarino G, Ceppi M, Pierre P. SUnSET, a nonradioactive method to monitor protein synthesis. Nat Methods. 2009;6(4):275-7.

84. Miao Y, Du Q, Zhang HG, Yuan Y, Zuo Y, Zheng H. Cycloheximide (CHX) Chase Assay to Examine Protein Half-life. Bio Protoc. 2023;13(11):e4690.

85. Eldeeb MA, Siva-Piragasam R, Ragheb MA, Esmaili M, Salla M, Fahlman RP. A molecular toolbox for studying protein degradation in mammalian cells. J Neurochem. 2019;151(4):520-33.

86. Moraes-Vieira PM, Yore MM, Sontheimer-Phelps A, Castoldi A, Norseen J, Aryal P, Simonyté Sjödin K, Kahn BB. Retinol binding protein 4 primes the NLRP3 inflammasome by signaling through Toll-like receptors 2 and 4. Proc Natl Acad Sci U S A. 2020;117(49):31309-18.

87. Choi SG, Olivet J, Cassonnet P, Vidalain PO, Luck K, Lambourne L, Spirohn K, Lemmens I, Dos Santos M, Demeret C, Jones L, Rangarajan S, Bian W, Coutant EP, Janin YL, van der Werf S, Trepte P, Wanker EE, De Las Rivas J, Tavernier J, Twizere JC, Hao T, Hill DE, Vidal M, Calderwood MA, Jacob Y. Maximizing binary interactome mapping with a minimal number of assays. Nat Commun. 2019;10(1):3907.

88. Kunec D, Osterrieder N, Trimpert J. Synthetically recoded virus sCPD9 - A tool to accelerate SARS-CoV-2 research under biosafety level 2 conditions. Comput Struct Biotechnol J. 2022;20:4376-80.

89. Nouailles G, Adler JM, Pennitz P, Peidli S, Teixeira Alves LG, Baumgardt M, Bushe J, Voss A, Langenhagen A, Langner C, Martin Vidal R, Pott F, Kazmierski J, Ebenig A, Lange MV, Mühlebach MD, Goekeri C, Simmons S, Xing N, Abdelgawad A, Herwig S, Cichon G, Niemeyer D, Drosten C, Goffinet C, Landthaler M, Blüthgen N, Wu H, Witzenrath M, Gruber AD, Praktiknjo SD, Osterrieder N, Wyler E, Kunec D, Trimpert J. Live-attenuated vaccine sCPD9 elicits superior mucosal and systemic immunity to SARS-CoV-2 variants in hamsters. Nat Microbiol. 2023;8(5):860-74.

90. Stukalov A, Girault V, Grass V, Karayel O, Bergant V, Urban C, Haas DA, Huang Y, Oubraham L, Wang A, Hamad MS, Piras A, Hansen FM, Tanzer MC, Paron I, Zinzula L, Engleitner T, Reinecke M, Lavacca TM, Ehmann R, Wölfel R, Jores J, Kuster B, Protzer U, Rad R, Ziebuhr J, Thiel V, Scaturro P, Mann M, Pichlmair A. Multilevel proteomics reveals host perturbations by SARS-CoV-2 and SARS-CoV. Nature. 2021;594(7862):246-52.

91. Yan Y, Tao H, He J, Huang SY. The HDOCK server for integrated protein-protein docking. Nat Protoc. 2020;15(5):1829-52.

92. Jung YS, Liu G, Chen X. Pirh2 E3 ubiquitin ligase targets DNA polymerase eta for 20S proteasomal degradation. Mol Cell Biol. 2010;30(4):1041-8.

93. Yue K, Yao B, Shi Y, Yang Y, Qian Z, Ci Y, Shi L. The stalk domain of SARS-CoV-2 NSP13 is essential for its helicase activity. Biochem Biophys Res Commun. 2022;601:129-36.

94. Duan S, Yao Z, Hou D, Wu Z, Zhu WG, Wu M. Phosphorylation of Pirh2 by calmodulin-dependent kinase II impairs its ability to ubiquitinate p53. Embo j. 2007;26(13):3062-74.

95. Lavigne M, Helynck O, Rigolet P, Boudria-Souilah R, Nowakowski M, Baron B, Brule S, Hoos S, Raynal B, Guittat L, Beauvineau C, Petres S, Granzhan A, Guillon J, Pratviel G, Teulade-Fichou MP, England P, Mergny JL, Munier-Lehmann H. SARS-CoV-2 Nsp3 unique domain SUD interacts with guanine quadruplexes and G4-ligands inhibit this interaction. Nucleic Acids Res. 2021;49(13):7695-712.

96. Nathans D. Puromycin Inhibition of Protein Synthesis: Incorporation of Puromycin into Peptide Chains. Proc Natl Acad Sci U S A. 1964;51(4):585-92.

97. Cao D, Duan L, Huang B, Xiong Y, Zhang G, Huang H. The SARS-CoV-2 papain-like protease suppresses type I interferon responses by deubiquitinating STING. Sci Signal. 2023;16(783):eadd0082.

98. Armstrong SR, Wu H, Wang B, Abuetabh Y, Sergi C, Leng RP. The Regulation of Tumor Suppressor p63 by the Ubiquitin-Proteasome System. Int J Mol Sci. 2016;17(12).

99. Xu G, Wu Y, Xiao T, Qi F, Fan L, Zhang S, Zhou J, He Y, Gao X, Zeng H, Li Y, Zhang Z. Multiomics approach reveals the ubiquitination-specific processes hijacked by SARS-CoV-2. Signal Transduct Target Ther. 2022;7(1):312.

100. Jacobson AD, Zhang NY, Xu P, Han KJ, Noone S, Peng J, Liu CW. The lysine 48 and lysine 63 ubiquitin conjugates are processed differently by the 26 s proteasome. J Biol Chem. 2009;284(51):35485-94.

101. Swatek KN, Komander D. Ubiquitin modifications. Cell Res. 2016;26(4):399-422.

102. Lei X, Dong X, Ma R, Wang W, Xiao X, Tian Z, Wang C, Wang Y, Li L, Ren L, Guo F, Zhao Z, Zhou Z, Xiang Z, Wang J. Activation and evasion of type I interferon responses by SARS-CoV-2. Nat Commun. 2020;11(1):3810.

103. Sui C, Xiao T, Zhang S, Zeng H, Zheng Y, Liu B, Xu G, Gao C, Zhang Z. SARS-CoV-2 NSP13 Inhibits Type I IFN Production by Degradation of TBK1 via p62-Dependent Selective Autophagy. J Immunol. 2022;208(3):753-61.

104. Vazquez C, Swanson SE, Negatu SG, Dittmar M, Miller J, Ramage HR, Cherry S, Jurado KA. SARS-CoV-2 viral proteins NSP1 and NSP13 inhibit interferon activation through distinct mechanisms. PLoS One. 2021;16(6):e0253089.

105. Shakhov AN, Collart MA, Vassalli P, Nedospasov SA, Jongeneel CV. Kappa B-type enhancers are involved in lipopolysaccharide-mediated transcriptional activation of the tumor necrosis factor alpha gene in primary macrophages. J Exp Med. 1990;171(1):35-47.

106. Pickart CM, Fushman D. Polyubiquitin chains: polymeric protein signals. Curr Opin Chem Biol. 2004;8(6):610-6.

107. Yao F, Zhou Z, Kim J, Hang Q, Xiao Z, Ton BN, Chang L, Liu N, Zeng L, Wang W, Wang Y, Zhang P, Hu X, Su X, Liang H, Sun Y, Ma L. SKP2- and OTUD1-regulated non-proteolytic ubiquitination of YAP promotes YAP nuclear localization and activity. Nat Commun. 2018;9(1):2269.

108. Johnson MA, Chatterjee A, Neuman BW, Wuthrich K. SARS coronavirus unique domain: three-domain molecular architecture in solution and RNA binding. J Mol Biol. 2010;400(4):724-42.

109. Dong W, Cheng Y, Zhou Y, Zhang J, Yu X, Guan H, Du J, Zhou X, Yang Y, Fang W, Wang X, Song H. The nucleocapsid protein facilitates p53 ubiquitination-dependent proteasomal degradation via recruiting host ubiquitin ligase COP1 in PEDV infection. J Biol Chem. 2024;300(4):107135.

110. Yuan L, Chen Z, Song S, Wang S, Tian C, Xing G, Chen X, Xiao ZX, He F, Zhang L. p53 degradation by a coronavirus papain-like protease suppresses type I interferon signaling. J Biol Chem. 2015;290(5):3172-82.

111. Muñoz-Fontela C, Mandinova A, Aaronson SA, Lee SW. Emerging roles of p53 and other tumour-suppressor genes in immune regulation. Nat Rev Immunol. 2016;16(12):741-50.

112. Aubrey BJ, Kelly GL, Janic A, Herold MJ, Strasser A. How does p53 induce apoptosis and how does this relate to p53-mediated tumour suppression? Cell Death Differ. 2018;25(1):104-13.

113. Rashedi I, Panigrahi S, Ezzati P, Ghavami S, Los M. Autoimmunity and apoptosis--therapeutic implications. Curr Med Chem. 2007;14(29):3139-51.

114. Xuan B, Qian Z, Torigoi E, Yu D. Human cytomegalovirus protein pUL38 induces ATF4 expression, inhibits persistent JNK phosphorylation, and suppresses endoplasmic reticulum stress-induced cell death. J Virol. 2009;83(8):3463-74.

115. Deng Y, Águeda-Pinto A, Brune W. No Time to Die: How Cytomegaloviruses Suppress Apoptosis, Necroptosis, and Pyroptosis. Viruses. 2024;16(8).

116. Kommagani R, Caserta TM, Kadakia MP. Identification of vitamin D receptor as a target of p63. Oncogene. 2006;25(26):3745-51.

117. Ishii M, Yamaguchi Y, Isumi K, Ogawa S, Akishita M. Transgenic Mice Overexpressing Vitamin D Receptor (VDR) Show Anti-Inflammatory Effects in Lung Tissues. Inflammation. 2017;40(6):2012-9.

118. Sethi I, Romano RA, Gluck C, Smalley K, Vojtesek B, Buck MJ, Sinha S. A global analysis of the complex landscape of isoforms and regulatory networks of p63 in human cells and tissues. BMC Genomics. 2015;16:584.

119. Rodriguez Calleja L, Lavaud M, Tesfaye R, Brounais-Le-Royer B, Baud'huin M, Georges S, Lamoureux F, Verrecchia F, Ory B. The p53 Family Members p63 and p73 Roles in the Metastatic Dissemination: Interactions with microRNAs and TGFβ Pathway. Cancers (Basel). 2022;14(23).

120. Yu VZ, So SS, Lung BC, Hou GZ, Wong CW, Chow LK, Chung MK, Wong IY, Wong CL, Chan DK, Chan FS, Law BT, Xu K, Tan ZZ, Lam KO, Lo AW, Lam AK, Kwong DL, Ko JM, Dai W, Law S, Lung ML. ΔNp63-restricted viral mimicry response impedes cancer cell viability and remodels tumor microenvironment in esophageal squamous cell carcinoma. Cancer Lett. 2024;595:216999.

121. Carlin AF, Plummer EM, Vizcarra EA, Sheets N, Joo Y, Tang W, Day J, Greenbaum J, Glass CK, Diamond MS, Shresta S. An IRF-3-, IRF-5-, and IRF-7-Independent Pathway of Dengue Viral Resistance Utilizes IRF-1 to Stimulate Type I and II Interferon Responses. Cell Rep. 2017;21(6):1600-12.

122. Yang A, Kaghad M, Wang Y, Gillett E, Fleming MD, Dötsch V, Andrews NC, Caput D, McKeon F. p63, a p53 homolog at 3q27-29, encodes multiple products with transactivating, death-inducing, and dominant-negative activities. Mol Cell. 1998;2(3):305-16.

123. Heaton SM, Borg NA, Dixit VM. Ubiquitin in the activation and attenuation of innate antiviral immunity. J Exp Med. 2016;213(1):1-13.

124. Isaacson MK, Ploegh HL. Ubiquitination, ubiquitin-like modifiers, and deubiquitination in viral infection. Cell Host Microbe. 2009;5(6):559-70.

125. Freitas BT, Scholte FEM, Bergeron É, Pegan SD. How ISG15 combats viral infection. Virus Res. 2020;286:198036.

126. Shi HX, Yang K, Liu X, Liu XY, Wei B, Shan YF, Zhu LH, Wang C. Positive regulation of interferon regulatory factor 3 activation by Herc5 via ISG15 modification. Mol Cell Biol. 2010;30(10):2424-36.

127. Ganesan M, Poluektova LY, Tuma DJ, Kharbanda KK, Osna NA. Acetaldehyde Disrupts Interferon Alpha Signaling in Hepatitis C Virus-Infected Liver Cells by Up-Regulating USP18. Alcohol Clin Exp Res. 2016;40(11):2329-38.

128. Frias-Staheli N, Giannakopoulos NV, Kikkert M, Taylor SL, Bridgen A, Paragas J, Richt JA, Rowland RR, Schmaljohn CS, Lenschow DJ, Snijder EJ, García-Sastre A, Virgin HWt. Ovarian tumor domain-containing viral proteases evade ubiquitin- and ISG15-dependent innate immune responses. Cell Host Microbe. 2007;2(6):404-16.

129. Park JH, Yang SW, Park JM, Ka SH, Kim JH, Kong YY, Jeon YJ, Seol JH, Chung CH. Positive feedback regulation of p53 transactivity by DNA damage-induced ISG15 modification. Nat Commun. 2016;7:12513.

130. Malone B, Urakova N, Snijder EJ, Campbell EA. Structures and functions of coronavirus replication-transcription complexes and their relevance for SARS-CoV-2 drug design. Nat Rev Mol Cell Biol. 2022;23(1):21-39.

131. Giraldo MI, Xia H, Aguilera-Aguirre L, Hage A, van Tol S, Shan C, Xie X, Sturdevant GL, Robertson SJ, McNally KL, Meade-White K, Azar SR, Rossi SL, Maury W, Woodson M, Ramage H, Johnson JR, Krogan NJ, Morais MC, Best SM, Shi PY, Rajsbaum R. Envelope protein ubiquitination drives entry and pathogenesis of Zika virus. Nature. 2020;585(7825):414-9.

132. Rahman MM, McFadden G. Modulation of NF-κB signalling by microbial pathogens. Nat Rev Microbiol. 2011;9(4):291-306.

133. Yang J, Li S, Feng T, Zhang X, Yang F, Cao W, Chen H, Liu H, Zhang K, Zhu Z, Zheng H. African Swine Fever Virus F317L Protein Inhibits NF-κB Activation To Evade Host Immune Response and Promote Viral Replication. mSphere. 2021;6(5):e0065821.

134. Fang X, Gao J, Zheng H, Li B, Kong L, Zhang Y, Wang W, Zeng Y, Ye L. The membrane protein of SARS-CoV suppresses NF-kappaB activation. J Med Virol. 2007;79(10):1431-9.

135. Krump NA, You J. Molecular mechanisms of viral oncogenesis in humans. Nat Rev Microbiol. 2018;16(11):684-98.

136. Stanley M. Pathology and epidemiology of HPV infection in females. Gynecol Oncol. 2010;117(2 Suppl):S5-10.

137. Tu T, Bühler S, Bartenschlager R. Chronic viral hepatitis and its association with liver cancer. Biol Chem. 2017;398(8):817-37.

138. Naseem M, Barzi A, Brezden-Masley C, Puccini A, Berger MD, Tokunaga R, Battaglin F, Soni S, McSkane M, Zhang W, Lenz HJ. Outlooks on Epstein-Barr virus associated gastric cancer. Cancer Treat Rev. 2018;66:15-22.

139. Khatun M, Ray RB. Mechanisms Underlying Hepatitis C Virus-Associated Hepatic Fibrosis. Cells. 2019;8(10).

140. Tagaya Y, Gallo RC. The Exceptional Oncogenicity of HTLV-1. Front Microbiol. 2017;8:1425.

141. Duyao MP, Kessler DJ, Spicer DB, Bartholomew C, Cleveland JL, Siekevitz M, Sonenshein GE. Transactivation of the c-myc promoter by human T cell leukemia virus type 1 tax is mediated by NF kappa B. J Biol Chem. 1992;267(23):16288-91.

142. Daks A, Petukhov A, Fedorova O, Shuvalov O, Merkulov V, Vasileva E, Antonov A, Barlev NA. E3 ubiquitin ligase Pirh2 enhances tumorigenic properties of human non-small cell lung carcinoma cells. Genes Cancer. 2016;7(11-12):383-93.

143. Scheffner M, Huibregtse JM, Vierstra RD, Howley PM. The HPV-16 E6 and E6-AP complex functions as a ubiquitin-protein ligase in the ubiquitination of p53. Cell. 1993;75(3):495-505.

Acknowledgements

The period of time passed rapidly, and my doctoral study in Germany approached its end. During the years of my doctoral study, I would like to express my gratitude to all those who supported the work described in this dissertation.

First, I express my deepest gratitude to my supervisor, PD Dr. rer. nat. Dr. habil. med. Albrecht von Brunn. Many thanks to him for providing me with the opportunity to work in his laboratory and for giving me the platform to study this great project. He was supportive and patient and always paid close attention to my research. Whenever I discussed the research progress with him, he provided me with careful guidance and encouraged me to overcome the challenges I faced.

It was a great pleasure to work with a friendly group of colleagues. I am grateful to the postdoctoral fellow Dr. Yue Ma-Lauer. She was full of enthusiasm and had a strong spirit of exploration in scientific research. Her constructive comments on my doctoral work often inspired me and gave me new ideas. I would also like to thank Brigitte von Brunn. She is a positive and optimistic person - a source of encouragement for everyone around her. Whenever I encountered difficulties in work or life, she always tried her best to help me without hesitation. I also wanted to thank my colleagues Pengyuan Li and Chengyu Xiang, who encouraged me when I felt upset and provided great help. I felt very lucky to have worked with everyone at AG von Brunn.

I am also grateful to Dr. Zhe Ma, Dr. Gregor Ebert, and Professor Andreas Pichlmair for their help in the SARS-CoV-2 infection studies in the S3 lab. I also thank the China Scholarship Council (CSC) for funding my doctoral studies.

Finally, I sincerely thank my family for their selfless support and care. They were my strongest support. I also appreciate the friends I met during my time in Germany—He Yi, Liu Sha, Wang Cai, He Jingyi, and A Zheng—who comforted me when I felt disappointed or lost faith, and were there for me when I needed them.

Affidavit

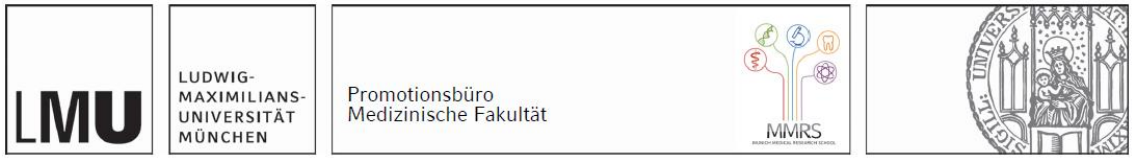

Affidavit

Ru, Yi

Surname, first name

I hereby declare, that the submitted thesis entitled:

SARS-CoV-2 Nsp3 and Nsp13 utilize host E3 ubiquitin ligase RCHY1 to suppress host antiviral responses and facilitate virus replication ……

is my own work. I have only used the sources indicated and have not made unauthorized use of services of a third party. Where the work of others has been quoted or reproduced, the source is always given.

I further declare that the dissertation presented here has not been submitted in the same or similar form to any other institution for the purpose of obtaining an academic degree.

Zhengzhou, 19.12.2025 Yi Ru

place, date Signature doctoral candidate

Confirmation of congruency

LMU LUDWIG-MAXIMILIANS-UNIVERSITÄT MÜNCHEN

Promotionsbüro
Medizinische Fakultät

MMRS

Confirmation of congruency between printed and electronic version of the doctoral thesis

Ru, Yi

Surname, first name

I hereby declare, that the submitted thesis entitled:

SARS-CoV-2 Nsp3 and Nsp13 utilize host E3 ubiquitin ligase RCHY1 to suppress host antiviral responses and facilitate virus replication

……

is congruent with the printed version both in content and format.

Zhengzhou, 19.12.2025 Yi Ru

place, date

Signature doctoral candidate

Curriculum vitae

RU YI

Education Background

Faculty of Medicine, The Ludwig Maximilian University of Munich (LMU) Munich, Germany

Doctoral Program of Natural Sciences, Virology 2021-2025

Department of Medical Genetics, Beijing University Beijing, China

Master of Science, Genetics 2017-2020

School of Life Sciences, Central China Normal University Wuhan, China

Bachelor's Degree in Biotechnology 2013-2017

Research Experience

Project Lead: Circular RNA in the pathogenic mechanism of glioma (Supervised by Dr. Wu Dan and Prof. Luo Jianyuan, Department of Medical Genetics, Peking University, 2017-2020)

Project Lead: The influence of SARS-CoV-2 proteins on human E3 ligase RCHY1 and its substrates (Supervised by PD Dr. Dr.von Brunn, Max von Pettenkofer-Institute, LMU, 2021-2025)

Project Lead: LMP7 Inhibited by Ixazomib and Targeted by SARS-CoV-2 Nonstructural Protein 13 and 16 Regulates Viral Replication (Supervised by PD Dr. Dr.von Brunn, Max von Pettenkofer-Institute, LMU, 2024-2025)

Oxysterole-binding protein (OSBP) targeted by SARS-CoV-2 viral proteins regulate coronavirus replication (Supervised by PD Dr. Dr.von Brunn, Max von Pettenkofer-Institute, LMU, 2021-2024)

Publications

Ma-Lauer, Y., Li, P., Niemeyer, D., Richter, A., Pusl, K., von Brunn, B., **Ru, Y.**, Xiang, C., Schwinghammer, S., Liu, J., Baral, P., Berthold, E. J., Qiu, H., Roy, A., Kremmer, E., Flaswinkel, H., Drosten, C., Jin, Z., & von Brunn, A. (2024). Oxysterole-binding protein targeted by SARS-CoV-2 viral proteins regulates coronavirus replication [Original Research]. Frontiers in Cellular and Infection Microbiology, 14. https://doi.org/10.3389/fcimb.2024.1383917

Ru, Y., et al. SARS-CoV-2 Nsp3 and Nsp13 utilize host E3 ubiquitin ligase RCHY1 to suppress host antiviral responses and enhance virus replication. (Submitted).

Ru, Y.#, Ma-Lauer, Y.#, Xiang, C., Li, P., von Brunn, B., Richter, A., Drosten, C., Pichlmair, A., Pfefferle, S., Klein, M., Damoiseaux, RD., Betz, UAK., & von Brunn, A. (2025). LMP7 as a Target for Coronavirus Therapy: Inhibition by Ixazomib and Interaction with SARS-CoV-2 Proteins Nsp13 and Nsp16. Pathogens, 2025,14(9), 871; https://doi.org/10.3390/pathogens14090871

List of publications

25-26 September, 2023

Conference

Deutsches Zentrum für Infektionsforschung (DZIF), **SARS-CoV-2 Nsp3 a.a.1-1363 down-regulates antiviral factors p53 and p63 by targeting RCHY1** (Poster)

13-15 February, 2025

Conference

Deutsches Zentrum für Infektionsforschung (DZIF), **RCHY1 targets and is utilized by SARS-CoV-2 Nsp13 to modulate Lys63-linked polyubiquitination of Nsp13 and inhibit NF-κB signaling** (Poster)

Journal Article

Ma-Lauer, Y., Li, P., Niemeyer, D., Richter, A., Pusl, K., von Brunn, B., **Ru, Y.**, Xiang, C., Schwinghammer, S., Liu, J., Baral, P., Berthold, E. J., Qiu, H., Roy, A., Kremmer, E., Flaswinkel, H., Drosten, C., Jin, Z., & von Brunn, A. (2024). Oxysterole-binding protein targeted by SARS-CoV-2 viral proteins regulates coronavirus replication [Original Research]. Frontiers in Cellular and Infection Microbiology, 14. https://doi.org/10.3389/fcimb.2024.1383917

Ru, Y.#, Ma-Lauer, Y.#, Xiang, C., Li, P., von Brunn, B., Richter, A., Drosten, C., Pichlmair, A., Pfefferle, S., Klein, M., Damoiseaux, RD., Betz, UAK., & von Brunn, A. (2025). LMP7 as a Target for Coronavirus Therapy: Inhibition by Ixazomib and Interaction with SARS-CoV-2 Proteins Nsp13 and Nsp16. Pathogens, 2025,14(9), 871; https://doi.org/10.3390/pathogens14090871